Travail de fin d'études en chimie et bio-industries : Understanding the Fate of Organic Matter and Nutrients in New Typologies of Organic Sludge Fertilizers.

Auteur : Burgess, Lucy
Promoteur(s) : 24100
Faculté : Gembloux Agro-Bio Tech (GxABT)
Diplôme : Master en bioingénieur : chimie et bioindustries, à finalité spécialisée
Année académique : 2025-2026
URI/URL : http://hdl.handle.net/2268.2/26059

European Master in Biological and Chemical Engineering for a Sustainable Bioeconomy

Master thesis report

submitted to obtain the degrees of:

Master in Biology AgroSciences (BAS) of the University of Reims Champagne-Ardenne

Master in Integrative Biology and Physiology (BIP) of the University Paris-Saclay, operated by AgroParisTech

Master in Bioengineering: Chemistry and Bioindustries of the University of Liège

Title of the Master thesis:

Understanding the Fate of Organic Matter and Nutrients in New Typologies of Organic Sludge Fertilizers

Presented by: ***BURGESS Lucy***

Defended the: **26/06/26**

Supervised by **PATUREAU Dominique, JIMENEZ Julie and SINISGALLI Erika**

at: INRAE, LBE, Av. des Étangs, 11100 Narbonne.

from: 02/02 /26 to 31/07/26.

Bioceb supervisors: BARANGER Claire, AgroParisTech

MANON Genva, University of Liège

Confidentiality: Yes □ No ■ Privacy expiration date: …/…/….

Acknowledgments

I would like to express my sincere thanks to all the people who gave me help and support. Without them the completion of this thesis would not have been possible.

My mentor, Erika Sinisgalli, for her invaluable advice and guidance throughout my internship. It has been a genuine pleasure to learn from her.

Thanks to Sophie Cuissette, for her help and chats in the lab. Without her, none of this work would have been possible.

Thank you to Dominique Patureau and Julie Jimenez for their direction and guidance throughout this project and for the opportunity to work on such stimulating and relevant research.

My colleagues at LBE were a great support and made my time there truly enjoyable. What an enriching experience to work within such a diverse and international community!

My Bioceb classmates and professors for making the last 2 years an unforgettable experience.

And of course, my deepest thanks to my family for their unwavering support and my friends, Daniel, Laura and Eimear for their understanding and encouragement throughout it all.

Abstract

Global population growth, urbanisation and intensifying pressure on natural resources have made the sustainable management of organic waste streams an increasingly urgent priority. The depletion of finite mineral resources and the decline of soil organic matter across European agricultural land have underlined the need to recover and recycle nutrients from waste rather than disposing of them – a need made more urgent by rising fertilizer costs and geopolitical instability in supply chains. In this context, the concept of a circular bioeconomy - in which waste streams are valorised as resources rather than discarded - has become central to EU environmental and agricultural policy.

Sewage sludge, generated in vast quantities across Europe, represents both a significant waste management burden and an underexploited source of organic matter and plant-available nutrients. When treated appropriately, SS can return to agricultural land as a biofertilizer, closing nutrient loops and reducing dependence on synthetic fertilizer inputs. However, it also contains a complex mixture of contaminants - including heavy metals, pharmaceuticals, PFAS and microplastics - whose behaviour during treatment and following land application is not fully understood.

The fate of organic matter, nutrients and pollutants during sludge treatment is a function of both the treatment process applied, and the chemical structure of the compounds involved. Biological treatments tend to stabilise organic matter and preserve nutrients. Thermochemical treatments achieve greater volume reduction and alter contaminant concentrations and their interactions with organic matter, thereby affecting pollutant bioavailability in soil. However, this comes at the cost of structural changes to organic matter itself and shifts in nutrient bioavailability. The impact of sludge application on agricultural soils depends on soil physicochemical properties, vegetation and crop type, application rate and environmental conditions. Evaluating SS-derived products for land application thus requires comprehensive, multicriteria characterisation of their physicochemical properties, agronomic benefits and associated risks. This study aimed to provide a comprehensive characterization of sludge and sludge-derived products with an emphasis on the bioavailability, bioaccessibility and complexity of organic matter and nutrients across these matrices. The main objectives are:

(i) to elucidate the transformation pathways of organic matter and nutrients across various sludge-derived products,
(ii) to identify the most impactful physicochemical and agronomical fate parameters affected by these transformations through multivariate statistical analyses,
(iii) to elucidate the links between treatment processes and their corresponding end-products and facilitate a reverse-engineering approach, to optimize process performance and product quality.

Table of Contents

Table of Figures

List of Tables

List of Tables in Annex

Abbreviations

AD	Anaerobic Digestion	NP	Nonylphenols
AMR	AntiMicrobial Resistance	OM	Organic Matter
ARG	Antimicrobial Resistance Genes	OWP	Organic Waste Product
BaP	Benzo(a)pyrene	PAH	Polycyclic Aromatic Hydrocarbons
BMP	Biochemical Methane Potential	PCA	Principal Component Analysis
CEC	Cation Exchange Capacity	PCB	Polychlorinated Biphenyls
CMC	Component Material Categories	PEOM	Poorly Extractible Organic Matter
COD	Chemical Oxygen Demand	PFAS	Per and polyfluoroalkyl Substances
CR	Complexity Ratio	PPCP	Pharmaceuticals and Personal Care Products
DOM	Dissolved Organic Metter	REOM	Readily Available Organic Matter
DS	Dry Solids	sCOD	Soluble Chemical Oxygen Demand
EC	Electrical Conductivity	SEOM	Slowly Extractible Organic Matter
EEM	Excitation Emission Matrix	SPOM	Soluble Organic Matter
EPS	Extracellular Polymeric Substances	SS	Sewage Sludge
FRI	Fluorescence Regional Integration	SSD	Sewage Sludge Directive
HCA	Hierarchical Clustering Analysis	TAN	Total Ammonia Nitrogen
HM	Heavy Metals	tCOD	Total Chemical Oxygen Demand
HTC	Hydrothermal Carbonization	TKN	Total Kjeldahl Nitrogen
ISBAMO	Indice de Stabilite et de BioAccessibilite de la Matiere Organique	TN	Total Nitrogen
LAS	Linear Alkylbenzene Sulfonate	TS	Total Solids
MP	MicroPlastics	VFA	Volatile Fatty Acids
NEOM	Non Extractible Organic Matter	VS	Volatile Solids

1 Introduction

1.1 What is Sewage Sludge (SS)

Water used by households and industries is collected and transported to wastewater treatment plants (WWTPs). Along the way, it may mix with surface runoff and other industrial effluent. This combination is commonly referred to as 'wastewater'. Prior to treatment, wastewater contains a complex mixture of pollutants and microorganisms harmful to human health and the environment, so it must be treated before re-entering the water cycle.

Sewage sludge (SS) is the solid by-product of wastewater treatment plants (Figure 1). Composed primarily of water, it is rich in valuable resources such as organic carbon (typically 25–35% of dry solids (DS)) as well as nitrogen (N, 4–5% DS), phosphorus (P, 1–3% DS) and potassium (K, 0.1-0.3% DS). It also contains hazardous pollutants like PAHs (Polycyclic Aromatic Hydrocarbons), PCBs (Polychlorinated Biphenyls) (Mailler et al., 2017), PFAS (Per and polyfluoroalkyl Substances) (Arvaniti et al., 2024), pharmaceuticals and personal care products (PPCPs) (Bourdat-Deschamps et al., 2017), heavy metals (HMs), microplastics (MPs), pathogens (Lamastra et al., 2018) and antimicrobial resistance genes (ARGs) (Yin et al., 2024).

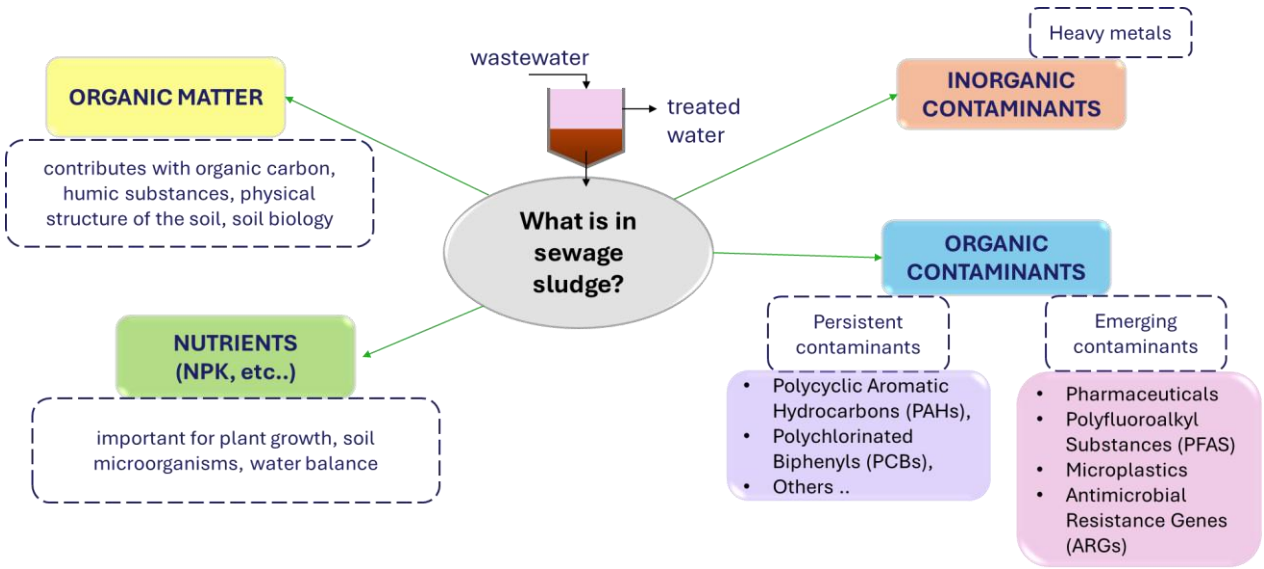

Figure 1: Conceptual overview of the main constituents of sewage sludge generated during wastewater treatment, including beneficial components (organic matter and nutrients) and contaminants (inorganic and organic; persistent and emerging).

1.2 Quantities and Disposal Routes

The production of SS has increased steadily over the last decade. According to Eurostat, total European production currently reaches approximately 13.5 million tonnes of DS per year, a figure

that continues to rise with population growth, urbanisation and increasingly efficient wastewater treatment (Eurostat, 2022). Consequently, sludge valorisation has become a priority within waste management policy and research.

Land application for agriculture accounts for 47.5% of European sludge, followed by incineration (27.2%), land reclamation (8.3%), and landfill (5.6%), as shown in Figure 2. Current management practices vary across European countries, reflecting differences in geography, regulation, and infrastructure. Agricultural recycling dominates in France, Spain, Denmark and Ireland, while incineration is the only permitted route in Flanders and the Netherlands. Land reclamation is favoured in Finland and Sweden, and several countries including Germany and Poland operate mixed strategies. These contrasts partly reflect underlying agronomic contexts: southern European soils often deficient in organic matter (OM) benefit from sludge amendment, whereas northern European countries facing nutrient surplus and eutrophication risks tend toward thermal treatments (EurEau, 2021)

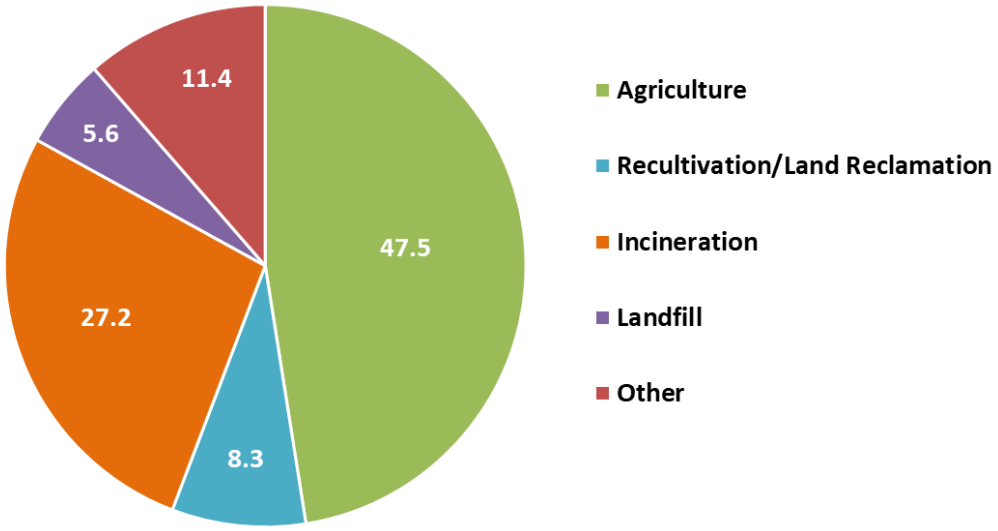

Figure 2: Sludge destination in Europe (% of total) according to the 2021 EurEau Survey 'Europe's Water in Figures (EurEau, 2021).

1.3 Policy context

To support a sustainable and circular society that protects both the environment and human health, updates to EU law governing the use of SS are urgently needed. The current legislative framework on SS presents significant differences among EU Countries and gaps on emerging but also already existing topics of concern. This limits safe treatment and application practices across EU Member States, slowing progress toward circular economy objectives.

1.3.1 The Sewage Sludge Directive (86/278/EEC)

The Sewage Sludge Directive (86/278/EEC; SSD), which came into effect on 18th June 1986, remains the primary legislative instrument governing the agricultural use of SS across the EU. Its objective is to regulate land spreading of treated SS to minimise risks to human, animal and plant health. The Directive sets maximum permissible concentrations of six HMs - cadmium (Cd), copper (Cu), nickel (Ni), lead (Pb), zinc (Zn) and mercury (Hg) - in both the receiving soil and the sludge itself, specifying annual application limits based on a ten-year average. It establishes requirements covering nutrient management planning, sampling and analysis of sludge and soils, record-keeping, and permitted treatment types and application sites (European Comission, 1986).

Now over 40 years old, this legislation urgently requires updates and revision. It addresses only a limited set of HMs and makes no provision for the growing suite of emerging contaminants now recognised as significant risks associated with sludge land application, including organic micropollutants, PFAS, PPCPs and MPs. Several Member States have already responded by applying more stringent national limits and extending regulation to additional contaminant classes. For example, France regulates 3 PAHs and 7 PCBs, Denmark sets limits for 9 PAHs, and Belgium for 7 PCBs (Hudcová et al., 2019). This has resulted in disparate approaches across the EU rather than coordinated progress.

1.3.2 Complementary EU Legislation

Sewage sludge application in agriculture must also comply with limits set by other EU legislation. The Nitrates Directive (91/676/EEC) has a particularly significant practical impact, regulating the maximum quantities of nitrogen permitted to be spread on an agricultural holding (Sutton et al., 2016). In practice, these nutrient thresholds impose a more binding constraint on sludge application rates than heavy metal limits in many contexts, yet emerging organic contaminants remain entirely unregulated at EU level.

1.3.3 The EU Fertilising Products Regulation (2019/1009)

The European Fertilising Products Regulation (FPR 2019/1009) sets common safety, quality and labelling requirements for fertilising products to shift dependency away from imported mineral fertilisers and expand EU market access to organic and recycled fertilisers (Green Horizon Farmers Network, 2019). The regulation covers seven component material categories (CMCs) but does not currently include sewage sludge or sludge derived products (EU Commission, 2019/1009). Thus,

SS and its derived products cannot be commercialised at EU level and can only be marketed under specific national or regional frameworks.

The FPR has introduced some organic contaminant limit values for the first time, namely for PAHs, providing a useful blueprint for how sludge-derived products could safely circulate the European market in future. The anticipated revision of the SSD and potential inclusion of SS-derived products within the FPR framework represent an opportunity to establish a coherent, risk-based regulatory approach that supports both environmental protection and nutrient circularity.

The regulatory gaps outlined above highlight the need for comprehensive, systematic characterisation of SS and its treatment derivatives across OM, nutrient and contaminant profiles. A deeper understanding of how different treatment processes transform OM and nutrients is essential for technology development, ensuring agronomic value, guaranteeing safety from pollutants and minimising environmental impact.

While there is growing research interest in optimizing innovative sludge treatment strategies such as hydrothermal carbonization (HTC) and pyrolysis, what is lacking is a data-driven comparative framework for evaluating treatments and sludge-derived products against consistent quality and safety benchmarks, as well as long-term studies on the effect on soil after agricultural application. The following section lists some of the existing and more innovative sludge treatment technologies and reviews their agronomic performance.

1.4 Sludge Treatment Processes

Fresh sludge is liquid, containing primarily water. It is usually thickened and dewatered on site or nearby (up to 20-35% DS) so that it can be processed and transported more easily (EurEau, 2021). Due to the presence of pathogens and other contaminants, sludge must be properly treated before use, to minimise its environmental and social impacts (Fan et al., 2022).

Sludge treatment processes can be broadly classified into three categories according to their mode of action (Pradel, 2019): biological processes, which stabilise OM and reduce pathogen load through microbial activity, as in anaerobic digestion and composting; physical processes, which reduce water content through thickening, dewatering and drying; and thermochemical processes, which transform OM structure and fix carbon into stable solid matrices, as in pyrolysis and hydrothermal carbonisation (HTC).

While physical and biological treatments are well-established, some innovative thermochemical approaches remain at an earlier stage of adoption, with wider deployment limited by techno-economic constraints (Durak, 2023).

1.4.1 Biological

1.4.1.1 Anaerobic Digestion (AD)

Anaerobic Digestion (AD) is a biological treatment comprising four sequential phases: hydrolysis, acidogenesis, acetogenesis, and methanogenesis. Sewage sludge, containing complex carbohydrates, proteins and fats, first undergoes hydrolysis, breaking down complex organic compounds through enzymatic reactions into soluble monomers. These are fermented during acidogenesis into volatile fatty acids (VFAs), which acetogenesis subsequently converts into acetic acid, hydrogen and carbon dioxide. Finally, methanogenesis transforms these substrates into biogas, a gas phase mostly composed of methane (CH_4) and carbon dioxide (CO_2) (Gizaw et al., 2024).

AD yields two main products. Biogas can be used for heat and electricity generation, offsetting operational energy costs and reducing CO_2 emissions associated with wastewater treatment (Gizaw et al., 2024). Digestate - the residue remaining after digestion - retains partially stabilised OM and a nutrient-rich composition, typically meeting minimum requirements for use as an organic soil amendment. The valorisation potential of each product is linked to the biodegradability of the input OM: higher biodegradability favours methane yields, while lower biodegradability is associated with greater soil amendment value, as more stable OM persists following land application (Fernández-Domínguez et al., 2022; Jimenez et al., 2017).

AD has been shown to effectively recover P and N as plant-available nutrients from digestate. It can provide OM and nutrients converted into mineral forms more readily available for plant uptake when applied to soil as fertilizer (Jimenez et al., 2020) However, mineral N can be temporarily immobilized by microbial biomass during OM biodegradation in soil (Lashermes et al., 2009). The partially stabilised OM fraction that persists following digestion can contribute to long-term soil organic carbon and support soil structure through water retention and increased microbial activity, adding further agronomic value beyond nutrient supply (Balkrishna et al., 2025; Lucia et al., 2025a). Better knowledge of OM and nutrient availability would improve the fertilizing potential of sludge-derived products (Jimenez et al., 2020).

1.4.1.2 Composting

Composting is a widespread biological process used to stabilise solid organic waste. Under aerobic conditions aeration promotes the hydrolysis of complex organic substances into simpler compounds through the production of hydrolytic enzymes and increased microbial activity, transforming raw waste into a stabilised product suitable for use as an organic fertiliser. Its performance is governed by a range of factors including feedstock composition, C/N ratio, moisture content, pH, aeration intensity and oxygen consumption rate. The process proceeds through three successive temperature-driven phases. First, an initial mesophilic stage in which

microorganisms break down labile organic compounds - including simple sugars, proteins and lipids – releasing energy and causing a rise in temperature. This is followed by a thermophilic stage characterised by peak temperatures (60-65 °C), at which most pathogens are eliminated and more complex organic structures begin to break down. Finally, there is a maturation phase during which temperatures gradually decline, mesophilic populations reestablish and recalcitrant compounds undergo humification, yielding a biologically stable product with stable organic matter and retained nutrients (Amir et al., 2004; Lucia et al., 2025; Salva et al., 2025; Zhao et al., 2016)

1.4.2 Physical

Fresh sludge is subjected to a series of physical treatment steps to progressively reduce its water content, facilitating further processing, transport and disposal (EurEau, 2021).

1.4.2.1 Thickening

One of the first steps in sludge treatment is thickening, which increases the total solids (TS) content from approximately 1-3% in fresh sludge to around 2–8% TS (Romero-Güiza et al., 2022). This is achieved through gravitational settling or mechanical processes such as lamellar settling, in which inclined plates increase the effective settling surface area and accelerate solids separation (Tarpagkou & Pantokratoras, 2014).

1.4.2.2 Dewatering

Thickened or digested sludge is subsequently de-watered to typically 15-30% TS (Romero-Güiza et al., 2022), producing a semi-solid product that is significantly easier and cheaper to handle, store and transport. Common mechanical dewatering technologies include centrifugation, which separates solid and liquid phases through centrifugal force and press filtration, by applying hydraulic or pneumatic pressure to compress the sludge and expel water, yielding a filter cake with high solids content (Zhang et al., 2022).

1.4.2.3 Drying

Drying further reduces water content beyond what mechanical dewatering can achieve. A general distinction is made between partial drying (less than 85% dry solids) and full drying (greater than 85% dry solids); as water content decreases, calorific value increases, which is particularly relevant when sludge is destined for thermochemical conversion processes such as pyrolysis or incineration (Schnell et al., 2020). Drying processes can be classified by their mode of heat transfer into contact, convection, radiation and mixed forms. Contact dryers - such as disc and thin-film dryers - transfer heat to the sludge via a heated surface using steam, hot water or thermal oil, without direct contact between the sludge and the heat transfer medium. Convection dryers, such as drum and belt dryers, bring sludge into direct contact with a hot gas stream such

as flue gas or steam. Some systems, including fluidized bed dryers, combine both principles (Schnell et al., 2020). On an industrial scale, solar drying is widely used, particularly for smaller wastewater treatment plants where throughputs are comparatively low. The process involves spreading sludge over large surface areas within glasshouses, where it is dried by solar radiation and ambient air ventilation; due to the low temperatures and large air volumes involved, vapour condensation and treatment are generally not required. Thermal drying, by contrast, applies direct or indirect heat, usually at a temperature of 105 °C for sludge treatment, though some driers operate at higher ranges of 300-800 °C, depending on the technology (Schnell et al., 2020; Voulvoulis & Lester, 2006).

While physical processes do not substantially alter the bulk chemical composition of OM or nutrients, drying can induce notable changes. Thermal drying at 85 °C has been shown to weaken sludge OM structure, increasing lipid, humic acid and fulvic acid fractions while reducing the insoluble OM fraction. Solar drying, by contrast, promotes progressive humification through microbial activity, resulting in increased humic-like substances and reduced lipid content over time - a transformation that may favour the production of stable soil amendments suited to long-term OM input, while thermally dried sludge is better suited for use as a fertilizer (Collard et al., 2017). Drying can also cause volatilisation of certain nitrogen compounds, particularly ammonia, which potentially reduces the nutrient content of the dried product relative to the input material (Horttanainen et al., 2017).

1.4.3 Thermochemical

1.4.3.1 Pyrolysis

Pyrolysis is a thermochemical process in which OM is decomposed at elevated temperatures (typically around 350−600◦C) under oxygen-limited (or inert) conditions and atmospheric to slightly elevated pressure, producing three co-products: a solid carbonaceous residue (biochar), a liquid fraction (bio-oil), and a syngas, composed of CO, CO_2, CH_4 and H_2 (Gizaw et al., 2024; Racek et al., 2020).

Process conditions, particularly temperature and residence time, govern the relative yield of these fractions: slow pyrolysis (350–450°C, residence time of minutes to hours) favours biochar production, while fast pyrolysis (400–600°C, residence time of seconds) shifts yield toward bio-oil and syngas. As temperature increases, biochar yield decreases as carbon is increasingly partitioned to gaseous and liquid fractions, while ash content rises.

Applied to SS, pyrolysis offers significant advantages including volume reduction, pathogen destruction, and immobilisation of HMs within the biochar matrix (Ahmad et al., 2014). At higher

pyrolysis temperatures, the progressive thermal decomposition of hemicellulose (220–315°C), cellulose (315–400°C) and lignin (160–900°C) releases volatile gases, further reducing the oxygen and hydrogen content of the biochar and eliminating polar functional groups. This enhances biochar stability, reflected in decreasing hydrogen-to-organic carbon (H/C) and oxygen-to-organic carbon (O/C) ratios with increasing temperature. However, the loss of functional groups simultaneously reduces cation exchange capacity (CEC), with implications for nutrient retention following soil application (Pokharel et al., 2025). The conditions for biochar production inhibit complete combustion of the biomass and preserve part of the carbon it contains as a recalcitrant carbon pool, making biochar very useful as a soil amendment and tool to mitigate climate change (Bona et al., 2023). Despite its proven agronomic potential, biochar derived from SS is not currently permitted as an EU fertilising product under Regulation 2019/1009, limiting its use to national frameworks and constraining wider adoption of pyrolysis as a sludge valorisation route (EU Commission, 2019).

1.4.3.2 Hydrothermal carbonisation (HTC)

Hydrothermal carbonisation (HTC) has emerged as a promising thermochemical process for SS treatment, offering a key advantage over conventional dry thermal processes by eliminating the need for energy-intensive drying of wet feedstock (Tasca et al., 2019). The process operates under subcritical water conditions at temperatures between 180 and 280°C and autogenous pressure. The organic fraction of SS is converted through hydrolysis, dehydration, decarboxylation and condensation reactions into a coal-like solid product known as hydrochar, a nutrient-rich liquid phase, and a minor gaseous fraction composed primarily of CO_2 along with small amounts of CO, CH_4 and other light hydrocarbons (IEA, 2021; Tasca et al., 2019).

Reaction temperature is the governing parameter controlling hydrochar properties: increasing process severity reduces atomic H/C and O/C ratios and enhances fixed carbon content, reflecting progressive aromatisation of the OM structure (Tasca et al., 2019). This transformation involves the conversion of labile, oxygen-rich functional groups (O-alkyl C associated with carbohydrates and carboxylic C) into more hydrophobic, alkyl-rich and aromatic structures, as confirmed by ^{13}C NMR and FTIR analyses (Bona et al., 2023; Zhang et al., 2014) Simultaneously, labile organic fractions are solubilised and partitioned into the process water, while more recalcitrant compounds are retained and stabilised within the hydrochar matrix.

Despite this structural transformation, hydrochar retains a substantial content of dissolved organic matter (DOM), characterised by low-molecular-weight compounds (organic acids, furans, phenols and their derivatives) generated during hydrolysis and partial condensation reactions (Bona et al., 2023; Tasca et al., 2019). Thermal characterisation confirms that hydrochar contains a higher proportion of thermally labile compounds compared to mature compost, indicating greater

susceptibility to microbial decomposition in soil (Bona et al., 2023). This has direct agronomic consequences: the capacity of raw hydrochar to contribute to long-term SOC stabilisation is constrained by its relatively high H/C ratios, typically well above the threshold of 0.6 recommended for recalcitrant soil amendments, making it more analogous to a labile organic input than a stable carbon sink (Tasca et al., 2019). Hydrochar is nonetheless proposed as a carbon-rich product capable of maintaining or enhancing soil organic carbon stocks, provided that biological stability is adequately addressed prior to land application (Bona et al., 2023). Aerobic co-composting with mature compost has been shown to reduce DOM content and phytotoxicity while improving plant growth response, suggesting that post-treatment is a necessary step before agronomic deployment (Bona et al., 2023).

Additionally, HTC presents opportunities for nutrient recovery. Phosphorus is largely retained within the hydrochar solid fraction following processing, though its bioavailability is highly dependent on process conditions and the speciation of metals present (Tasca et al., 2019; Zhang et al., 2014). Nitrogen concentration in the solid fraction is reduced, as proteins contained in SS are degraded above 150 °C. This is reflected by the increase of ammonium-N in the liquid phase produced after HTC treatment (Tasca et al., 2019). As well as this increase in total N, the TOC value usually increases due to the decomposition of organic compounds in the aqueous phase (Zhang et al., 2014). This high organic content left in process water offers an attractive potential and can be used in either gasification or cultivation medium for biomass or to recover nutrients (Tasca et al., 2019; Tekin et al., 2014). Conversely, the accumulation of HMs and residual organic contaminants, including pharmaceuticals and potentially phytotoxic compounds in the hydrochar, needs a thorough risk assessment before land application (Bona et al., 2023; Tasca et al., 2019; Wang et al., 2018).

SS and SS derived products hold considerable potential as a source of recoverable resources including OM, nitrogen, and phosphorus for fertilizer applications, mineral constituents for use as adsorbents in environmental remediation, and feedstocks for energy recovery. Achieving this potential, however, requires detailed knowledge of the agronomical fate of OM and nutrients, a prerequisite for optimising treatment processes and positioning SS-derived products as viable, sustainable alternatives to conventional fossil-based fertilizers and soil amendments.

1.5 Sewage Sludge – Advantages

1.5.1 The Effect of Sludge Application on Soil

Sewage sludge represents a significant source of OM and essential plant nutrients with considerable potential as a soil amendment and fertilizer substitute. Mineral fertilisers have

dramatically increased soil fertility and food production since the latter half of the 20th century, yet their manufacture relies on finite geological deposits in the case of phosphorus and potassium, and energy-intensive processes for nitrogen fixation. Sewage sludge offers an opportunity to recycle these nutrients back to agricultural land, reducing dependency on synthetic inputs. Depending on origin and treatment process, SS contains 2.80–8.06% nitrogen and 0.1–14% phosphorus per tonne of dry solids (Liu et al., 2026), representing valuable nutrients that can contribute meaningfully to sustainable agricultural practice.

Sewage sludge contains a range of essential macro- and micronutrients that contribute to soil fertility and plant growth. Nitrogen, phosphorus and potassium are the primary macronutrients of agronomic relevance, with SS also providing micronutrients including iron, zinc, copper and manganese. Despite lying within the contaminants category, elements Zn and Cu are important for chlorophyll synthesis and plant vitality and contribute to biofortification (Bolan et al., 2021; McGrath et al., 1995). However, nutrient concentrations in SS are generally lower than in conventional mineral fertilisers. Additionally, the slow-release nature of nitrogen, which is a consequence of its predominantly organic form, means nutrient availability is gradual rather than immediate. While this can reduce leaching risks compared to synthetic fertilisers, it may require higher application rates, supplementary inputs or appropriately timed application (e.g., autumn application to align nutrient release with crop demand the following spring) to meet crop needs. The OM fraction of SS can further enhance nutrient availability indirectly, through improved CEC and the gradual mineralisation of bound nutrient forms, releasing plant-available phosphorus and nitrogen progressively throughout the growing season (Balkrishna et al., 2025; Lucia et al., 2025)

Beyond nutrient supply, OM in SS plays a significant role in improving soil health. Nearly 50% of the solid fraction of SS is OM, which significantly affects the physical, chemical and biological characteristics of the soil when applied, by increasing porosity, improving water retention and circulation, and promoting aggregate stability and microbial balance (Lucia et al., 2025). Ippolito et al. (2021) found that increasing sludge application rates significantly elevated soil organic carbon, potentially mineralizable nitrogen and extractable phosphorus compared to mineral fertiliser application alone, suggesting broader benefits for soil biogeochemical processes. However, the quantity of SS that can be applied is constrained by nutrient thresholds and heavy metal limits set by national regulations, a tension that underscores the need for precise characterisation of sludge-derived products.

In a two-year study that used secondary- and tertiary-treated sludge as an organic soil amendment on rainfed wheat, improvements in soil water content, CEC and available phosphorus were observed, with OM accumulation identified as the driving mechanism (Abou Jaoude et al., 2025). Similarly, SS applied at 10 g/kg soil in a controlled field experiment significantly improved

plant growth, biomass production and soil water holding capacity, with no toxic accumulation of HMs in plant tissues at this application rate (Eid et al., 2026).

In the 18-year SOERE-PRO field experiment, dehydrated sewage sludge (SLU) achieved the highest nitrogen fertiliser replacement value (this estimates the N contribution of organic waste) at 58%, among the organic wastes tested, second only to digestate (69%), and provided the largest mineral fertiliser savings (57.3 kg N, 23.1 kg P_2O_5, and 5.7 kg K_2O ha^{-1} yr^{-1}), attributed to its relatively high mineral N content. However, the same study found that SLU was the only organic waste tested that did not significantly increase soil organic carbon stocks relative to the control, attributed to its lower humification coefficient (i.e., greater biodegradability) compared with the other organic wastes. In contrast, the SLU-derived compost (GWS) showed a significantly higher SOC stock increase than SLU (+5.4 t C ha^{-1} over 18 years under N-, vs. no significant change for SLU), consistent with its higher humification coefficient (72% vs. 49% for SLU), although GWS achieved a lower nitrogen fertiliser replacement value of 30% (Chen et al., 2022).

The high OM content of SS provides an energy source for heterotrophic soil microorganisms, driving increases in microbial biomass carbon and nitrogen following application. Several studies have demonstrated significant increases in microbial biomass carbon, in some cases exceeding 90% compared to unamended controls, alongside enhanced enzymatic activities including dehydrogenase, phosphatase and urease, which are key indicators of soil biological activity and nutrient cycling (Lucia et al., 2025). These effects reflect a broader improvement in soil biodiversity and ecosystem functioning, supporting nutrient cycling and disease suppression. However, the magnitude and persistence of these effects depend on application rate, sludge quality and soil characteristics. The presence of HMs and organic contaminants in sludge can, in some cases, reduce microbial diversity, emphasizing the importance of sludge characterisation prior to land application (Lucia et al., 2025).

The agronomic properties of SS-derived products vary considerably depending on the treatment process applied, with thermochemical products such as biochar and hydrochar exhibiting significantly distinct characteristics from raw or biologically treated sludge.

1.5.2 The Effect of Biochar Application on Soil

The pyrolysis of SS produces biochar, whose agronomic and environmental properties differ substantially from those of the raw feedstock, with implications for both carbon soil dynamics and contaminant behaviour. The long-term persistence of biochar in soil has been demonstrated in a 15-year vineyard study, in which 22 t/ha of biochar was deployed and the soil monitored under conventional agricultural practices including tillage and fertilisation (Chiaramonti et al., 2024).

Although this study used lignocellulosic rather than SS-derived biochar, its findings are relevant to the broader question of biochar stability in agricultural soils. It was found that biochar remained in soil throughout this period: during this time, exogenous organic and inorganic matter was incorporated into the material, penetrating the biochar structure and diluting the carbon content of analysed particles. Critically, the inertinite fraction - the most thermodynamically stable form of organic carbon, used to assess potential degradation - remained unchanged over the 15 years, confirming the permanence of this fraction under real agricultural conditions. In terms of agronomic potential, increases in soil organic carbon following biochar amendment have also been reported at the same site under a different treatment regime, with TOC remaining significantly elevated relative to controls several years after application (Rombolà et al., 2015).

Turning to contaminant behaviour, the sorption capacity of SS-derived biochars towards PAHs - specifically phenanthrene and pyrene, among the most commonly found hydrophobic organic contaminants in contaminated sites, was investigated by Zielińska & Oleszczuk, 2015. It was found that pyrolysis of SS significantly improved sorption capacity towards these compounds, suggesting that SS-derived biochar may serve as both a soil amendment and a contaminant immobilisation agent. Trace metal behaviour following SS pyrolysis is more variable than that observed for PAHs. Khan et al. (2013) found that, although pyrolysis increased the total concentration of all measured metals in the resulting sewage sludge biochar, soil amendment decreased the bioavailable (EDTA-extractable) concentrations of As, Co, Cr, Ni and Pb relative to the unamended control, while bioavailable Cu, Zn and Cd increased (Ahmad et al., 2014).

1.5.3 The Effect of Hydrochar Application on Soil

Hydrochar derived from hydrothermal carbonisation of sewage sludge has demonstrated promising agronomic potential, particularly in terms of N dynamics. Application of SS-derived hydrochar has been shown to immobilise soil nitrogen and regulate its release, reducing leaching to groundwater while improving availability during crop growth (Tasca et al., 2019). At the agronomic level, bean dry matter yield following hydrochar amendment was found comparable to that achieved with mineral fertiliser application (Melo et al., 2018), while ryegrass production increased substantially relative to peat substrate (Álvarez et al., 2017). These results have been further supported by field-scale additions of 10 and 60 t/ha of hydrochar from stabilised SS, which increased dry biomass yield of bean and rice, respectively compared to unamended controls (Melo et al., 2019).

The potential of hydrochar derived from SS as a nitrogen fertiliser has been further demonstrated in net-house conditions (semi-controlled, shade-netted), where hydrochar application alone or

combined with urea improved soil fertility, plant growth and reduced N leaching; however, the combination with urea significantly increased N_2O emissions, highlighting a trade-off between agronomic performance and greenhouse gas release that requires careful consideration before large-scale adoption (Gebretsadkan et al., 2024).

In addition to nutrient dynamics, hydrochar production raises important questions regarding contaminant fate. HMs in SS are thermally stable under HTC and are not degraded; instead, they redistribute from exchangeable to more stable, oxidisable and residual fractions via complexation with OM and minerals, with solid-phase immobilisation increasing with reaction severity (Nahar et al., 2024). This produces an apparent concentration effect: total metal content rises relative to feedstock due to mass loss during carbonisation, while leachability and bioavailability decrease. However, some HMs may remain in the aqueous phase and efforts should be made to reduce HMs or immobilize them. Organic contaminants behave differently: PAHs and PCBs were substantially reduced under HTC at 180°C, with removal efficiencies above 48% for PAH and above 68% for PCBs in hydrochar derived from stabilised sludge and sludge cake (Alipour et al., 2022). However, despite this reduction, resulting PAH concentrations in hydrochar remained above the limit proposed in the STRUBIAS report for soil-applied char and gasification materials, whereas pyrolysis at 450°C brought concentrations below this threshold (Alipour et al., 2022), suggesting HTC alone may not be sufficient to meet regulatory thresholds for organic contaminants. Elevated contaminant concentrations in hydrochar should therefore not be read as increased risk without considering speciation, mobility and compound class.

1.6 Disadvantages and Public Concern

Despite the widely demonstrated agronomic value of SS, its agricultural application raises legitimate concerns due to the presence of potentially harmful substances whose behaviour and fate following soil application are not yet fully understood. Contaminants fall into two broad categories: inorganic contaminants, mainly heavy metals (HMs), and a growing and diverse suite of organic contaminants, including the polycyclic aromatic hydrocarbons (PAHs), polychlorinated biphenyls (PCBs), pharmaceuticals and personal care products (PPCPs), per- and polyfluoroalkyl substances (PFAS), microplastics (MPs), anti-microbial resistance genes (ARGs).

1.6.1 Inorganic Contaminants

HMs are the most historically documented concern associated with SS land application. Unlike organic contaminants, they are not biodegradable and accumulate persistently in topsoil following repeated applications, with long residence times. Low doses of SS do not cause a significant

increase in heavy metal concentrations, however, excessive application has been found to increase HM bioavailability, with negative consequences for soil health (Hudcová et al., 2019a).

While some HMs, like copper and zinc, are essential micronutrients at low concentrations, at elevated levels they can become phytotoxic and impair the proper functioning of soil organisms and biological processes (Michaud et al., 2026). Cd, Pb and arsenic (As) are of particular concern given their toxicity even at very low concentrations (Kominko et al., 2024).

The behaviour of HMs in SS-amended soils is influenced by soil pH, cation exchange capacity, OM content and the specific form of each metal (Hudcová et al., 2019a). Among these factors, pH plays a particularly significant role: acidic conditions increase the solubility of metals such as Cd and Zn, enhancing their mobility and plant uptake, while alkaline pH reduces solubility through precipitation and adsorption (Lucia et al., 2025a). Heavier soils, with near neutral pH and high OM content, can further reduce metal bioavailability through binding of metals to OM, reducing their toxic effects on soil organisms (McGrath et al., 1995).

It is not only the total concentration but also the speciation, that is, the chemical form in which a metal is present, that determines its mobility, bioavailability, and ecotoxicity. Feng et al. (2023) reported that over 70% of Zn and Ni in SS were present in exchangeable or acid-soluble fractions, posing greater environmental risk compared to more stable forms bound to OM or mineral phases (Feng et al., 2023). In contrast, Pb and chromium (Cr) tend to occur in less mobile forms, while Cd remains more available, particularly in acidic soils. These findings suggest that amendments capable of raising soil pH, such as biochar, can effectively immobilize labile metal fractions and reduce their potential toxicity in agricultural applications (Michaud et al., 2026).

This distinction between total content and bioavailable fraction is reflected in long-term field data: an 18-year study within the SOERE PRO network found that repeated SS-derived organic waste application increased soil HM availability over time, correlating with cumulative HM input, particularly for Cu and Zn. However, total HM concentrations remained below conservation thresholds throughout, with no detectable transfer to crop grains (Chen, 2023).

As mentioned above, HM content in SS is currently regulated under the EU Directive 86/278/EEC, which sets maximum limits for a set of HMs (Cd, Cu, Hg, Ni, Pb and Zn) in both sludge and receiving soils. Given that the SOERE PRO findings suggest total concentrations can remain within regulatory thresholds even as bioavailable fractions increase, an open question is whether total-content-based regulation is sufficient to manage the long-term bioavailability risks discussed above, or whether speciation-based criteria would offer better protection from HM toxicity.

1.6.2 Organic and Emerging contaminants

A second, more recently recognised category of concern includes:

i. several categories of organic contaminants — including Polycyclic Aromatic Hydrocarbons (PAHs), Polychlorinated Biphenyls (PCBs), and other families such as Nonylphenols (NPs), Linear Alkylbenzene Sulfonate (LAS);
ii. emerging contaminants — substances not yet adequately addressed by existing EU regulation, i.e. pharmaceuticals and Personal Care Products (PPCPs), per- and polyfluoroalkyl substances (PFAS), microplastics (MPs) and Antimicrobial Resistance Genes (ARGs).

The fate and impact of these organic contaminants following sludge land application are strongly governed by their physicochemical properties, particularly hydrophobicity and sorption affinity as well as soil characteristics such as pH and organic carbon content. While hydrophobic compounds tend to accumulate in the solid phase and persist over long timescales, more mobile compounds may leach to groundwater or can be taken up by plants, with degradation, accumulation, and transfer rates varying across compound classes.

PAHs are by-products of incomplete combustion of OM. Some natural phenomena like wildfires or eruptions can also exacerbate their spread in the environment. They are hydrophobic in nature, exhibit high sorption coefficient (K_D) values and therefore easily adsorb to solid particles of SS during biological treatment, resulting unavailable for degradation and difficult to eliminate (Annori et al., 2022).

PCBs are a class of ubiquitous chemical compounds originating from a range of industrial materials. These molecules can be introduced into the environment from combustion processes like waste incineration and are by-products from a variety of chemical processes. PCBs, in particular dioxin-like and indicator congeners are of great environmental concern because of their high persistence, lipophilic properties, bioaccumulation, and toxicity to the ecosystem and to humans (Guo et al., 2009).

PPCPs enter wastewater through human excretion and can accumulate in sludge during treatment. Most pharmaceuticals exhibit low sorption coefficient (K_D) values and therefore have a greater affinity for the water phase (Ternes et al., 2004). However, they can be removed from wastewater through processes including adsorption to sludge and microbial and abiotic degradation. Removal rates of nonsteroidal anti-inflammatory drugs (e.g., ibuprofen and diclofenac) in WWTPs exceed 75%, whereas carbamazepine is recalcitrant to biological treatments. Mean removal rates of fluoroquinolones approach 70% due to strong sorption to sludge rather than biodegradation. Primary risks are from antibiotics which can contribute to antimicrobial resistance and the

distribution of all types of PPCPs (i.e., antibiotics, antidepressants, and endocrine disruptors, amongst others) into the environment. This has ecotoxicological impacts on soil organisms — earthworms, plant seeds, and microorganisms (Bourdat-Deschamps et al., 2017).

PFAS are emerging contaminants of growing concern, comprising a large and diverse group of highly persistent synthetic compounds characterised by strong carbon-fluorine bonds, rendering them resistant to biological and chemical degradation (Arvaniti et al., 2024; Bolan et al., 2021). PFAS can be distinguished into short-chain and long-chain compounds according to carbon chain length, a distinction with important implications for their environmental fate: short-chain PFAS tend to remain in the aqueous phase and are more mobile, while long-chain PFAS exhibit greater hydrophobicity and partition preferentially onto sludge solids through sorption mechanisms (Arvaniti et al., 2024; C. Zhang et al., 2013). Sewage sludge, therefore, acts as a significant sink for long-chain PFAS, with concentrations in sludge matrices reported up to 8.2 µg/g dry weight across 182 detected substances worldwide (Arvaniti et al., 2024). Their high persistence, combined with demonstrated toxicity to soil organisms, plants and human health through dietary and inhalation exposure routes, makes PFAS a contaminant of particular concern in the context of sludge land application. Examples from the French context illustrate this concern across multiple environmental compartments. Munoz et al. (2022) characterised 160 PFAS across 42 classes in 47 organic waste products (OWP) applied in French agricultural fields, including SS, composts, and manures, and found that urban-sourced OWP contained PFAS at concentrations several orders of magnitude higher than livestock-derived materials (median PFAS: 265 vs. 0.63 µg/kg dry matter). Sludge samples were dominated by PFOS (perfluorooctane sulfonate) and its electrochemical fluorination-derived precursors, while contemporary samples showed a shift towards zwitterionic fluorotelomers, reflecting broader regulatory and industrial transitions (Munoz et al., 2022). Field-scale work by Michaud et al. (2025) demonstrated that repeated sludge application over decades led to significant PFAS accumulation in topsoils (up to ~21 µg/kg), with leaching waters at 45 cm depth containing short-chain perfluoroalkyl carboxylic acids at concentrations exceeding EU drinking water guidelines, indicating a long-term groundwater contamination risk (Michaud et al., 2025). Saliu et al. (2025) showed that despite elevated soil PFAS burdens, concentrations in harvested grains remained low (generally below 2.5 µg/kg), with PFBA dominating plant uptake due to its low soil-water partitioning coefficient and high mobility. Notably, a significant negative correlation was observed between soil organic carbon and plant bioaccumulation. PFAS adsorb to soil OM through hydrophobic and electrostatic interactions, reducing their mobility and bioavailability for root uptake (Saliu et al., 2025). Nevertheless, PFAS transfer to soil and groundwater remains a concern where OWP originate from wastewater treatment plants receiving industrial or municipal effluents, underscoring the importance of monitoring PFAS levels in OWP prior to land application.

With the increased production of plastics from fossil fuels and the growing use of bioplastics, the presence of microplastics in the environment is of growing concern, particularly the accumulation in wastewater streams (Landeros Gonzalez et al., 2022). A 23-year field trial by Adhikari et al., 2024 reported over 90 % of microplastics to be removed from the wastewater effluent and accumulated in sewage sludge. This SS is then applied to land where microplastics will accumulate in soil. It was demonstrated that repeated biosolids applications resulted in microplastic concentrations significantly higher than unamended control soils, with polyurethane, polyethylene and polyamide being the dominant polymer types detected (Adhikari et al., 2024). Atmospheric deposition was also identified as a significant independent source of microplastic input, complicating the attribution of soil contamination to sludge application alone. Evidence from the French SOERE PRO long-term field network similarly demonstrates that repeated application of urban waste composts leads to substantial microplastic accumulation in agricultural soils, with coarse microplastic concentrations ranging from 26.9 to 417 kg per hectare after 22 years of biannual application depending on compost type (Colombini et al., 2022). Composts derived from unsorted municipal solid waste produced the highest accumulation, while those from more selectively sorted biowastes introduced significantly lower microplastic loads, underscoring the importance of upstream waste sorting in limiting soil contamination. The long-term ecological consequences of the accumulation of MPs in soils remain poorly characterised and understood, as well as the combined effects with additional contaminants.

With the consumption of antibiotics as therapeutic agents, there is a transfer of multiple antibiotic resistance genes (ARGs) into bacteria, which have evolved and spread to produce antimicrobial resistance (AMR). Large amounts of antibiotic residues and ARGs then end up in wastewater. WWTPs receive wastewater from residential areas, hospitals, livestock, aquaculture and pharmaceutical plants. The high microbial density, growth and nutrient content of the wastewater provides the essential environment for the proliferation of AMRs. The antibiotics do not biodegrade fully and adsorb to the surface of sludge particles (Yin et al., 2024).

Taken together, these concerns have fuelled significant public scepticism toward SS land application, often amplified by high-profile contamination incidents and media coverage that does not always distinguish between raw sludge and treated products, or between contaminant presence and demonstrated impact or risk.

2 Aims and Objectives

Addressing these knowledge and regulatory gaps requires moving beyond threshold-based contamination limits. Instead, more comprehensive characterisation strategies are needed - ones that better capture parameters related to the quality and the fate of OM and nutrients. This approach is not limited to the simple measure of total concentrations and is essential for evaluating both the agronomic potential and environmental safety of sludge-derived products.

By applying a biochemical fractionation methodology able to characterise OM accessibility and complexity, this work aims to advance understanding of OM fate across sludge and sludge-derived products from both conventional and more innovative treatment processes, providing the data needed to observe, evaluate and ultimately optimise sludge treatment and valorisation strategies.

In terms of agronomic efficiency, biochemical fractionation of OM (accessibility and complexity) will be carried out according to the ISBAMO® methodology (Indice Stabilité et Bioaccessibilité MO, Jimenez et al., 2014, 2015, 2017, 2020). This characterization is performed on a collection of different sludge products coming from different processes, namely: anaerobic digestion, thermal hydrolysis, thermal treatment, pyrolysis, hydrothermal carbonization and physical and mechanical treatment such as gravitational thickening and centrifugation.

2.1 Specific Objectives

- Analyse physicochemical characteristics of different sludge products: raw sludge, digested sludge, dehydrated sludge, thickened sludge, thermally treated sludge, sludge cake, hydrochar, biochar;
- Perform biochemical fractionation and 3D fluorescence analyses on the same set of samples;
- Apply multivariate statistical methods, namely principal component analysis (PCA) and hierarchical clustering analysis (HCA) to find correlations between variables, simplify the dataset of collected data, and support interpretation of results.

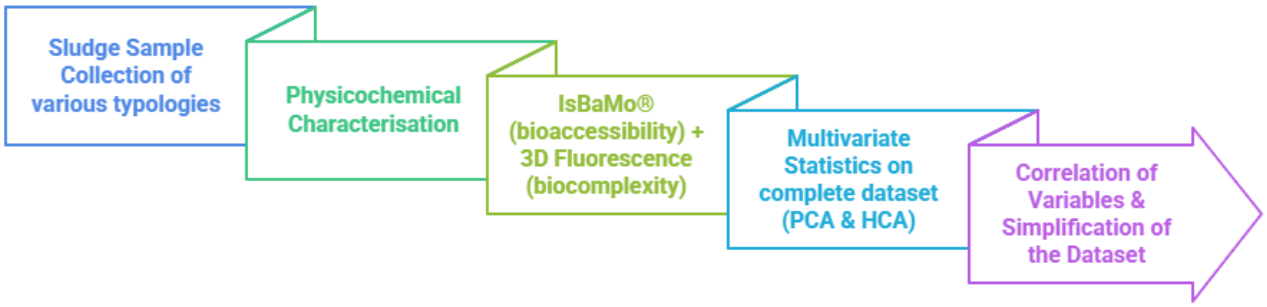

Figure 3: Overview of the methodological workflow: sludge samples undergo physicochemical characterisation, ISBAMO fractionation and 3D fluorescence spectroscopy, and multivariate statistical analysis is performed on the resulting dataset.

3 Materials and Methods

3.1 Sample set

For this study, 29 sludge samples were analysed. The samples covered a range of typologies from several wastewater treatment plants (WWTP): 4 raw sludge, 4 anaerobically digested sludge, 4 thickened sludge and 4 sludge cake all from WWTP1, 4 hydrochar from 4 different hydrothermal carbonization (HTC) pilot-scale plants, 2 dehydrated sludge from WWTP2 and WWTP3, the input and output of a thermal hydrolysis treatment at WWTP2, the input and output of AD process in WWTP2, 2 solid fractions after centrifugation collected at WWTP2, and 1 biochar sample collected at a lab scale pyrolysis system. Raw sludge, digested sludge and thickened sludge samples were in the liquid phase, while sludge cake, hydrochar and solid fractions collected after centrifugal treatment were in the solid phase. Nomenclature was created according to Table 1.

Table 1: Nomenclature of sample names, sample descriptions, treatment processes applied and different sample sources; either wastewater treatment plants or hydrothermal carbonisation pilot-scale plants.

SHORT CODE	SAMPLE NAME	SAMPLE DESCRIPTION	TREATMENT PROCESS	SOURCE
R1	RS_080725	raw sludge	aerobic	WWTP 1
R2	RS_160725	raw sludge	aerobic	WWTP 1
R3	RS_220725	raw sludge	aerobic	WWTP 1
R4	RS_280125	raw sludge	aerobic	WWTP 1
D1	DS_040325	digested sludge	anaerobic digestion	WWTP 1
D2	DS_290725	digested sludge	anaerobic digestion	WWTP 1
D3	DS_050825	digested sludge	anaerobic digestion	WWTP 1
D4	DS_120825	digested sludge	anaerobic digestion	WWTP 1
T1	TS_280125	thickened sludge	thickening	WWTP 1
T2	TS_080725	thickened sludge	thickening	WWTP 1
T3	TS_160725	thickened sludge	thickening	WWTP 1
T4	TS_220725	thickened sludge	thickening	WWTP 1
SC1	SC_080725	sludge cake (after AD + thermally treated + filter press)	anaerobic digestion/thermal conditioning	WWTP 1
SC2	SC_160725	sludge cake (after AD + thermally treated + filter press)	anaerobic digestion/thermal conditioning	WWTP 1
SC3	SC_220725	sludge cake (after AD + thermally treated + filter press)	anaerobic digestion/thermal conditioning	WWTP 1
SC4	SC_280125	sludge cake (after AD + thermally treated + filter press)	anaerobic digestion/thermal conditioning	WWTP 1
H1	H_ES	hydrochar	hydrothermal carbonisation	HTC 1
H2	H_ES.d	hydrochar from digested sludge	hydrothermal carbonisation	HTC 1
H3	H_SE	hydrochar	hydrothermal carbonisation	HTC 2
DH	DeH_F	dehydrated sludge (output of rotating filter press -hydrochar input)	dehydration	HTC 3
H4	H_F	hydrochar (output of incinerator - hydrochar output)	hydrothermal carbonisation	HTC 3
HIN	HT_IN	thermally treatment input (before AD)	aerobic	WWTP 2
HOUT	HT_OUT	thermally treatment output (before AD)	hydrothermal treatment	WWTP2
AIN	AD_IN	primary sludge + thermally treated sludge - AD input	thermal treatment	WWTP 2
AOUT	AD_OUT	primary sludge + thermally treated sludge - AD output	anaerobic digestion	WWTP 2
cAD	Centri_AD	solid fraction before AD (inlet to AD) -primary	dehydration	WWTP 2
cINC	Centri_INC	solid fraction before incineration (inlet to incinerator) - primary	dehydration	WWTP 2
DH2	DH_2	dehydrated sludge (output of rotating filter press)	dehydration	WWTP 3
B4	Biochar 4	Biochar	pyrolysis	Biochar plant

The samples from WWTP1 were part of the same treatment process chain, which is outlined in Figure 4 (a). In this work, the results of bioaccessibility, complexity and fluorescence distribution are analysed for these typologies from WWTP1 and for hydrochar samples. Figure 4 (b) presents additional typologies according to treatment category (mechanical, thermochemical and

biological). The data for these typologies, as well as typologies from WWTP1, are included in the database used to conduct the statistical analysis.

Temperatures of thermal conditioning used in the treatment of sludge cake (Figure 4 (a)) were 195 °C and temperatures for hydrochar processing (Figure 4 (b)) ranged from 200-210 °C.

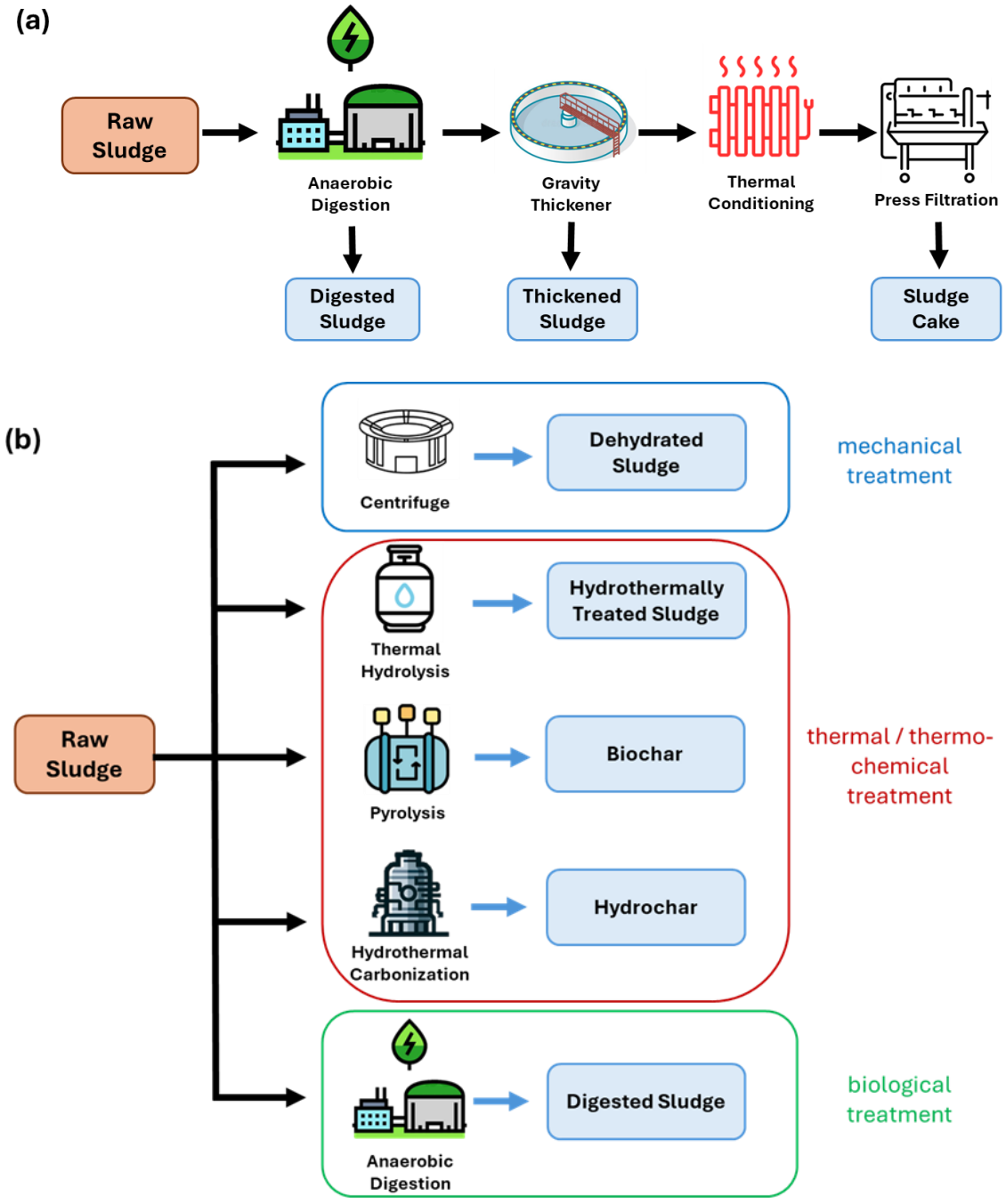

Figure 4: Process diagram for sludge treatments and corresponding sludge products: (a) shows treatment chain for typologies for WWTP1 samples and (b) shows typologies for the additional samples included in the principal component analysis, presented according to treatment category.

3.1.1 Sample Preparation

Figure 5 represents an overview of sample preparation and analyses conducted during this project for (a) liquid samples and for (b) solid samples. This shows all analyses performed for each sample type, although it should be noted that not all analyses were conducted for every sample.

Sample pretreatment and several physicochemical measurements (phase separation for liquid samples, TS, VS, pH, EC (Electrical Conductivity) and elemental analysis (CHNS)) were completed prior to the author's work.

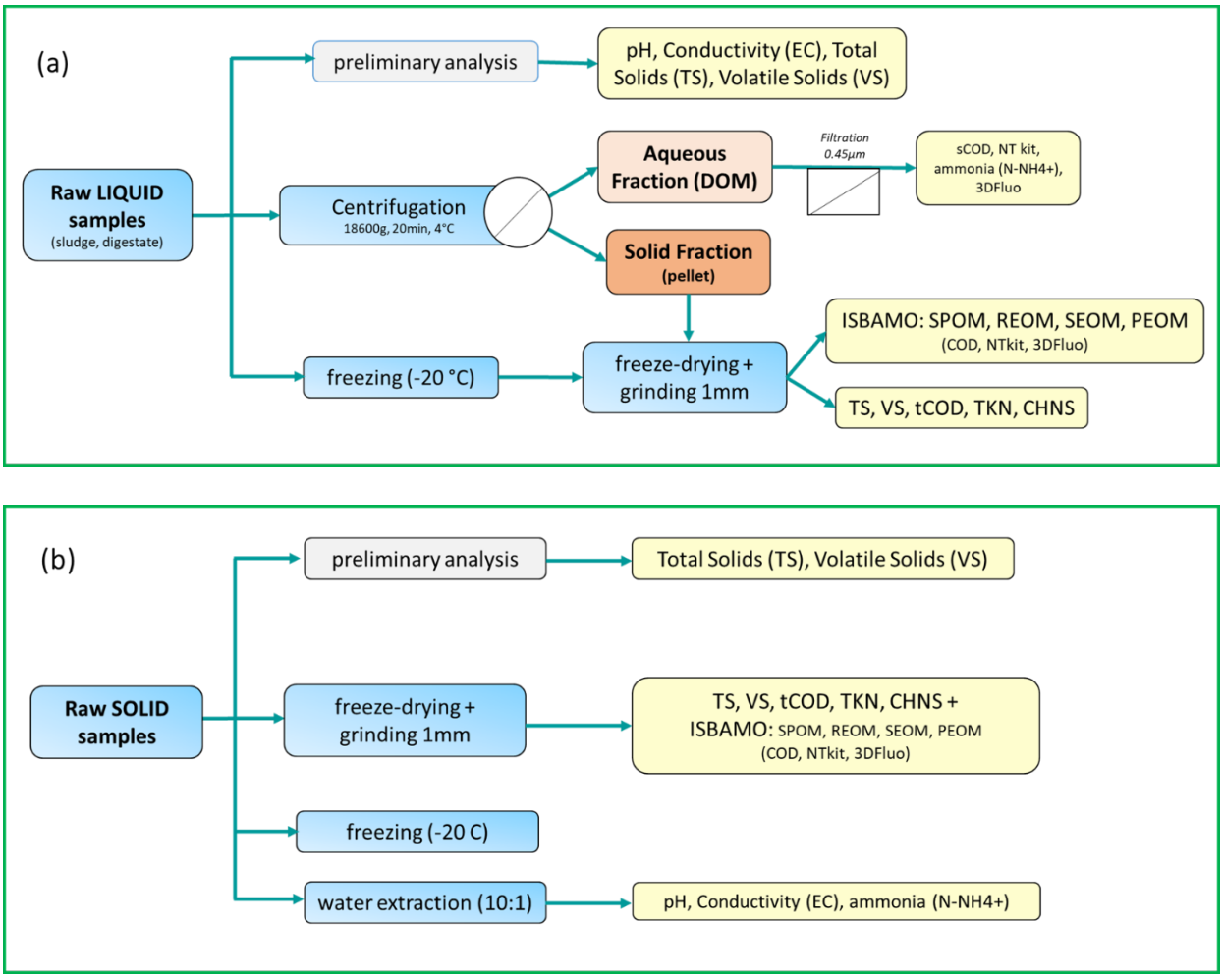

Figure 5: Flow diagram of sample preparation and analytical procedures for (a) liquid samples and (b) solid samples. Key pre-treatment steps include centrifugation and 0.45 µm filtration for DOM isolation (a) and freeze-drying and grinding to 1 mm prior to ISBAMO sequential extraction (a, b). Analyses performed on resulting fractions include COD, NTkit, TKN, CHNS, and 3D fluorescence spectroscopy.

3.1.2 Sample Pretreatment

Phase separation using centrifugation was complete so that analysis could be done on both the liquid and solid fractions of the sample. A Beckman Coulter Avanti J-26 XP centrifuge was used to separate the samples into a solid fraction and a liquid fraction. The centrifuge was set at 18,600

g for 20 minutes at 4 °C. The centrifugation ratio is calculated by dividing the total mass of the solid fraction by the total mass of the samples centrifuged.

The liquid fraction, representing the DOM (Dissolved Organic Matter), was recovered after centrifugation, filtered at 0.45 µm (with glass fiber cellulose acetate, Sartorius) and frozen at -20 °C for further analyses.

The solid fraction was frozen at -20 °C and freeze-dried using a Cryotec Cosmos 20k freeze-drier. Freeze-drying is a process that eliminates all water from a sample by sublimation, without altering its fundamental properties. After freeze-drying, a knife mill (IKA MF 10 basic) was used to grind the freeze-dried samples into a powder of < 1 mm diameter.

For solid samples, no centrifugation was needed and after preliminary characterization, they were directly frozen at -20°C to be subsequently freeze-dried and used for further analysis.

3.2 Physicochemical characterization

3.2.1 Total Solids (TS) and Volatile Solids (VS)

The concentration of Total Solids (TS) and Volatile Solids (VS) was determined by weighing and drying. TS represent all dry solids contained in a sample, including organic and inorganic solids. TS were analysed by gravimetry after 24 h at 105 °C, while VS were analysed by gravimetry after 2 h at 550 °C. The VS was obtained by subtraction of the mineral matter obtained after 550 °C and of the TS. Both measurements are performed in duplicate and values are expressed as a percentage of the sample.

$$\text{TS}\,(\%) = \frac{\text{Mass}_{105°C} - \text{Mass}_{\text{Dish}}}{\text{Mass}_{\text{Dish+Sample}} - \text{Mass}_{\text{Dish}}} \times 100$$

$$\text{VS}\,(\%) = \frac{\text{Mass}_{105°C} - \text{Mass}_{550°C}}{\text{Mass}_{\text{Dish+Sample}} - \text{Mass}_{\text{Dish}}} \times 100$$

3.2.2 Chemical Oxygen Demand (COD)

The Chemical Oxygen Demand (COD) corresponds to the amount of oxygen required to oxidise the OM contained in a raw sample under acid medium, high temperature (150 °C), a specific oxidising agent (K dichromate ($K_2Cr_2O_7$)), and time (120 min). The COD is defined as the amount of O_2 chemically equivalent to the $Cr_2O_7^{2-}$ consumed during the oxidation. It is frequently used in wastewater treatment as an indicator to assess the organic contamination in various effluents.

Soluble and total COD (sCOD and tCOD) were measured using AqualyticO® kits (0–1500 mg $O_2.L^{-1}$). The measurements were done using a spectrophotometer which follows Beer-Lambert's law. For sCOD analysis, the sample was previously filtered through 0.45 µm filter. The tCOD of solid samples and solid fractions was determined using an acid extraction method. A known mass of freeze-dried sample is mixed with H_2SO_4 (98 % w w $^{-1}$) and agitated for 24 hours. Afterwards, the sample is diluted with distilled water before measuring COD using kits. Units were expressed in mg $O_2.L^{-1}$ for the liquid phases and mg $O_2.gTS^{-1}$ for the solid fraction and total phases.

For liquid samples (raw sludge, digested sludge and thickened sludge) the tCOD of the sample is considered as the sum of the tCOD from the freeze-dried solid fraction and the sCOD of the liquid fraction. First, the total COD of the solid freeze-dried sample is calculated on raw samples basis:

$$tCOD_{solid\ fraction}(mg\ g\ TS^{-1}) = \frac{\frac{mgCOD}{L} \times \frac{mL\ H_2O\ total}{1000\ mL}}{g\ RS_{freeze-dried} \times TS_{freeze-dried}(\%)}$$

$$tCOD_{solid\ fraction}(mg\ g\ RS^{-1}) = tCOD_{solid\ fraction}(mg\ g\ TS^{-1}) \times TS_{raw\ solid\ fraction}(\%)$$

The sum of soluble COD and total COD of the solid fraction will be the tCOD of the sample:

$$tCOD_{sample}(mg\ g\ RS^{-1}) = \left(COD_{soluble}(mg\ g\ RS^{-1}) \times (1-r)\right) + \left(r \times tCOD_{solid}(mg\ g\ RS^{-1})\right)$$

Where RS is raw sample and r is the centrifugation rate (the mass of solid fraction after centrifugation over the mass of the initial sample centrifuged (%)).

3.2.3 Total Kjeldahl Nitrogen and Ammonia Nitrogen

Total Kjeldahl Nitrogen (TKN) was measured for freeze-dried solid samples and solid fractions (sludge cake, hydrochar and solid fractions collected after centrifugal treatment), using the Kjeldatherm and Vapodest 500 (Gerhardt) apparatus. The protocol involves 3 steps: first, the digestion of OM using concentrated H_2SO_4, heat, K_2SO_4 and a selenium catalyst. This converts nitrogen to ammonium sulfate. With the addition of NaOH, ammonium sulfate is converted to NH_3, which is distilled and collected in excess boric acid to produce ammonium borate. Finally, the residual boric acid is titrated with a standard acid using a suitable indicator point to estimate the total nitrogen content. TKN value is considered the sum of organic nitrogen and ammonia nitrogen ($N\text{-}NH_4^+$).

Ammonia nitrogen and total nitrogen is measured in the soluble fractions (DOM) and extracted fractions obtained through the ISBAMO® methodology (explained in section 3.3), using Hach Lange kits. TN was expressed as a proportion of total TKN of the original solid sample. Organic N-content can be calculated as the difference between TKN and $N\text{-}NH_4^+$.

3.3 ISBAMO® Methodology

The ISBAMO® (Indice de Stabilité et de BioAccessibilité de la Matière Organique) methodology is based on sequential chemical extractions of the OM contained in a sample and their subsequent spectral analysis. The values obtained assess the biochemical and structural nature of the matrix by means of its bioavailability and complexity (Jimenez et al., 2014, 2015, 2017, 2020).

A total quantity of 1 g of freeze-dried sample was sealed in two fibre bags (0.5 g each bag) and subjected to the sequential chemical extractions using an automated extraction system (Thermo Scientific Dionex ASE 350 Automated Accelerated Solvent Extraction System) in extraction cells, as seen in Figure 6 below. The system operates at a temperature of 40°C to achieve the automatic extraction using 3 increasingly aggressive solvents. The oven design ensures uniform heating and temperature control for the extraction cell. The system allows in-line filtration and in-cell clean-up to ensure homogeneous extraction. The software used was Chromaleon 7. N_2 gas is used to purge the cells.

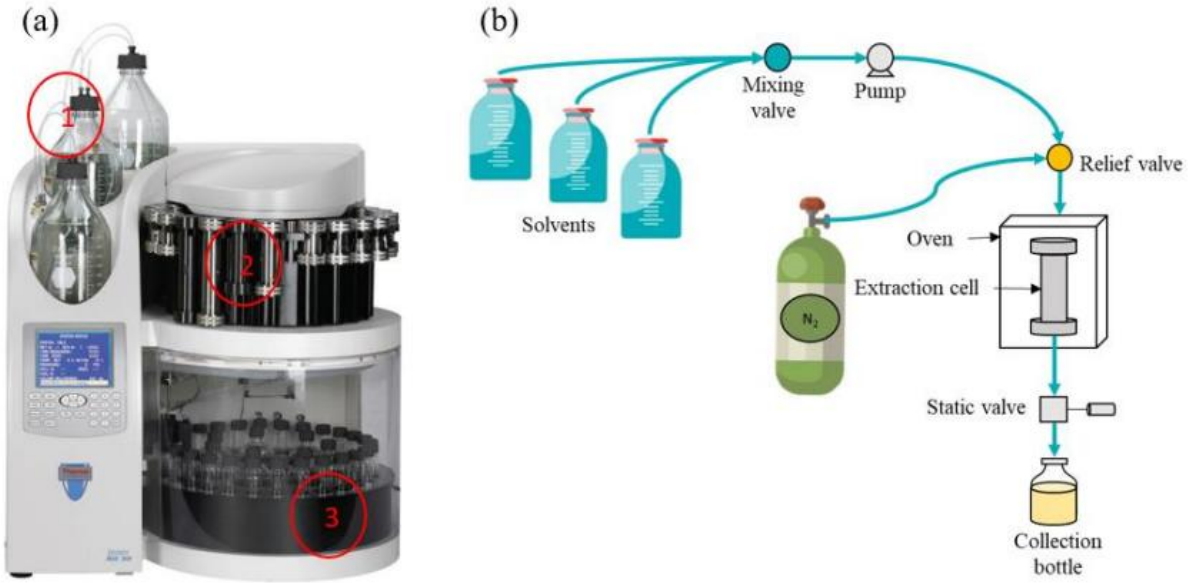

Figure 6: Thermo Scientific™ Dionex™ ASE™ 350 (a): 1) Solvents bottles 2) Zirconium cells containing the samples. 3) Collection bottles. b) Schematic of the ASE process (Fernandez-Dominguez, 2023).

Using the ASE system, three fractions were obtained by this extraction process:

- SPOM = soluble extracted from particulate organic matter;
- REOM = readily available organic matter;
- SEOM = slowly extractible organic matter.

The 3 fractions were collected in a total of 6 glass bottles. The SPOM is extracted into 1 bottle, the REOM is extracted into 3 bottles (equal volume in each) and the SEOM is extracted into 2 bottles (equal volume in each).

The final sample of each fraction after extraction was obtained by mixing an equal part of volume from each extraction step. For SPOM, the final fraction is contained in 1 single bottle, so can be transferred to a container directly. For REOM equal volumes (10mL) from each bottle were mixed in one container and for SEOM equal volumes (20mL) from each bottle were mixed in one container.

An additional extraction (PEOM = poorly extractible organic matter) is performed manually on the fibre bags from the ASE cells, using H_2SO_4 72%. The PEOM extraction is complete after the extraction using the ASE system. The non-extractable organic matter (NEOM) represents the unextractable fraction.

Each fraction could be associated with a different family of biochemically similar compounds with the aim to simulate biological accessibility. Table 2 defines all the obtained fractions using the ISBAMO® methodology and clarifies the biochemical molecules extracted.

Table 2: All fractions obtained using the ISBAMO methodology. [a]Fraction extracted using the ASE system. [b]Manually extracted fraction. [c]Residual solid fraction after PEOM extraction. [d]The extraction solvents used, the biochemical molecules extracted and the resulting number of extraction bottles.

Fraction	Solvent[d]	Biochemical molecules extracted	No. of extraction bottles
Soluble from Solid Organic Matter (SPOM)[a]	$CaCl_2$ 10 mM	Protein-like and sugars	1
Readily Extractable Organic Matter (REOM)[a]	NaCl 10 mM and 10 mM NaOH	EPS (Extracellular Polymeric Substances), protein-like, nucleic acid-like, sugars, lipids	3
Slowly Extractable Organic Matter (SEOM)[a]	NaOH 0.1	Protein-like, humic-like substances, remaining lipids	2
Poorly Extractable Organic Matter (PEOM)[b]	H_2SO_4, 72 % w:w	Hemicellulose and cellulose-like	
Non-Extractable Organic Matter (NEOM)[c]		Residual OM (lignin-lignin, humins, insoluble lipids)	

As for the DOM fraction, all extracted fractions were kept at -20°C. At the end of each extraction step, COD and TN of each fraction were measured (according to methodology explained in section 3.2.2 and 3.2.3) to calculate the accessibility profile of the sample as well as the extraction yield based on the total sample COD and N concentrations. The NEOM fraction represents COD remaining after sequential chemical extraction and is calculated by difference. To assess the complexity of the sample, each fraction was analysed using 3D-Fluorescence spectroscopy.

3.4 COD and TN Mass Balance and Extraction Yield Calculations

The amount of extract for each extraction step was measured. The extraction volumes of the same fraction, collected in different bottles, were mixed (as outlined above), and the COD and TN (mg L^{-1}) were measured for each fraction (SPOM, REOM, SEOM, PEOM). With these values, the equations below were used to obtain the relative COD % and N % of each fraction over the total COD and N in the raw sample.

$$Fraction_{mass}(mg) = conc.(mg/L) \times \frac{V_{extractant}}{1000}(L)$$

$$Fraction_{mass,FD}\left(\frac{mg}{gTS_{FD}}\right) = \frac{\text{Fraction}_{mass}(mg)}{m_{sample}(\text{g}) \times TS_{FD}(g/g)}$$

$$Fraction_{mass,RS}\left(\frac{mg}{gRS}\right) = Fraction_{mass,FD}\left(\frac{mg}{gTSFD}\right) \times TS_{RS}(g/g)$$

$$Fraction_{mass,r}\frac{mg}{gRS} = \text{Fraction}_{mass,RS}\left(\frac{mg}{gRS}\right) \times r$$

$$Fraction_{x}(\%X) = \frac{\text{Fraction}_{mass,r}\left(\frac{mg}{gRS}\right)}{tconc._{sample}\left(\frac{mg}{gRS}\right)} \times 100$$

$$DOM_{x}(\%X) = \frac{C_{DOM}(mg/L) \times \frac{(1-r)}{1000}}{tconc._{sample}\left(\frac{mg}{gRS}\right)} \times 100$$

Where X refers to a specific fraction, FD, freeze-dried; RS, raw sample; m_{sample}, is the mass of the solid fraction; conc., the concentration of either COD or TN. Please note that for solid samples, DOM fraction (liquid fraction) is not present.

3.5 3D fluorescence spectroscopy

The fluorescence spectroscopy analyses were conducted on the extracted liquid fractions using a fluorescence spectrometer (Perkin Elmer LS55). The liquid sample was introduced into a SUPRASIL quartz cell from HELLMA type 110-Q5, where the excitation wavelength passed through the quartz cell and the emission could be detected at an angle of 90°. Pulsed radiation is produced by a xenon lamp between 200 and 600 nm with a 10 nm incrementation. The monochromators presence in the excitation and emission compartments allow the acquisition of the excitation-emission spectra and 3D spectra. The processing of the Excitation Emission Matrix (EEM) subsequent data from the 3D spectra was performed with fluorescence regional integration (FRI) analysis as a quantitative data approach. The spectra can be divided into seven zones (I-VII) corresponding to a biochemical family with common complexity level as seen in Figure 7 below.

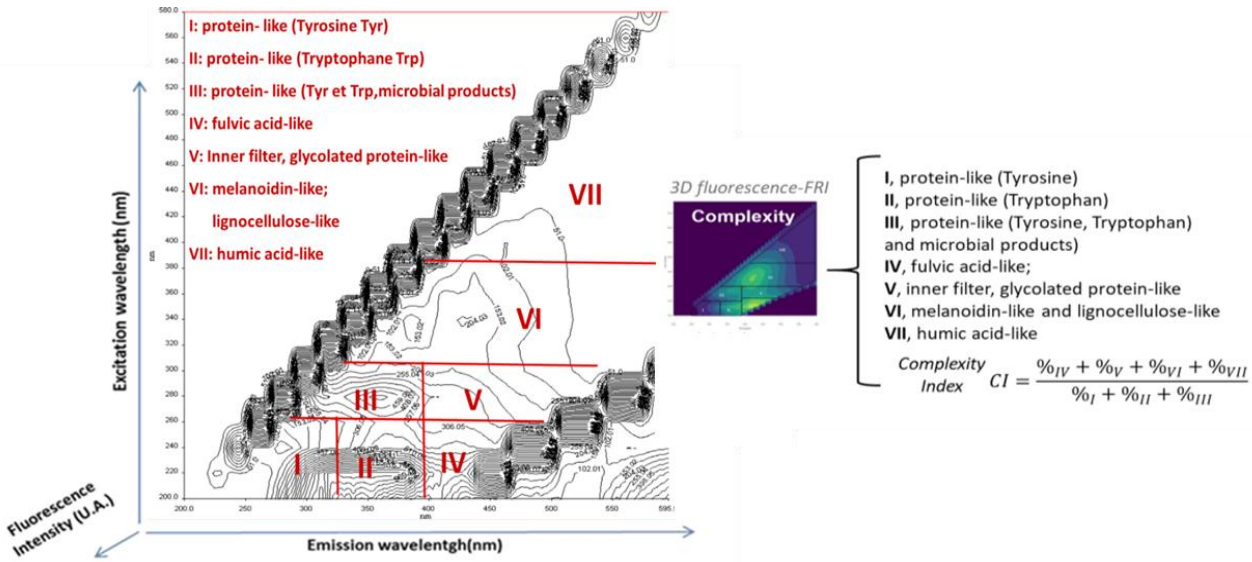

Figure 7: Fluorescence regionalization integration for spectra interpretation and quantification, outlining the location of each zone and the complexity index calculation (Jimenez et al., 2014).

Zones I–III correspond to the simplest molecules with protein-like fluorescence, while the more complex molecules are located in zones 4–7. The different molecules corresponding to each zone are described in the table below (Table 3).

Table 3: 3D fluorescence spectral zones, their corresponding biochemical families and excitation and emission wavelength regions.

Zone	Biochemical family	λex, λem
I	Aromatic protein-like (Tyrosine-like)	220, 300-310
II	Aromatic protein-like (Tryptophan)	220, 360
III	Protein-like (Trp, Tyr, microbial products)	280, 350-360
IV	Fulvic acid-like	230, 400-420
V	Intern filter (glycolated protein-like)	280, 440-450
VI	Glycolated protein-like (melanoidin), lignocellulose-like	340, 420-450
VII	Lipofuscin-like (condensed protein) lignin-like Humic acid-like	400, 480-500

The complexity of OM is assessed through the proportions of fluorescence volumes of the most recalcitrant molecules such as humic-like substances, fulvic-like acids, lipofuscin-like (i.e. a lignocellulosic marker) as well as amino acids and less complex molecules.

The proportion of fluorescence for a given zone "i" P_f (i) was calculated using the fluorescence zone volumes V_f (i) according to the equations below (Jimenez et al., 2017):

$$V_f(i)(U.A./mg \cdot COD \cdot L^{-1}) = \frac{V_{f\_raw}(i)}{COD_{sample}} \times 1/\frac{S(i)}{\sum_{i=1}^{7} S(i)}$$

$$P_f(i)(\%) = \frac{V_f(i)}{\sum_{i=1}^{7} V_f(i)} \times 100$$

with:

V_f (i) (U.A. mg $O_2.L^{-1}$): the normalized volume of the zone i,

V_{f_raw} (i) (U.A. mg $O_2.L^{-1}$): the raw volume of the zone i,

COD_{sample} (mg $O_2.L^{-1}$): the COD concentration of the sample,

S(i) (nm^2): the area of a zone i,

P_f (i) (%): the fluorescence proportion of a zone i.

To compare several samples, a "complexity index" (CI) was used to simplify interpretation. This index is defined by the ratio of the sum of the fluorescence volumes of the most complex fluorescence zones (IV–VII) over the sum of the fluorescence volumes of the protein-like zones (I–III). The complexity index used here incorporates the OM content of the sample through normalisation by COD concentration, lending greater analytical significance to the index by accounting for differences in sample OM load (Jimenez et al., 2015). The CI is calculated as follows:

$$\text{Complexity Index} = \%\text{COD}_{\text{fraction}} \times \frac{\sum_{i=4}^{7} V_f(i)}{\sum_{i=1}^{3} V_f(i)}$$

3.6 Statistical analysis

Principal Component Analysis (PCA) was used to investigate the collected variables, find correlations, reduce the complexity of the dataset and identify treatment gradients. PCA summarizes information contained in many correlated variables into fewer dimensions. The first two dimensions, which explain the highest share of variance in the dataset, are normally visualized through Cartesian axes.

Hierarchical Clustering (HC) was applied to the PCA results. This method groups samples according to their composition and allows us to determine whether materials naturally cluster according to their treatment origin and/or shared physicochemical properties. It helps to reveal compositional similarities among different materials. Using these statistical analysis tools, it was possible to determine correlations between biodegradability, indicators from OM characterization and the different type of sludge products. All data processing and statistical analyses were performed in Excel and R Studio (R version 4.5.1). Descriptive statistics and data visualization were generated using Excel and standard R packages. Multivariate analyses were conducted using the Factoshiny (Vaissie et al., 2025) application for PCA and hierarchical clustering analysis (HCA).

4 Results

Firstly, the results for bioaccessibility, complexity and 3D-Fluorescence data will be presented. This analysis was completed on 5 typologies: raw sludge, digested sludge, thickened sludge, sludge cake (all samples from WWTP1 that form a process chain) and hydrochar (sourced from 4 different treatment plants). These samples were selected as they represent the principal stages of conventional and innovative sludge treatment; from minimally processed raw sludge through biological stabilisation, mechanical dewatering, thermal conditioning and hydrothermal carbonisation. Each comprised four replicate samples, enabling typology-level comparison. The biochar sample was excluded from this analysis as the solid-phase pyrolysis matrix is not compatible with the ASE extraction system. Raw data is shown in the annex in section 8.2, Table A 3.

4.1 Bioaccessibility

4.1.1 OM Distribution Across Fractions

The proportion of total COD distributed across the chemically extracted fractions of the 5 sludge typologies (raw, digested, thickened, sludge cake, hydrochar) is summarised in Figure 8. The fractionation profiles obtained were typology-specific, reflecting the distinct processing history of each sample type.

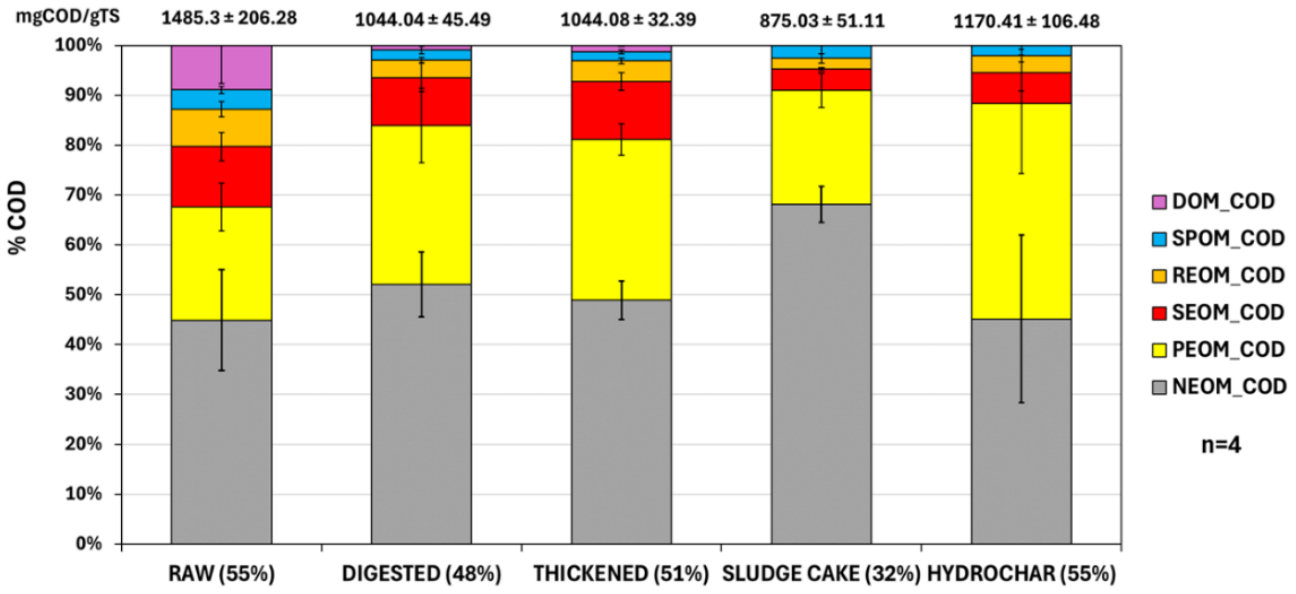

Figure 8: Total COD and biochemical fractionation profiles across five sludge typologies (n=4 per typology; left to right: raw sludge, digested sludge, thickened sludge, sludge cake, and hydrochar). Bar segments represent chemically extracted COD fractions; values at bar tops indicate total COD; percentage values in brackets indicate the total extracted COD. Black error bars show standard deviation.

Raw sludge exhibits the highest tCOD content of the solid fraction (1485.3 ± 206.28 mgCOD/gTS) and the greatest proportion of bioaccessible fractions. The DOM fraction, representing water-soluble organic substances, is highest in raw sludge compared to other typologies (9%). Raw sludge also contains the highest COD proportions in the SPOM (4%) and REOM (7%) fractions out of all typologies. The considerable variability observed (±206.28 mgCOD/gTS) is attributable to the inherent heterogeneity of influent sewage sludge composition.

Digested sludge shows a reduction in tCOD (1044.04 ± 45.49 mgCOD/gTS) relative to raw sludge, consistent with the poor biodegradability of secondary sludge. The fractionation profile reflects a shift toward less accessible fractions, with a marked increase in the PEOM fraction from raw sludge (23% to 32%) and reduction in DOM, SPOM and REOM fractions, indicating preferential degradation of more accessible OM during AD. Variability is substantially reduced compared to raw sludge, suggesting that AD homogenises the organic composition of the sludge.

Thickened sludge displays a fractionation profile closely resembling that of digested sludge and the same value of tCOD (1044.08 ± 32.39 mgCOD/gTS), with a similar distribution across fractions (± 3%) and low variability. This suggests that thickening, as a purely physical process, does not significantly alter the organic composition or bioaccessibility of the sludge relative to digested material.

Sludge cake shows the lowest proportion of extractable COD (32%) and the lowest tCOD (875.03 ± 51.11 mgCOD/gTS) of all typologies. Following AD and thickening, the sludge undergoes thermal conditioning at 195°C, prior to press filtration. The low extractable COD proportion and narrow variability reflect the cumulative effect of sequential processing steps on OM bioaccessibility. Despite this, a substantial PEOM fraction remains, indicating that a portion of OM persists in a moderately accessible form even after extensive processing.

Hydrochar exhibited a moderate level of bioaccessibility (55%) with a tCOD of 1170.41 ± 106.48 mgCOD/gTS. The fractionation profile is dominated by the PEOM fraction (43%) and a portion of the SEOM fraction remains (6%). The elevated variability (±106.48 mgCOD/gTS) is expected given that hydrochar samples derived from different municipal sludge samples and sourced from different processing facilities.

4.1.2 Nitrogen Distribution Across Fractions

The proportion of total nitrogen distributed across the chemically extracted fractions of the five sludge typologies (raw, digested, thickened, sludge cake, hydrochar) was measured and is summarised in Figure 9. Here, the PEOM fraction and the non-extractable organic matter (NEOM) fraction are grouped and represent the total nitrogen remaining after sequential chemical

extractions by the ASE. Like the COD fractionation data, the nitrogen fractionation profiles obtained were typology-specific, reflecting the distinct processing history of each sample type.

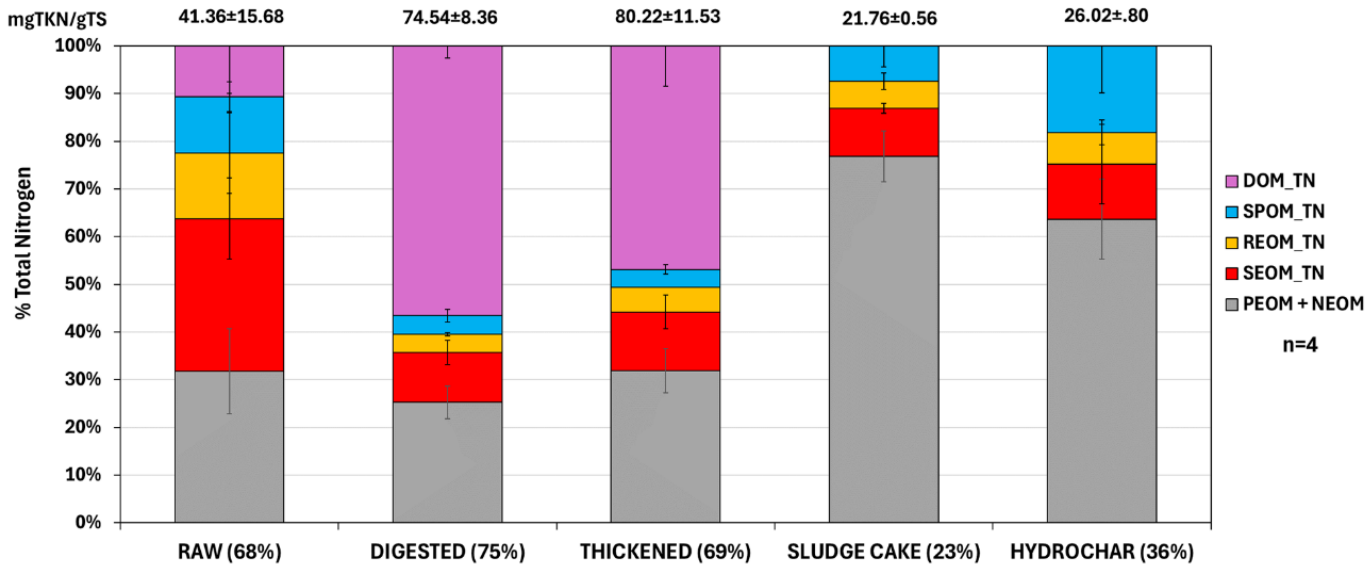

Figure 9: Total nitrogen and accessibility nitrogen profiles across the five chemically distinct sludge typologies from left to right; raw sludge, digested sludge, thickened sludge, sludge cake and hydrochar, n=4 per typology. Bar segments represent chemically extracted nitrogen fractions; values at bar tops indicate total nitrogen (TKN); percentage values in brackets indicate the extracted nitrogen. Black error bars show standard deviation.

Raw sludge has a TKN of 41.36 ± 15.68 mgTKN/gTS with 68% extractable nitrogen. Nitrogen is distributed relatively evenly across SPOM (12%), REOM (14%) and SEOM (32%) fractions, with SEOM fraction dominating. There is a substantial non-extractable fraction (31%) which may reflect poorly and non-accessible organic N. Once again, the high variability reflects the inherent heterogeneity of raw sludge composition.

Digested sludge shows the most striking shift in nitrogen distribution, with the DOM fraction accounting for 57% of total extractable nitrogen, compared to 11% in raw sludge. TKN curiously yields 74.54 ± 8.36 mgTKN/gTS, a higher value compared to the raw sludge it derives from, with 75% extractable nitrogen. The SEOM fraction decreases markedly relative to raw sludge (10% vs 32%), consistent with degradation of protein-like compounds during digestion. Variability is substantially reduced relative to raw sludge, consistent with the homogenising effect of AD observed as well in the COD fractionation data.

Thickened sludge presents the highest absolute TKN of all typologies (80.22 ± 11.53 mgTKN/gTS) with 69% extractable nitrogen. The DOM fraction remains dominant at 47%, though slightly reduced relative to digested sludge (57%), with a corresponding slight increase in SEOM (12% vs 10%) and NEOM (31% vs 25%). Overall, there is a subtle redistribution away from the DOM

fraction toward less accessible fractions and a slight increase in absolute TKN relative to digested sludge.

Sludge cake shows a reduction in both absolute TKN (21.76 ± 0.56 mgTKN/gTS) and extractable proportion (23%), with NEOM dominating at 75%. The SPOM, REOM and SEOM fractions are all substantially reduced relative to upstream typologies. The extremely low variability (±0.56 mgTKN/gTS) reflects the high reproducibility of the industrial sludge cake process.

Hydrochar presents a TKN of 26.02 ± 6.80 mgTKN/gTS with 36% extractable nitrogen. The nitrogen distribution is closest in similarity to sludge cake but distinct from all other typologies, with a higher SPOM fraction (18%) relative to sludge cake. The SEOM fraction (12%) remains comparable to other typologies while the PEOM+NEOM fraction dominates at 64%. The DOM fraction is absent as hydrochar is the solid fraction after hydrothermal carbonization processing. Most of the soluble nitrogen is moved to the process liquid phase during treatment. The variability (±6.80 mgTKN/gTS) is expected given that hydrochar samples originate from different processing facilities.

4.2 Evolution of 3D Spectra: Characteristic Fluorescence Footprint

Representative 3D excitation-emission matrix (EEM) fluorescence spectra for selected representative samples from each typology across the five extracted fractions are presented in Figure 10 (WWTP1 typologies) and Figure 11 (hydrochar) below. Although one sample is chosen to represent each typology, the spectra produced for each typology was consistent across the 4 samples. The red arrows indicate the dominant fluorescence peaks within each spectrum. Spectral profiles are discussed in detail in Section 5.2, in conjunction with complexity ratio and fluorescence zone distribution data.

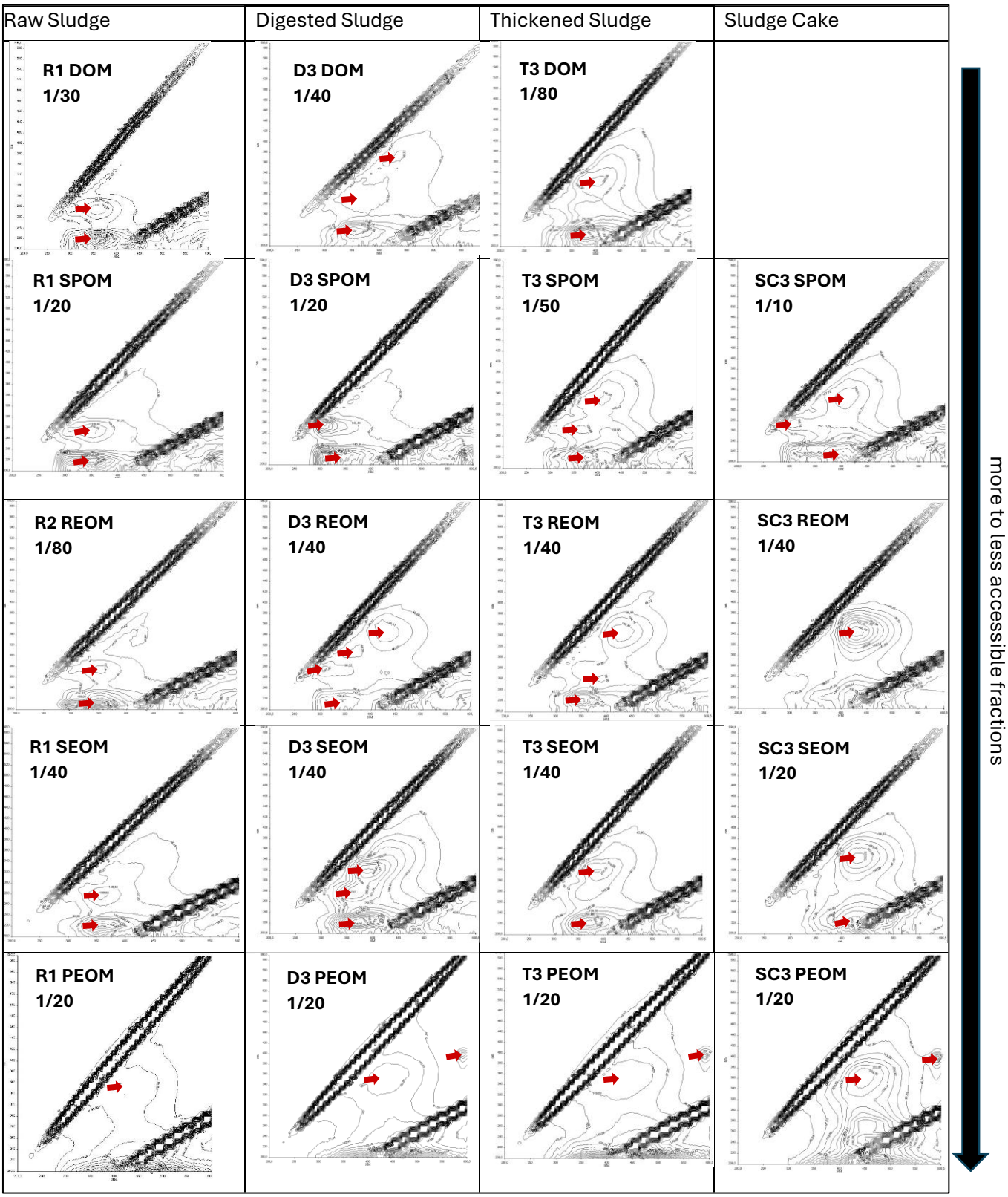

Figure 10: 3D-Fluorescence fluorescence spectra at each extraction step from DOM (row 1) to PEOM (row 5) for the sludge typologies from WWTP 1, column 1 = raw sludge (R1), column 2 = digested sludge (D3), column 3 = thickened sludge (T3), column 4 = sludge cake (SC3). Fluorescence intensity in arbitrary units is plotted as iso-lines. Arrows indicate the main fluorescence peaks.

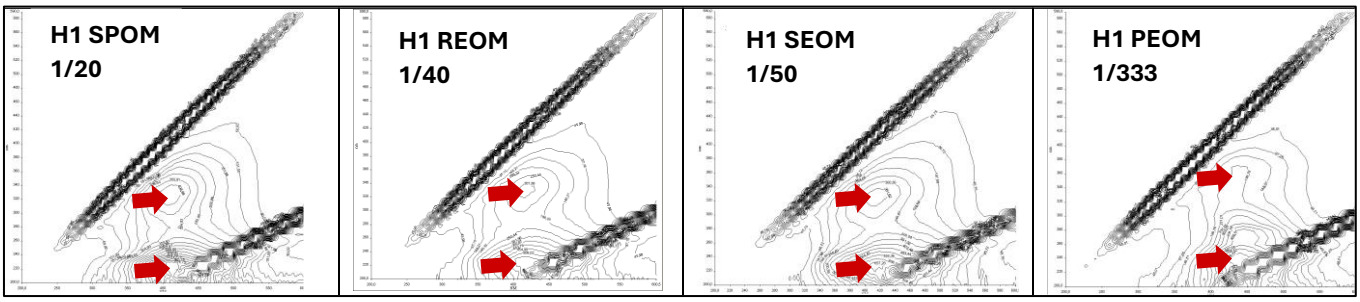

Figure 11: 3D-Fluorescence spectra at each extraction step from SPOM (left) to PEOM (right) for a hydrochar sample (H1 sample). Fluorescence intensity in arbitrary units is plotted as iso-lines. Arrows indicate the main fluorescence peaks.

4.3 OM Fluorescence Distribution

The fluorescence zone distribution across the five extracted fractions (DOM, SPOM, REOM, SEOM, PEOM) for each typology is summarised in Figure 12. The split line divides simple protein-like fluorescence zones (I–III) from complex fluorescence zones (IV–VII), with a higher proportion above the split line indicating greater OM complexity. Results are expressed as the percentage fluorescence contribution of each zone within each extracted fraction. The distribution is these graphs are directly correlated with the zone distribution of the 3D-fluorescence spectra. Raw data can be found in the annex section 8.2 in Table A 4.

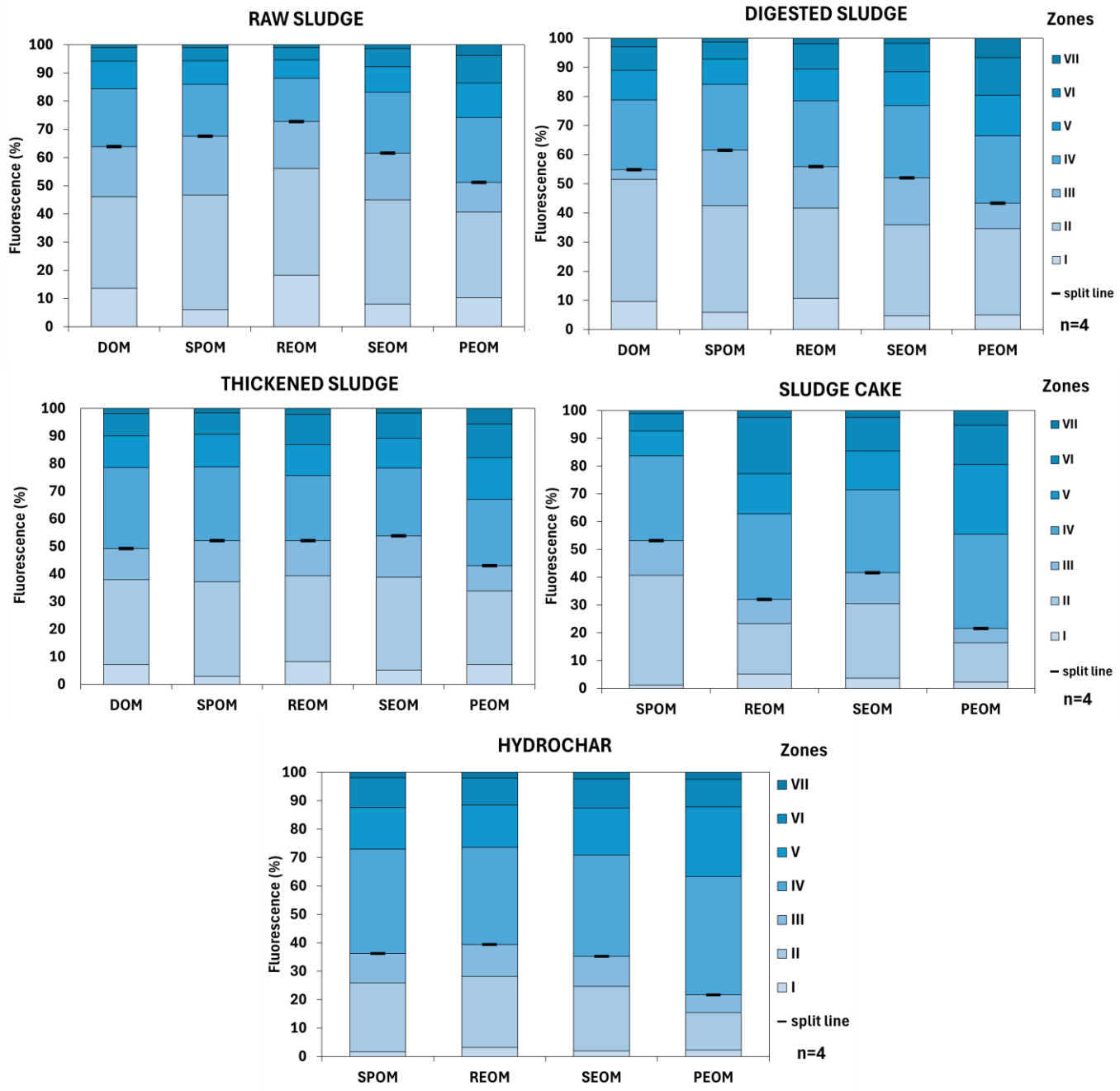

Figure 12: Distribution of fluorescence (%) of the seven spectral regions in each fraction for the five sludge typologies, n=4 for each typology. The horizontal line splits the simple fluorescent OM from the complex one.

Raw sludge presents the highest overall proportion of simple fluorescence zones across all fractions, with the split line ranging from 51% (PEOM) to 73% (REOM), indicating that the majority of OM in the accessible fractions is composed of relatively simple, protein-like compounds. Zones I–III dominate particularly in the DOM, SPOM and REOM fractions and complexity increases progressively toward less accessible fractions, with the PEOM fraction showing the lowest proportion of simple zones (51%) and the highest contribution of zone IV (fulvic acid-like, 23%) and zone VII (humic acid-like, 3.8%) of all raw sludge fractions.

Digested sludge shows a marked reduction in simple zone proportions relative to raw sludge across all fractions, with the split line ranging from 43% (PEOM) to 62% (SPOM). The DOM fraction shows a notable decrease in simple zones compared to raw sludge with split line decreasing from 64% to 55%. Zone VII (humic acid-like) increases in the PEOM fraction relative to raw sludge (6.7% vs 3.8%).

Thickened sludge presents a fluorescence distribution broadly consistent with digested sludge across all fractions, with split line values ranging from 43% (PEOM) to 52% (SPOM and REOM).

Sludge cake shows a distinct fluorescence profile characterised by high complexity in the less accessible fractions. While the SPOM fraction retains a relatively high proportion of simple zones (53%), complexity increases sharply toward less accessible fractions, with the PEOM fraction showing only 22% simple zones, the lowest of any fraction across typologies along with hydrochar. Zone V (glycolated protein-like) increases substantially in the PEOM fraction (25%) relative to upstream typologies. Zone IV (fulvic acid-like) increases progressively across fractions, reaching 34% in PEOM. In addition, zone VI (melanoidin-like compounds) increases substantially in the REOM fraction (20%) from thickened sludge (7.7%).

Hydrochar presents the most complex fluorescence profile of all typologies, with consistently low simple zone proportions across all fractions (the split line ranges from 22% in PEOM to 39% in REOM). Zone IV (fulvic acid-like) dominates across all fractions, reaching 42% in the PEOM fraction, substantially higher than any other typology. Zone V (glycolated protein-like) is elevated in the PEOM fraction (24%) and zone VI (melanoidin-like compounds) is consistently present, ranging from 9.5-10.4% across all fractions.

4.4 Sludge Complexity Indicator

The complexity ratio (CR) across the extracted fractions of the five sludge typologies is presented in Figure 13 and the data plotted by typology. A graph of CR plotted by fraction can be found in the annex section 8.1.1 in Figure A 1. The CR is defined as the ratio of the sum of fluorescence volumes of complex zones (IV–VII) to the sum of fluorescence volumes of protein-like zones (I–III), normalised by COD concentration to account for differences in OM load between samples. Higher CR values indicate greater molecular complexity and recalcitrance of the extracted OM (Jimenez et al., 2017). The CR increases consistently with processing intensity across all fractions and typologies, reflecting progressive stabilisation of OM through biological, mechanical and thermochemical treatment stages. Raw data is found in the annex section 8.2, Table A 5.

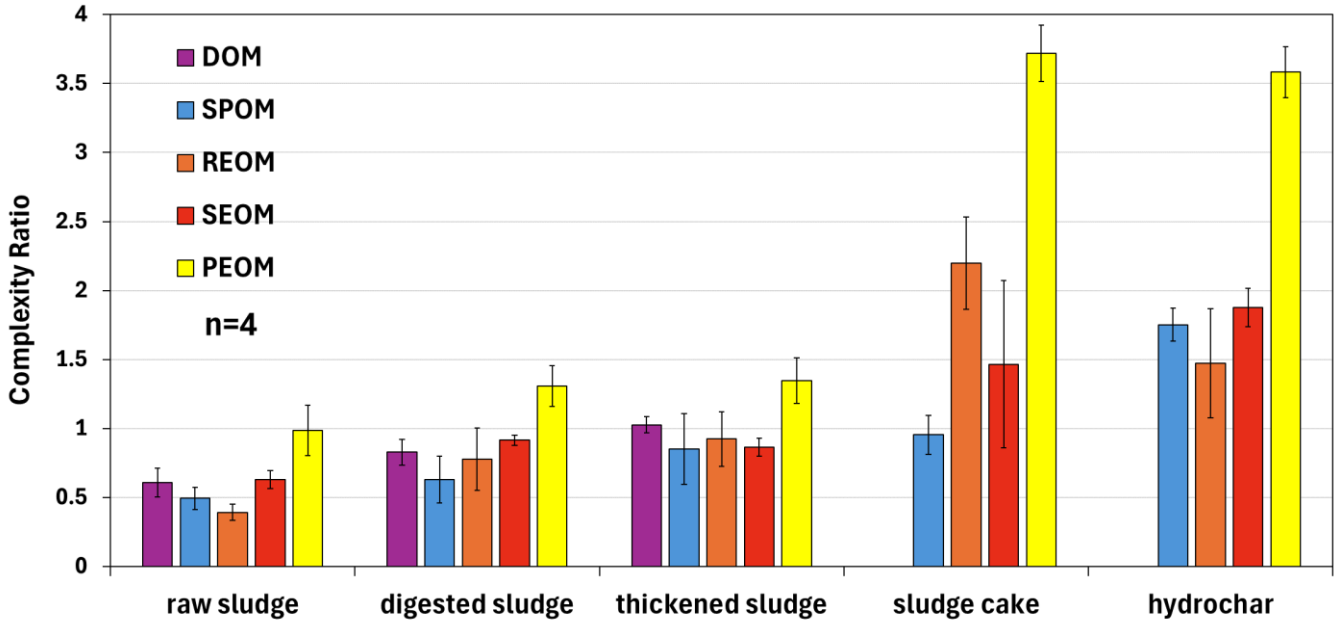

Figure 13: The complexity ratio (CR) of each fraction across the five sludge typologies (raw sludge, digested sludge, thickened sludge, sludge cake and hydrochar), n=4 for each typology. Black error bars show standard deviation.

Raw sludge presents the lowest CR values of all typologies across all fractions, ranging from 0.39 (REOM) to 0.99 (PEOM). The PEOM fraction shows the highest CR within raw sludge.

Digested sludge shows a moderate increase in CR across all fractions relative to raw sludge, ranging from 0.63 (SPOM) to 1.31 (PEOM). The increase is most pronounced in the DOM (0.83) and SEOM (0.91) fractions.

Thickened sludge presents CR values broadly comparable to digested sludge across most fractions, ranging from 0.85 (SPOM) to 1.35 (PEOM). The DOM fraction shows a slight increase relative to digested sludge (1.03 vs 0.83), though the overall profile remains consistent.

Sludge cake shows a dramatic increase in CR relative to upstream typologies, with REOM (2.20) and PEOM (3.72) showing the most pronounced increases. The PEOM CR of 3.72 represents an approximately 3.8-fold increase relative to raw sludge and approximately 2.8-fold increase relative to thickened sludge. The SPOM fraction shows a more moderate increase of 0.95.

Hydrochar presents PEOM CR (3.58) comparable to sludge cake (3.72), confirming that both thermochemical treatments produce poorly and non-accessible organic OM. However, the distribution of complexity across fractions differs between the two typologies: hydrochar presents elevated CR in the SPOM (1.75) and SEOM (1.88) fractions relative to sludge cake (0.95 and 1.46 respectively), whereas sludge cake shows higher REOM CR (2.20 vs 1.47), suggesting that HTC and thermal conditioning complexify OM through different structural pathways in different fractions.

4.5 Principal Component Analysis and Hierarchical Clustering of the Dataset

PCA and hierarchical clustering were performed on two datasets: one comprising physicochemical variables and one comprising fluorescence zone distribution data, across the 29 samples (as outlined in (Table 1) representing the sludge typologies investigated in this study.

4.5.1 PCA of Physicochemical Parameters

First, PCA according to physicochemical properties was applied to the dataset. The set of physicochemical characteristics considered as variables were pH, EC, TS, VS/TS, COD, TKN, N, C, H, P, K, Benzo(a)pyrene (BaP) and Total Ammonia Nitrogen (TAN). BaP is one of the 16 PAHs classified by the United States Environmental Protection Agency (Alipour et al., 2022). It was considered in this analysis because it is one of the most toxic PAHs found in SS and is classified as a level 1 carcinogen (Mohammed et al., 2021).

Considering its low representativeness in the database (only 1 sample) and its extreme physicochemical signature, the analysis was done with and without the biochar sample data. To focus on functional convergence and avoid one typology dominating the principal components, the results and discussion will focus on the analysis excluding biochar data. By excluding biochar, the PCA-HCA analysis of remaining products better resolves more subtle functional gradients among sludge products that share intermediate characteristics but originate from diverse biological and thermochemical processes. The PCA and HCA of the data including biochar is presented in the annex section 8.1.2, Figure A *2*.

4.5.1.1 PCA and HC of Physicochemical Properties Without Biochar

Scores and loadings from the PCA of physicochemical properties excluding biochar are presented in Figure 14. The first two components accounted for 67.44% of the total variance (Dim 1: 36.99%; Dim 2: 30.45%). Dimension 1 represents a gradient from high C, H, mgCOD/gTS and N on the positive axis toward high P and pH on the negative axis. Dimension 2 separates individuals with high TKN, EC, TAN and K from those with high TS and BaP.

Where the results differ are in distribution of the typologies across the PCA graph of individuals which shows typologies form a decreasing gradient from left to right; thickened and digested sludge (negative Dim 1), dehydrated sludge and thermally treated sludge (near origin) and raw and hydrothermally treated sludge (positive Dim 1). Sludge cake and hydrochar are further separated toward negative Dim 2.

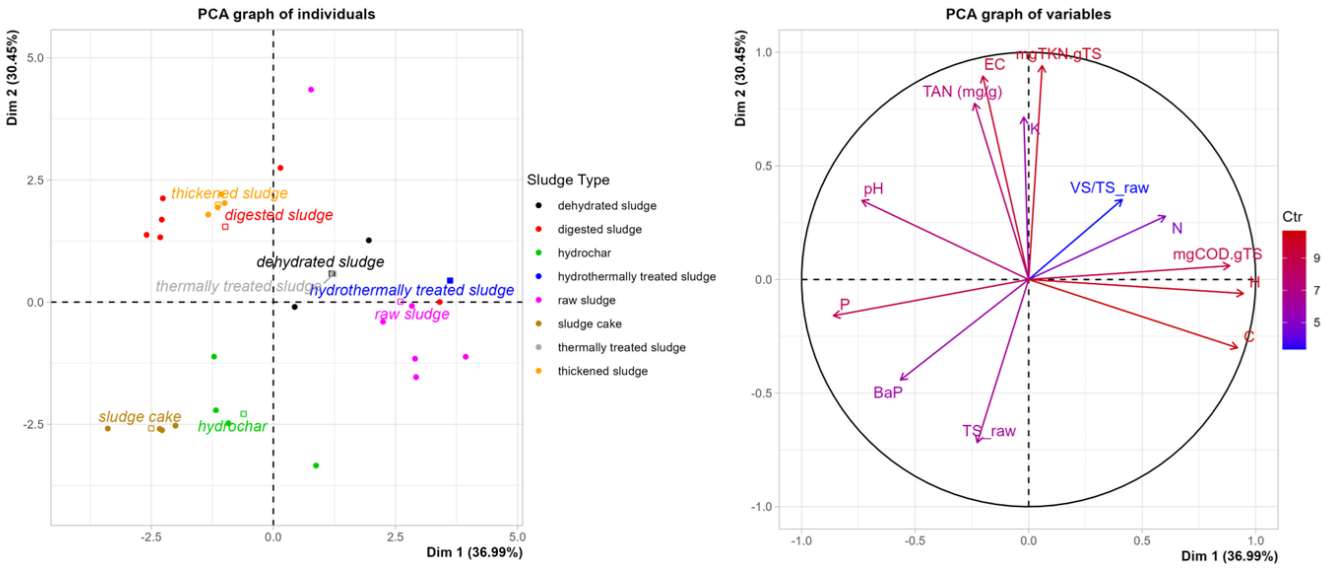

Figure 14: Scores plot (a) and loadings (b) obtained from the PCA analysis of the database (biochar excluded) with the considered set of physicochemical characteristics (pH, EC, TS, VS/TS, COD, TKN, N, C, H, P, K, BaP, TAN) as active variables; left is the graph of individuals (sludge types) and right is the PCA graph of variables (physicochemical properties).

The correlation values of the quantitative variables on Dimensions 1 and 2 are presented in Table 4. On Dimension 1, H, C, mgCOD/gTS and N showed the strongest positive correlations, while P and pH showed the strongest negative correlations. On Dimension 2, mgTKN/gTS, EC, TAN and K were most positively correlated, while TS and BaP were negatively correlated.

Table 4: Correlation data of the variables for dimension 1 and dimension 2 of PCA graph of physicochemical characteristics using data excluding biochar.

Correlation of quantitative variables on **Dimension1**		**Correlation** of quantitative variables on **Dimension2**	
H	9.457E-01	mgTKN.gTS	9.414E-01
C	9.197E-01	EC	8.954E-01
mgCOD.gTS	8.857E-01	TAN (mg/g)	7.754E-01
N	6.022E-01	K	7.150E-01
VS/TS_raw	4.118E-01	BaP	-4.424E-01
BaP	-5.648E-01	TS_raw	-7.181E-01
pH	-7.347E-01		
P	-8.599E-01		
H	9.457E-01		

Hierarchical clustering analysis of the physicochemical properties identified four clusters, selected on the basis of the inertia gain plot (Figure 15). Cluster 1 (black) grouped sludge cake and hydrochar, Cluster 2 (pink) grouped digested and thickened sludge, Cluster 3 (green) comprised dehydrated sludge samples, and Cluster 4 (blue) grouped raw sludge samples.

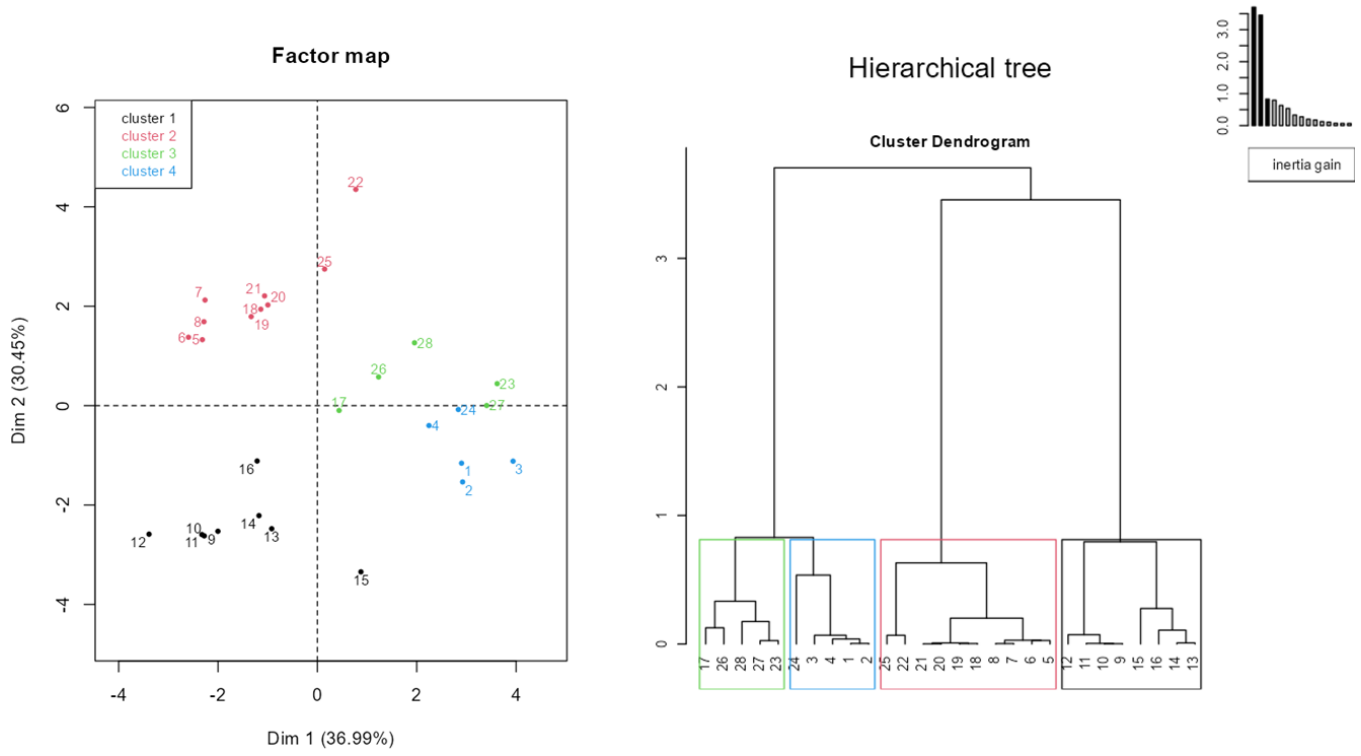

Figure 15: Hierarchical Clustering Analysis of the physicochemical properties excluding biochar with 4 clusters; Cluster 1 (black) = sludge cake and hydrochar, Cluster 2 (pink) = digested and thickened sludge, Cluster 3 (green) = dehydrated sludge, Cluster 4 (blue) = raw sludge.

4.5.2 PCA of the % Fluorescence of Fractions across Zones without DOM

PCA and HCA analyses was performed on 28 variables to describe the accessibility and complexity of the OM for 27 samples. For this analysis, the percentage fluorescence of each fraction (SPOM, REOM, SEOM and PEOM) across the 7 zones of complexity was used, providing the 28 variables. Scores and loadings from the PCA are presented in Figure 16 below and HCA results shown in Figure 17. Labels of variables correspond to Fraction_Zone. For example, PEOM_7 corresponds to the PEOM fraction that sits in zone 7 of the fluorescence spectrum.

As outlined previously, biochar was excluded from the analysis as well as the AD_IN sample due to missing data (ISBAMO fractionation was not performed on this sample). DOM fraction variables were also excluded from the fluorescence PCA because data for the DOM fraction is absent in sludge cake and hydrochar (DOM fluorescent data is not measurable for solid samples), rendering the dataset incomplete. This exclusion also improved the interpretability of the resulting biplot.

When removing DOM variables from the data, over 60% of the variance is explained in dimension 1 alone. Together, the first two dimensions explain 75.62 % of variance. Dimension 1 discriminates between sludge products with higher complexity, containing compounds in zones IV, V, VI and VII from sludges and sludge products with lower complexity, containing compounds

from zones I, II and III. Dimension 2 separated individuals with lower accessibility (PEOM fractions) from individuals with higher accessibility (SPOM fractions).

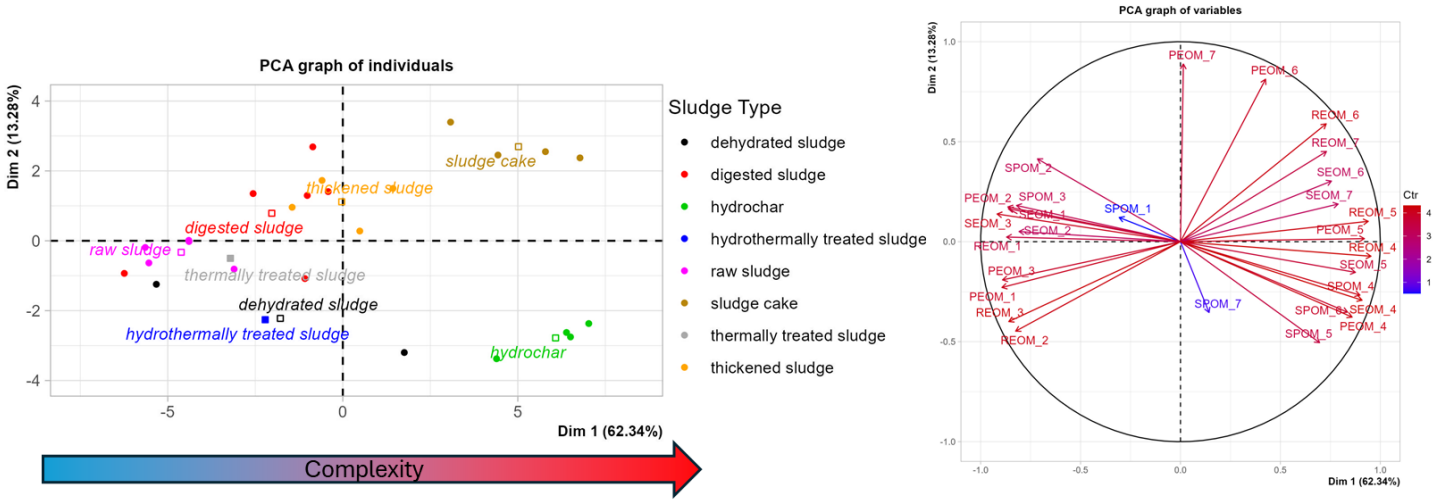

Figure 16: P Scores plot (a) and loadings (b) obtained from the PCA analysis of the database (biochar excluded) with the % fluorescence of fractions (SPOM, REOM, SEOM, PEOM) across the 7 complexity zones as active variables; left is the graph of individuals (sludge types) and right is the PCA graph of variables (% fluorescence of each fraction across zone I-VII). Labels of variables correspond to Fraction_Zone, e.g. PEOM_7 = PEOM fraction in fluorescence zone 7.

The correlation values of variables on Dimensions 1 and 2 are presented in Table 5. On Dimension 1, the strongest positive correlations were observed for zone IV and V fluorescence across the REOM, PEOM, SEOM and SPOM fractions and all top contributing variables are from zones IV-VII. On Dimension 2, fluorescence zones VII and VI in the PEOM and REOM fractions showed the strongest positive correlations, while zone II and V fluorescence in the REOM and SPOM fractions were negatively correlated.

Table 5: Correlation data of the variables for dimension 1 and dimension 2 of PCA graph of % fluorescence of fractions.

Correlation of quantitative variables on **Dimension1**		**Correlation** of quantitative variables on **Dimension2**	
REOM_4	9.537E-01	PEOM_7	8.882E-01
REOM_5	9.400E-01	PEOM_6	8.126E-01
PEOM_5	9.205E-01	REOM_6	5.895E-01
SEOM_4	9.090E-01	REOM_7	4.513E-01
SPOM_4	8.982E-01	SPOM_2	4.143E-01
SEOM_5	8.757E-01	REOM_3	-3.994E-01
PEOM_4	8.589E-01	REOM_2	-4.473E-01
SPOM_6	8.363E-01	SPOM_5	-5.048E-01
SEOM_7	7.892E-01		
SEOM_6	7.556E-01		
REOM_7	7.307E-01		

Hierarchical clustering analysis of the percentage fluorescence intensity across zones I–VII identified four clusters, selected on the basis of the inertia gain plot (Figure 17). Cluster 1 (black)

grouped mainly raw and dewatered sludge samples, Cluster 2 (pink) grouped digested and thickened sludge, Cluster 3 (green) comprised sludge cake samples, and Cluster 4 (blue) grouped hydrochar samples.

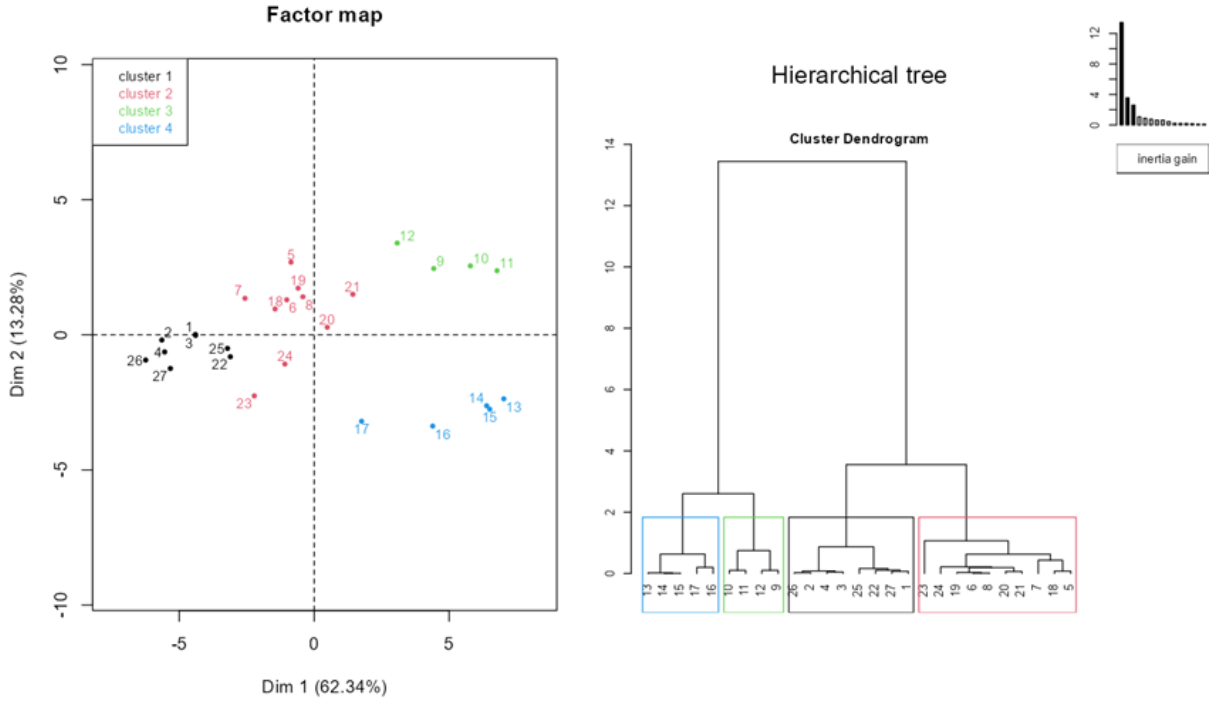

Figure 17: Hierarchical Clustering Analysis of the % fluorescence of fractions (SPOM, REOM, SEOM, PEOM) across the 7 complexity zones with 4 clusters: Cluster 1 (black): raw and dehydrated sludge, Cluster 2 (pink): digested and thickened sludge, Cluster 3 (green): sludge cake, Cluster 4 (blue) hydrochar.

5 Discussion

5.1 COD and Nitrogen Fractionation Profile: typology-specific bioaccessibility

The typology-specific fractionation profiles observed across the five sludge-derived matrices which reflect the cumulative effect of successive treatment stages on the chemical accessibility of both OM (Figure 8) and nitrogen (Figure 9). The progressive shift from accessible to less accessible fractions along the processing chain is consistent with the selective transformation and stabilisation of OM during each treatment stage, as established by Muller et al. and Parnaudeau et al. (Muller et al., 2014; Parnaudeau et al., 2004).

Raw sludge presents the highest absolute tCOD of all typologies (1485.3 ± 206.28 mgCOD/gTS) the highest proportion of labile COD fractions (DOM, SPOM and REOM) and the most evenly distribution of nitrogen across extracted fractions. The dominance of DOM (9%), SPOM (4%) and

REOM (7%) in the COD profile reflects the biochemically active character of raw sludge, which is rich in microbial biomass, extracellular proteins, simple sugars and water-soluble organic compounds (Jimenez et al., 2017; Laera et al., 2019). This result is in keeping with research by Ciaciuch et al., 2017, in which readily biodegradable substrates and slowly biodegradable substrates (fractions that can be correlated to REOM and SEOM), were dominant in raw sludge samples compared to thermally treated sludge and digestate, where COD increased in the less extractable fractions (Ciaciuch et al., 2017).

In contrast, the absolute TKN of raw sludge (41.36 ± 15.68 mgTKN/gTS) is the second lowest of all typologies, lower than digested (74.54 mgTKN/gTS) and thickened sludge (80.22 mgTKN/gTS). This inconsistent value of TN may reflect an analytical error or inconsistency in the sampling procedure seeing as this is also evidenced by anomalous TS and pH values for these samples. The nitrogen is distributed across SPOM (12%), REOM (14%) and SEOM (32%) fractions, with SEOM dominant, reflecting the association of organic nitrogen with proteins and microbial biomass compounds that require stronger alkaline conditions used in the SEOM extraction to solubilise. This is consistent with previous studies showing a high content of proteins in secondary sludge (Jimenez et al., 2014). The parallel between COD and nitrogen fractionation in raw sludge, both showing the highest proportion of accessible fractions in this typology, confirms that at this stage of processing, organic carbon and nitrogen exist predominantly in bio-accessible forms. The high variability in both tCOD (±206.28 mgCOD/gTS) and TKN (±15.68 mgTKN/gTS) reflects the inherent compositional heterogeneity of influent sewage sludge, despite coming from the same wastewater treatment plant. SS is known to be a challenging matrix that can lead to variability due to the heterogeneity of the input and the varying degrees of mixing during processing (Babić & Mutavdžić Pavlović, 2013).

After AD there is a reduction in tCOD from 1485 to 1044 mgCOD/gTS. This decrease of approximately 30% reflects the transformation of labile organic carbon to biogas (CH_4 and CO_2) (Yu & Schanbacher, 2010), with preferential consumption of DOM, SPOM and REOM fractions. This selectivity is consistent with the established preference of anaerobic microbial communities for accessible organic substrates over more recalcitrant compounds (Jimenez et al., 2015; Muller et al., 2014). The concomitant increase in PEOM (23% to 32%) and NEOM (45% to 52%) reflects the relative accumulation of holocellulose-like and lignin-like compounds as labile fractions are consumed.

Absolute TKN increases markedly from raw sludge (41.36 mgTKN/gTS) to digested sludge (74.54 mgTKN/gTS) by approximately 80%. This imbalance reflects, as previously mentioned, an analysis failure or sampling issue at the WWTP as normally TKN is conserved during this process, or else lost due to ammonia volatilisation. The nitrogen fractionation profile of digested sludge shows a

shift of nitrogen to the DOM fraction (11% in raw sludge to 57% in digested sludge) reflecting the mineralisation of organic nitrogen to ammonium (NH_4^+) during AD, which partitions preferentially into the aqueous phase. The marked decrease in SEOM nitrogen (32% to 10%) as well as decreases in SPOM and REOM fractions, is consistent with the degradation of nitrogen-containing compounds during digestion and partitioning to the liquid phase (the DOM fraction) (Guilayn et al., 2020).

The observed redistribution across fractions explains why nitrogen bioaccessibility increases to 75% in digested sludge, while COD bioaccessibility decreases slightly. Organic carbon is degraded and stabilised into recalcitrant forms; nitrogen is simultaneously released into accessible inorganic form. The reduced variability in both COD (±45.49 mgCOD/gTS) and nitrogen (±8.36 mgTKN/gTS) fractionation following digestion confirms the homogenising effect of AD on sludge OM composition.

Thickened sludge presents COD and nitrogen fractionation profiles broadly consistent with digested sludge, as expected for a purely physical concentration process involving no chemical or biological transformation. The tCOD remains essentially unchanged (1044.08 ± 32.39 mgCOD/gTS vs 1044.04 ± 45.49 mgCOD/gTS for digested sludge) and the COD fractionation profile is similar across all fractions (within ±3%), confirming that thickening does not alter the chemical accessibility of OM.

The absolute TKN increases slightly from digested (74.54 mgTKN/gTS) to thickened sludge (80.22 mgTKN/gTS). The slight increase (7%) may be a result of sampling inconsistency and since nitrogen is mainly present in the form of organic nitrogen, it is not separated and remains in the solid phase after the thickening process (Horttanainen et al., 2017).The nitrogen profile similarly retains DOM dominance (47%), though slightly reduced relative to digested sludge (57%), with a corresponding slight increase in SEOM and NEOM fractions, likely reflecting partial removal of soluble nitrogen with the separated liquid phase after thickening and subsequent concentration of solid sludge.

Sludge cake shows the most pronounced reduction in both total COD and nitrogen content and bioaccessibility out of all typologies with a tCOD of 875.03 ± 51.11 mgCOD/gTS, the lowest of all typologies. This is a ~41% reduction relative to raw sludge and ~16% relative to thickened sludge. The COD fractionation profile reflects the cumulative stabilising effect of the full treatment sequence; AD, thickening, thermal conditioning and press filtration, with NEOM dominating at 68% and extractable COD reduced to 32%. Following AD and thickening, which have already consumed the most labile COD fractions, thermal conditioning acts on an already-stabilised matrix, further solubilising residual accessible organic compounds including proteins and lipids (Aboulfoth et al., 2015). These solubilised compounds are subsequently removed during press filtration,

stripping the most accessible organic fraction from the solid product and leaving a matrix dominated by non-extractable, stable OM.

Thermal conditioning is known to accelerate the mineralisation of organic nitrogen in sludge, promoting its conversion to ammonium (NH_4^+) which partitions into the aqueous phase (Mustonen et al., 2018). The nitrogen profile of sludge cake is consequently dominated by the subsequent press filtration step, which removes this NH_4^+-rich liquid phase from the solid product. Absolute TKN drops to 21.76 ± 0.56 mgTKN/gTS, the lowest of all typologies, representing a loss of ~73% of the solid-phase TKN relative to thickened sludge. This high reduction reflects the removal of the NH_4^+-rich liquid phase during dewatering, leaving predominantly nitrogen-containing compounds that resist the milder extraction conditions, reflected in the PEOM+NEOM fraction dominating at 77%. Sludge cake is consequently the only typology where COD bioaccessibility (32%) exceeds nitrogen bioaccessibility (23%). While some extractable organic carbon is retained in the solid following thermal conditioning, the accessible nitrogen fraction is removed with the press filtrate and there is also some condensation of proteins into the NEOM fraction. The extremely low variability in both COD (±51.11 mgCOD/gTS) and nitrogen (±0.56 mgTKN/gTS) fractionation reflects the high reproducibility of the industrial thermal conditioning and press filtration process.

Hydrochar presents a fundamentally different pattern of OM and nitrogen transformation compared to sludge cake, despite both undergoing thermochemical treatment at comparable temperatures (SC = 195°C, H = 200-210°C). The tCOD of hydrochar (1170.41 ± 106.48 mgCOD/gTS) is higher than sludge cake (875.03 mgCOD/gTS) and comparable to digested sludge (1044 mgCOD/gTS), reflecting that HTC retains organic carbon in the solid product rather than removing it through dewatering or biological mineralisation. The COD fractionation profile is dominated by the PEOM fraction at 43% (the highest of any typology), while total extractable COD (55%) is comparable to raw sludge. This paradox of having similar overall extractability to raw sludge yet fundamentally different fraction distribution, reflects the structural transformation of OM during HTC. The HTC process is applied directly on raw sludge with no prior COD reduction, unlike sludge cake, which derives from a combination of treatments, of which AD has a high impact in reducing COD due to biogas production.

Hydrothermal carbonisation promotes the hydrolysis and decomposition of major biopolymer components such as carbohydrates, with subsequent condensation polymerisation of intermediates driving the formation of aromatic carbon structures (Zhang et al., 2014). This is consistent with 13C-NMR and FTIR analyses confirming that hydrochar contains lower proportions of oxygen-containing organic carbon (including O-alkyl, carboxylic and carbonyl C) and reduced aliphaticity, alongside higher aromatic carbon content and aromaticity relative to the original

sludge (Zhang et al., 2014). These condensed aromatic structures resist the milder aqueous and alkaline extractions but are solubilised under the strongly acidic PEOM conditions, explaining the concentration of extractable COD in the PEOM fraction.

The DOM fraction is absent in hydrochar, consistent with the transfer of water-soluble organic compounds to the HTC process water during treatment. The HTC process water is known to contain a range of soluble organic compounds; phenolic compounds, organic acids (acetic, formic, glycolic and levulinic acids), furan derivatives and 5-hydroxymethylfurfural (5-HMF) (Tasca et al., 2019), which are products of the hydrolysis and depolymerisation of carbohydrates and proteins during HTC. The elevated variability in tCOD (±106.48 mgCOD/gTS) reflects the heterogeneity of feedstock and process conditions across the different processing facilities from which hydrochar samples originate.

The absolute TKN of hydrochar (26.02 ± 6.80 mgTKN/gTS) is low, comparable to sludge cake (21.76 mgTKN/gTS) and substantially lower than digested and thickened sludge, showing transfer of nitrogen to the HTC process liquid during treatment (Wang et al., 2018). The nitrogen profile is distinct from all other typologies, with notably elevated SPOM nitrogen (18%) relative to sludge cake, consistent with reports of NH_4^+ adsorption onto hydrochar particles during HTC (Zhang et al., 2014). The dominant PEOM+NEOM nitrogen fraction (64%) likely reflects the incorporation of nitrogen into recalcitrant heterocyclic structures during HTC (principally pyridine-N and pyrrole-N), formed through thermal condensation reactions at elevated temperature and pressure (Liu et al., 2026). The variability in TKN (±6.80 mgTKN/gTS) is relatively low given that hydrochar samples originate from different processing facilities, suggesting that HTC consistently redistributes nitrogen regardless of feedstock variability.

The fractionation profiles presented here collectively illustrate the divergent fates of organic carbon and nitrogen across the sludge processing chain, a distinction that is central to understanding the agronomic and environmental character of each sludge-derived product and their possible functionality in soil application. Organic carbon follows a trajectory of progressive stabilisation: labile, accessible fractions are selectively consumed during AD and further complexified during thermochemical treatment, leaving an increasingly recalcitrant residue enriched in PEOM and NEOM fractions. Nitrogen, by contrast, is governed more strongly by phase separation processes: mineralised to NH_4^+ during biological treatment and concentrated in the soluble phase, then either retained (digested and thickened sludge) or removed (sludge cake) depending on whether a liquid-solid separation step follows. Hydrochar represents a distinct case where both carbon and nitrogen are simultaneously transformed by thermochemical reactions: carbon condensed into aromatic structures retained in the solid, nitrogen partially transferred to the process water and partially adsorbed or incorporated into recalcitrant heterocyclic structures.

These divergent transformation pathways mean that no single typology optimises both organic carbon and nitrogen bioaccessibility simultaneously. Importantly, the sequential chemical extraction approach demonstrates that chemical accessibility effectively simulates sludge bioaccessibility, successfully resolving the readily and slowly bio-accessible fractions across typologies in a way that bulk physicochemical parameters alone cannot (Muller et al., 2014). This observation will be further contextualised through the molecular complexity analysis presented in the following section.

5.2 Molecular Complexity as an Additional Layer of Characterisation

Classic characterisation of SS OM involves extracting and quantifying compounds according to biochemical families (proteins, lipids, carbohydrates, fibres), but this approach does not divulge which components constitute the biodegradable and non-biodegradable fractions of the OM (Muller et al., 2014). Chemical sequential extractions simulate the bioavailability of OM according to its chemical accessibility, providing a more functionally relevant characterisation by fractionating OM into compartments of decreasing accessibility rather than by biochemical origin (Muller et al., 2014).

Bioaccessibility alone is insufficient to predict biodegradability. A fraction may be chemically accessible yet molecularly complex and therefore resistant to microbial degradation, or conversely, simple in structure yet physically inaccessible. Both bioaccessibility and complexity must therefore be simultaneously determined to accurately characterise sludge OM and predict its behaviour during biological treatment or following land application (Muller et al., 2014). The 3D EEM spectra (Figure 10 and Figure 11), fluorescence zone distribution (Figure 12) and complexity ratio data (Figure 13) presented here provide this second dimension, revealing not just how much OM is accessible but how molecularly complex and recalcitrant that matter is across typologies and treatment stages. It is important to note that the chemical sequential extraction approach simulates bioaccessibility. It does not directly measure bioavailability, which would require biological assay data. The fractionation profiles therefore represent a proxy for the potential accessibility of OM to microbial degradation under defined chemical conditions. Across all typologies, the PEOM fraction consistently presents the highest complexity ratio, confirming that the least chemically accessible OM is systematically the most molecularly complex, consistent with findings from Muller et al. (2014).

Raw sludge presents the lowest complexity ratios across all fractions (0.39–0.99) and the highest proportion of simple fluorescence zones (51–73% above the split line), consistent with its predominantly protein-like, microbial biomass-derived OM. The dominance of zones I–III in the

DOM, SPOM and REOM fractions confirms that the most accessible compartments of raw sludge are composed of relatively simple compounds, consistent with the high labile COD fractions observed in the accessibility data. The moderate complexity of the PEOM fraction (CR: 0.99) reflects the presence of some more complex lignocellulose-like compounds even in untreated sludge, likely derived from lignocellulosic material in the wastewater influent.

The EEM spectra provide direct visual confirmation of this characterisation. The R1 DOM spectrum shows a dominant peak in the lower excitation/emission region (approximately Ex/Em 220–280/340–360 nm), characteristic of tyrosine and tryptophan-like fluorescence associated with fresh, relatively labile protein-like OM (Muller et al., 2014; Mayer et al., 1999), with a second peak in zone III (Ex/Em 280/350 nm) also present. The R1 SPOM and R1 REOM spectra show a similarly protein-dominated profile with contours concentrated in the lower spectral zones (I–III), and the R1 SEOM spectrum shows some spreading of contours toward higher excitation/emission wavelengths, reflecting the more complex character of alkaline-extractable compounds. The R1 PEOM spectrum presents notably sparser contours with the arrow pointing toward the mid-zone region. This could reflect partial dissolution of carbon structures by the 72% H_2SO_4 extractant, consistent with the lower OM content and moderately complex character of the acid-extractable fraction in untreated sludge.

AD produces a moderate but consistent increase in complexity across all fractions. Two complementary mechanisms drive this increase. First, the preferential consumption of simple protein-like compounds during digestion reduces the proportion of zones I–III across all fractions, proportionally enriching the residual OM in more complex structures. Second, microbial synthesis and cell lysis release intracellular components, including humic precursors and complex polymers (Aemig et al., 2019). Biological humification produces humic acid-like and fulvic acid-like substances reflected in the increase in zones IV, V and VI of the SEOM fraction (Jimenez et al., 2015; Muller et al., 2014), while an increase in upper zones of the PEOM fraction may reflect complex lignocellulose-like compounds related to the feedstock composition (Jimenez et al., 2015). The distinguishing feature of the digested sludge complexity profile is the intermediate CR levels across all fractions, indicating the presence of both simple and complex fluorescent molecules at all levels of chemical accessibility (Jimenez et al., 2015). The COD profile of digested sludge reflects these changes in complexity. The increase in NEOM COD in particular shows the stabilisation of OM into more recalcitrant humic acid-like forms during AD, a humification process associated with the formation of complex, slowly degradable organic structures from simpler precursors (Fernández-Domínguez et al., 2022; Jimenez et al., 2017)

The EEM spectra confirm this visually. The digested sludge DOM spectrum shows a significant shift relative to raw sludge, with peaks in zone I/II and zone III regions, indicating tyrosine, tryptophan

and other microbial-derived compounds. A peak appears in the upper right melanoidin/humic-like region (Ex/Em 340–400/420–480 nm, zones VI–VII), contrasting with the protein-dominated in the raw sludge DOM showing the fundamental transformation of dissolved organic matter during AD; simple protein-like compounds are consumed, reducing zones I-III and complex glycolated protein and lignocellulose-like compounds are produced. The D3 SPOM and D3 REOM spectra similarly show contours extending toward higher excitation/emission wavelength relative to raw sludge and the D3 SEOM spectrum shows a prominent peak in the complex upper zone VI/VII region, consistent with humic-like and fulvic acid-like accumulation. The D3 PEOM spectrum remains relatively sparse however a second peak appears in zone VII that is absent in R1 PEOM, consistent with the quantitative increase in zone VII (3.8% to 6.7%). Notably, protein-like fluorescence (zones I–III) persists across all fractions except PEOM, confirming that simple organic molecules exist at multiple levels of chemical accessibility. Their biodegradability potentially is not reduced by molecular complexity but by their inaccessibility, as demonstrated by Muller et al. (2014).

Thickened sludge presents complexity ratios broadly comparable to digested sludge across most fractions. However, the DOM fraction shows a slight increase in CR relative to digested sludge (1.03 vs 0.83) despite thickening involving no chemical or biological transformation. Since no new complex structures are formed during thickening, this likely reflects the preferential removal of simpler, soluble organic compounds with the separated water phase which may proportionally increase the complexity of the remaining solid matrix. This interpretation is consistent with the slight reduction in nitrogen in the DOM fraction. The CR increase through physical concentration rather than chemical transformation suggests the complexity is sensitive not only to chemical and biological transformation but also to physical processing, specifically changes in water content.

The T3 EEM spectra broadly reflect this pattern. The DOM and SPOM spectrum for the thickened sample shows peaks populating zone VI, indicating greater complexity. This confirms the hypothesis that the removal of water-soluble compounds like proteins and sugar (found in the SPOM fraction) will concentrate molecules in the remaining solid sample and increase complexity. The T3 PEOM spectrum is similar to D3 PEOM, which is expected. The least accessible fraction contains hemicellulose and cellulose compounds that are not removed with the water phase; therefore, complexity remains unchanged. Together, the T3 spectra confirm that thickening does not fundamentally alter the molecular character of OM but produces a subtle, visually detectable (3D spectra) shift toward greater complexity in the REOM, SEOM and PEOM fractions, consistent with the slight increase in the CR of the DOM fraction, observed in the quantitative data.

Sludge cake shows the most dramatic increase in complexity of all typologies within the biological-mechanical treatment chain, with REOM CR increasing to 2.20 and PEOM CR to 3.72: a 2.8 and

3.8-fold increase relative to thickened sludge, respectively. This increase in complexity is consistent with thermal conditioning promoting Maillard-type condensation reactions between proteins and reducing sugars, producing glycolated protein-like and melanoidin-like structures (Li et al., 2024; Muller et al., 2014; Yang et al., 2026). This is evidenced by the increase in zone VI fractions (in REOM, SEOM and PEOM) relative to upstream typologies (Jimenez et al., 2014; Muller et al., 2014). Zone IV (fulvic acid-like) increases to 34% in PEOM, consistent with thermal formation of fulvic acid-like compounds from simpler precursors (Collard et al., 2017). The SPOM fraction retains a relatively moderate CR (0.95) and simple zone proportion (53%), showing that the most accessible OM retains relatively simpler molecular character even after thermal conditioning. This asymmetry, a dramatic complexification of less accessible fractions alongside retention of simpler character in the most accessible fraction, reflects the specific effect of thermal conditioning acting on an already biologically stabilised matrix where labile fractions have largely been consumed by prior treatment. This is supported by Jimenez et al., (2014), whose correlation data demonstrated that thermally treated sludge shows a positive influence on biodegradability through DOM fraction variables, but a negative influence through complex compounds present at high temperatures from fluorescence zones IV to VI. This suggests that while the most accessible fraction retains some biodegradable character, the less accessible fractions are substantially complexified and recalcitrant.

The DOM fraction is absent in sludge cake, consistent with removal of the soluble phase during dewatering. The EEM spectra show shift away from simple protein-like zones (I/II) toward zone IV (fulvic acid-like, Ex/Em 230/400-420 nm) across all fractions relative to upstream typologies, reflecting the thermal formation of fulvic acid-like compounds (Muller et al., 2014). The SC3 SPOM spectrum shows a modest shift toward zone IV at the lower excitation region, consistent with its moderate CR and the relatively small decrease in simple zone proportion (4%), observed in the fluorescence distribution data. The SC3 REOM spectrum shows a prominent zone VI peak, populating higher excitation/emission wavelengths than any upstream typology, with dense contours reflecting the high fluorescence intensity of thermally modified structures, such as glycolated protein-like and melanoidin-like compounds associated with slow biodegradability (Jimenez et al., 2014; Muller et al., 2014). The SC3 SEOM spectrum shows a dominant peak in highly complex upper region of zones VI–VII, while simpler zones decrease and zone IV increases, consistent with molecules extracted from the SEOM fraction; humic-like and fulvic acid-like structures as well as complex proteins and certain lignocellulosic compounds (Jimenez et al., 2015; Laera et al., 2019). The PEOM spectrum of sludge cake shows contours shifting further toward zone VII, indicating the accumulation of humic acid-like and lipofuscin-like structures in the least accessible fraction, consistent with the elevated PEOM CR (3.72) and low simple zone proportion (22%). Together, the spectra for sludge cake paint a consistent picture of a matrix where thermal

conditioning has fundamentally transformed the molecular character of OM through complexification of less accessible OM.

Hydrochar presents the most complex fluorescence profiles of all typologies, with consistently low simple zone proportions across all fractions (split line of 22–39 %) and PEOM CR (3.58) comparable to sludge cake (3.72). However, the distribution of complexity across the other fractions differs from sludge cake. Hydrochar presents elevated CR across SPOM (1.75), SEOM (1.88) and PEOM (3.58) while sludge cake complexity is concentrated in REOM (2.20) and PEOM (3.72). This reflects the distinct structural pathways of the two thermochemical processes; in sludge cake, thermal conditioning acts on an already biologically stabilised matrix, concentrating its effects on residual less accessible OM, while HTC acts on a less pre-processed matrix producing comprehensive structural transformation across all OM compartments simultaneously through dehydration, decarboxylation and condensation reactions (Zhang et al., 2014).

The dominance of zone IV (fulvic acid-like, Ex 230/Em 400-420nm) across all hydrochar fractions (41.7% in PEOM, 36.8% in SPOM, 35.7% in SEOM and 34.2% in REOM), is particularly distinctive and not observed in any other typology, suggesting that HTC produces fulvic acid-like aromatic structures across the full spectrum of chemical accessibility, consistent with 13C-NMR and FTIR analyses confirming the formation of condensed aromatic structures during HTC (Zhang et al., 2014). Zone V (glycolated protein-like, Ex 280/Em 440-450nm) is elevated in PEOM (24.4%), comparable to sludge cake PEOM (25.0%), consistent with Maillard-type reactions during HTC producing melanoidin structures alongside aromatic condensation products (Li et al., 2024).

Although there is Zone VI (melanoidin/lignocellulose-like) compounds present across all fractions (9.5-10.4%), the values are comparatively lower in hydrochar than in sludge cake across most fractions. Hydrochar REOM zone VI (9.5%) is substantially lower than sludge cake REOM (20.2%), suggesting that the melanoidin/lignocellulose-like structures associated with zone VI are more characteristic of the multi-step, sludge cake production process than of HTC. Zone VII remains consistently low across all hydrochar fractions (1.9–2.4%), confirming that HTC produces fulvic acid-like and melanoidin-like structures through thermal condensation rather than promoting the biological humification pathway that produces humic acid-like fluorescence in digested sludge (Collard et al., 2017; Jimenez et al., 2015).

The hydrochar EEM spectra provide the most visually distinctive profiles of all typologies and directly confirm the breadth of complexity across fractions. The H1 SPOM spectrum shows two distinct peaks: one at Ex~240nm/Em~400nm corresponding to zone IV (fulvic acid-like) and one at Ex~280-300nm/Em~450-480nm, corresponding to zone V/VI (glycolated protein-like/melanoidin-like). This peak pattern is not observed in any other typology at the SPOM level. The presence of both zone IV and zone V/VI peaks even in the most accessible water-soluble

fraction confirms that HTC produces fulvic acid-like and melanoidin-like aromatic structures that remain associated with the solid hydrochar surface and are captured by the mild $CaCl_2$ extraction, alongside the adsorbed NH_4^+, as discussed in the nitrogen fractionation section. The H1 REOM spectrum shows similarly dense and complex contours with dominant peaks in zones V/VI (Ex ~280-300nm/Em ~450-480nm) alongside zone IV contributions, reflecting the accumulation of glycolated protein-like, melanoidin-like and fulvic acid-like structures. The H1 SEOM spectrum shows broad, dense contours extending across zones IV, V and VI with additional signal toward zone VII (Ex ~400nm/Em ~480-500nm), suggesting the presence of both humic-like and fulvic acid-like compounds alongside the full range of thermally condensed structures. The H1 PEOM spectrum shows complex contours with contributions from zones IV, V, VI and VII simultaneously, consistent with the accumulation of the full spectrum of thermally condensed aromatic structures in the acid-extractable fraction, confirmed by the highest PEOM CR of all typologies (3.58) and the lowest simple zone proportion (21.7%).

Notably, zone VII (humic acid-like) in the PEOM fraction of sludge cake (5.3%) is lower than digested sludge PEOM (6.7%), despite more intensive processing, suggesting that thermal conditioning does not enhance biological humification but instead produces structurally distinct complex compounds dominated by zones IV and VI through a thermal condensation pathway.

5.3 PCA: which parameters best discriminate typologies?

5.3.1 PCA of Physicochemical Parameters

As already noted, the PCA results without the biochar sample will be discussed. The PCA of physicochemical parameters (Figure 14) explains 67.44% of total variance across the first two dimensions (Dim 1: 36.99%; Dim 2: 30.45%), indicating that the major axes of compositional differentiation among the sludge typologies are well captured by this reduced representation. Dimension 1 is defined by high organic content variables loading positively (Table 4); H (0.946), C (0.920), mgCOD/gTS (0.886), N (0.602), VS/TS (0.412), and mineralisation-associated variables loading negatively; P (-0.860), pH (-0.735), BaP (-0.565). This axis therefore represents a gradient from organic-rich, hydrogen-rich typologies toward more mineralised, phosphorus-enriched and alkaline typologies. Typologies scoring positively on dimension 1 are raw sludge and hydrothermally treated (T=140°C, WWWTP2) sludge that retain high elemental organic content and elevated COD per unit total solids and have a high volatility due to organic solids present. This is consistent with limited degradation and mineralisation of OM in raw sludge at the start of the processing chain, and thermally treated sludge at lower temperatures of 140°C. The negative

dimension 1 scores of sludge cake and hydrochar reflect a relative depletion of labile organic fractions and hydrogen-rich structures.

Dimension 2, driven by mgTKN/gTS (0.941), EC (0.895), TAN (0.775) and K (0.715) loading positively, and BaP (-0.442) and TS_raw (-0.718) loading negatively, separates typologies on the basis of nitrogen speciation and ionic composition against total solids content. The high positive dimension 2 scores of digested and thickened sludge reflect the accumulation of nitrogen and ammonia as well as an elevated electrical conductivity following AD, where the breakdown of proteins and deamination reactions release inorganic nitrogen into the liquid phase (Park et al., 2014).

Sludge cake and hydrochar are seen at negative values along dimension 2 indicating a high total solids content which is expected after dewatering and carbon condensation. The negative dimension 2 scores of sludge cake and hydrochar are consistent with TAN loss during thermal processing, where volatilisation of ammonia under elevated temperature conditions occurs (Horttanainen et al., 2017; Qin & Hu, 2018).

An interesting point is the elevated benzo(a)pyrene (BaP) in both sludge cake and hydrochar. BaP is a polycyclic aromatic hydrocarbon formed through pyrolytic condensation reactions. Its association with both typologies confirms that thermal processing, both thermal conditioning (sludge cake) and hydrothermal carbonisation (hydrochar), does not reduce PAH contamination, consistent with literature, reporting increased levels of BaP in sludge with increasing hydrothermal temperature (Peng et al., 2017). This is a significant finding for agronomic valorisation since BaP is a regulated contaminant in many jurisdictions for land application; the limits of BaP for sludge use in agriculture are 2 mg/kg in France and the proposed limits for the EU are 6 mg/kg (the EU limit is the sum of several common occurring PAHs) (Hudcová et al., 2019b). Values of BaP found in the samples in this database fall below these limits and are in the range of 0.079 mg/kg DM – 0.419 mg/kg DM.

The high levels of P in both thermally processed typologies relative to biologically processed ones reflect the concentration of phosphorus as OM is destroyed during thermal treatment, increasing P on a per-TS basis. This enrichment of P during the thermal treatment of sewage sludge has been reported in literature (Meng et al., 2019). In terms of fertiliser valorisation this could be of great advantage as thermally processed sludge products can be P-rich however, the agronomic availability of P depends on its speciation (Meng et al., 2019)

The positioning of dehydrated and thermally treated sludge in intermediate positions on the factor map in Figure 15, reflects the transitional nature of these typologies, retaining characteristics of their biological precursors while exhibiting partial physicochemical transformation.

The hierarchical clustering (Figure 15) of the physicochemical dataset yields four clusters.

Cluster 1 (negative Dim 1, negative Dim 2) groups sludge cake and hydrochar together, characterised by high TS_raw (v-test: 4.50), BaP (2.32) and P (3.23), and strongly negative contributions from mgTKN/gTS (-4.11), TAN (-2.70) and VS/TS (-2.81), reflecting the solid-phase, thermally processed character of both typologies and their depletion of labile nitrogen relative to total solids. The clustering of sludge cake and hydrochar together based on physicochemical characteristics is notable given their distinct thermal processing pathways. This may suggest that these bulk compositional properties, principally high solids content, low volatile fraction and elevated BaP, overlap across both thermal treatment routes.

Cluster 2 (negative Dim 1, positive Dim 2) groups digested and thickened sludge, defined by high EC (4.68), mgTKN/gTS (3.86), TAN (3.97) and K (2.66), consistent with nitrogen mineralisation during AD and the release of intracellular ions through microbial cell lysis. The products in this cluster could contribute to nutrient supply and balancing acidic content in soils. The clustering of digested and thickened sludge together confirms that thickening does not substantially alter bulk physicochemical composition.

Cluster 3 (near origin, positive Dim 2) contains dehydrated sludge, distinguished by elevated N (3.60), H (2.63) and VS/TS (2.17), suggesting retention of organic nitrogen and volatile matter relative to thermally processed typologies. This is further confirmation that mechanical dewatering does not alter the chemical composition of the solid fraction. From an agronomic perspective, these products could contribute primarily to OM input and nitrogen supply.

Cluster 4 (positive Dim 1, near-zero Dim 2) comprises raw sludge, characterised by high mgCOD/gTS (3.35), C (3.12) and H (2.82) and strongly negative P (-3.95) and pH (-3.60), consistent with high organic content and the absence of alkalinity or phosphorus enrichment associated with downstream processing. The primary division in the dendrogram separates the thermally processed solid-phase typologies (cluster 1) from all biologically processed typologies (clusters 2, 3 and 4), with the secondary division separating nitrogen-enriched digested and thickened sludge (cluster 2) from organic-rich raw and dehydrated sludge (clusters 3 and 4). Sludge products in this cluster have the potential to increase OM in depleted contexts and to help increase biological diversity in the soil.

5.3.2 PCA of Percentage Fluorescence across Fractions and Complexity Zones

The PCA applied to fluorescence variables in Figure 16, explains 75.62% of total variance across the first two dimensions (Dim 1: 62.34%; Dim 2: 13.28%), with Dim 1 alone accounting for the majority of variance. This strongly dominant first component indicates that the single primary axis

of differentiation (fluorescence complexity) structures the dataset markedly, with dimension 2 capturing a secondary yet meaningful gradient.

Dimension 1 is defined by a clear opposition between zones IV–VII variables loading positively ((Table 5) REOM_4: 0.954, REOM_5: 0.940, PEOM_5: 0.921, SEOM_4: 0.909, SPOM_4: 0.898, SEOM_5: 0.876, PEOM_4: 0.859, SPOM_6: 0.836) and zones I–III variables loading negatively across all fractions. This axis therefore represents a gradient from simple, protein-like fluorescent OM (negative Dim 1) to complex, aromatic and humic-like fluorescent OM (positive Dim 1), in accordance with findings in literature (Fernández-Domínguez et al., 2021; Jimenez et al., 2014). Raw sludge, digested sludge and thickened sludge occupy negative dimension 1 positions, confirming the predominance of protein-like and tyrosine/tryptophan-like fluorophores in biologically derived typologies. Sludge cake and hydrochar occupy strongly positive dimension 1 positions, reflecting the thermal condensation and aromatisation reactions that shift fluorescent OM toward zones IV–VI in both typologies. The consistency of this pattern across all four fractions demonstrates that the complexity shift induced by thermal processing is not confined to a single accessibility level but is expressed throughout the entire OM pool. This demonstrates the discriminatory power of fluorescent OM complexity as a characterisation parameter, and the capacity of the fractionation methodology to generate diagnostic data for evaluating the fertilisation and amendment potential of diverse sludge-derived products.

Dimension 2 represents a secondary gradient of OM accessibility within the complex fraction, showing a positive correlation for high zone VI–VII contributions in less accessible fractions (PEOM_7 (0.888), PEOM_6 (0.813) and moderately accessible fractions REOM_6 (0.590), REOM_7 (0.451)) and negative for zone II–III contributions in more accessible fractions (SPOM_5 (-0.505), REOM_2 (-0.447), REOM_3 (-0.399)). This confirms the bioaccessibility axis, affording a matrix representation of indicators, in agreement with findings by Jimenez et al., 2014.

Sludge cake scores positively on dimension 2, indicating that its complex OM is concentrated in the less accessible PEOM fraction in zones VI–VII, consistent with Maillard-type condensation products accumulating in recalcitrant structural fractions (Li et al., 2024). Hydrochar scores negatively on dimension 2, indicating that despite its high overall complexity (positive Dim 1), its fluorescent OM is more evenly distributed across accessible fractions with greater contributions from zones II–III in SPOM, suggesting that hydrothermal carbonisation produces aromatic structures that are comparatively more accessible than the thermally condensed compounds of sludge cake.

The hierarchical clustering (Figure 17) presents four clusters; Cluster 1 (negative Dim 1, near-zero Dim 2) comprises raw sludge samples, characterised by high zone I–III contributions across all fractions, the highest positive v-test scores in this cluster are for PEOM_1, REOM_1, SEOM_1

and PEOM_3, confirming protein-like OM dominance. Cluster 2 (negative Dim 1, slightly positive Dim 2) groups digested and thickened sludge together, distinguished from raw sludge by higher PEOM_7 and reduced zone I contributions, reflecting labile OM consumption during AD (Jimenez et al., 2015). Cluster 3 (positive Dim 1, positive Dim 2) contains sludge cake samples, defined by high zone IV–VII contributions across REOM and SEOM fractions and elevated PEOM_6, consistent with thermally induced condensation producing structurally complex recalcitrant compounds. Cluster 4 (positive Dim 1, negative Dim 2) comprises hydrochar samples, characterised by high zone IV–V contributions in SPOM, REOM and SEOM and low zone VI–VII in PEOM, reflecting the dominance of aromatic but less humified structures produced by hydrothermal carbonisation.

The large inertia gain at the two-cluster partition visible in the dendrogram confirms that the primary division in the dataset is between thermochemically processed typologies (clusters 3 and 4) and biologically processed typologies (clusters 1 and 2), with thermochemical processing representing the dominant source of fluorescent OM complexity differentiation across the sample set.

Taken together, the fluorescence PCA resolves the sludge typologies along two orthogonal compositional gradients that jointly characterise the fate of OM across the treatment sequence. The dominant gradient, dimension 1, represents a progression from simple, protein-dominated fluorescent OM in biologically derived typologies toward thermally condensed, aromatic and humic-like fluorescent OM in thermally processed products. This gradient is driven consistently across all four accessibility fractions, confirming that fluorescent OM complexity is the single most discriminating parameter in the dataset. The secondary gradient further resolves the thermally processed typologies by the accessibility distribution of their complex OM, separating sludge cake (recalcitrant, PEOM-concentrated zone VI–VII structures) from hydrochar (comparatively accessible, SPOM-distributed zone IV–V structures). This suggests that indicators of bioaccessibility and OM complexity may offer greater predictive power for fertiliser or soil amendment quality than treatment type alone.

In terms of typology distribution, the PCA space describes a trajectory from raw sludge (simple, protein-rich, biologically labile) through digested and thickened sludge (intermediate complexity, protein-rich and biologically humified) to thermally processed products (highly complex, recalcitrant, aromatised), broadly corresponding to increasing treatment intensity and decreasing biological availability of OM.

In this specific dataset, the fluorescence fractionation approach resolves this trajectory with a greater clarity than physicochemical parameters alone, demonstrating its particular utility as a diagnostic framework for

i. evaluating the organic matter quality and fate;
ii. evaluating the agronomic valorisation potential;
iii. identifying treatment gradients;
iv. providing a clear summary of multiple types of variables.

6 Conclusion

The chemical characterisation of sludge organic matter and nutrients is a crucial field of investigation which can supply knowledge and innovative tools to optimize the recycling of sludge (Muller et al., 2014). Despite extensive prior research on organic fertilisers, no studies have comprehensively characterised SS and its diverse derivatives across organic matter accessibility, molecular complexity and nutrient distribution within a single, internally consistent dataset**.** This study addresses that gap by applying a deep characterisation methodology - the ISBAMO sequential extraction framework combined with 3D fluorescence spectroscopy – uniformly, across 29 sludge samples within a single analytical campaign. This integrated approach resolves sludge products specific differences in organic matter bioaccessibility, molecular complexity and nutrient distribution that bulk physicochemical parameters alone cannot capture, providing a basis for evaluating the agronomic efficiency and environmental safety of diverse sludge-derived fertiliser products.

A fundamental finding is the decoupling of carbon and nitrogen transformation fates across the treatment chain. Organic carbon follows a pathway of progressive stabilisation: labile, accessible fractions are selectively consumed during anaerobic digestion and further complexified during thermochemical treatment, producing an increasingly recalcitrant residue enriched in poorly accessible and non-accessible organic matter fractions. Nitrogen, by contrast, is governed primarily by phase separation processes: mineralised to ammonium during biological treatment and concentrated in the soluble phase (digested and thickened sludge), then either retained in the solid product or removed with the press filtrate (sludge cake). Hydrochar represents a distinct case in which both carbon and nitrogen are simultaneously transformed by thermochemical reactions: carbon condensed into aromatic structures retained in the solid fraction, and nitrogen partially transferred to the process water and partially incorporated into recalcitrant heterocyclic structures. These divergent pathways mean that no single typology simultaneously optimises organic carbon accessibility and nitrogen accessibility, a distinction with direct implications for agronomic valorisation strategy and fertiliser product design. Depending on the objective (soil organic matter stabilisation, mineral nitrogen supply, readily available carbon), the process can be optimised accordingly. An integrated approach is therefore required, in which soil requirements

are first assessed and sludge-derived fertiliser products are subsequently selected and tailored to meet these needs using multiple treatment pathways.

The physicochemical clustering analysis provides a basis for differentiating the agronomic potential of sludge-derived products beyond treatment classification. Cluster 1, grouping sludge cake and hydrochar, is characterised by high total solids, elevated phosphorus (P) and Benzo(a)pyrene (BaP), and severely depleted labile nitrogen, suggesting potential application for phosphorus supply on P-deficient soils, subject to regulatory constraints on BaP content. Cluster 2, comprising digested and thickened sludge, is defined by high ammonia, electrical conductivity and potassium (K), positioning these products as the most promising for nitrogen and potassium fertilizer supply to crops. Cluster 3, containing dehydrated sludge, retains elevated organic nitrogen and volatile matter, suggesting a role primarily in organic matter input and gradual nitrogen release in crop rotations. Cluster 4, comprising raw sludge, is characterised by high organic carbon content and low pH, indicating potential for organic matter replenishment in soils at risk of erosion and structural degradation or for targeting pH correction on marginal lands. However, pathogen and contaminant risk associated with untreated sludge must be considered. This cluster-based differentiation supports the principle that soil requirements should first be assessed and sludge-derived fertiliser products subsequently selected and tailored to meet these needs, rather than treating sludge products as interchangeable based on treatment type alone.

The environmental safety of these typologies is shaped principally by contaminant profiles. The association of elevated BaP concentrations with both thermochemically processed typologies, sludge cake and hydrochar, confirmed through their shared physicochemical cluster in the PCA, constitutes a significant regulatory constraint on direct land application under current European legislation and must be central to any valorisation pathway assessment. Although this data includes only one contaminant, this finding underlines the fundamental tension in thermochemical sludge treatment: while high-temperature processing eliminates pathogen risk, it does not necessarily eliminate PAH contamination and checking the compliance to regulation is mandatory before soil application (Meng et al., 2019). However, the actual risk depends not only on the concentration of a contaminant per se, but the application rate and the resulting exposure. Soil assays are therefore needed to simulate field applications and account for nutrient losses, plant uptake dynamics and, critically, the contrasting bioavailability and fate of contaminants for the diverse sludge-derived products, which can strongly alter contaminant mobility and risk in soil. Only through such integrated assessment can appropriate application rates be established, enabling controlled land use of sludge-derived products that minimises contaminant risk while maximising agronomic benefit.

Another key finding of this work is the compositional trajectory observed for typologies into the PCA space. The clustering based on fluorescence PCA data shows sludge products occupying a distinct gradient, demonstrating that organic matter complexity is the single most discriminating parameter across the typology dataset, explaining 62.34% of total variance on the primary axis alone. The secondary accessibility gradient further distinguishes sludge cake from hydrochar despite their similar bulk complexity. This distinction is invisible to physicochemical characterisation but clearly resolved by the fractionation-fluorescence variables. Together, these two gradients define a compositional space in which typologies distribute according to treatment intensity and thermochemical pathway, suggesting that bioaccessibility and complexity indicators offer greater predictive power for fertiliser and soil amendment quality assessment than treatment or physicochemical classification alone.

This work shows how the ISBAMO sequential extraction framework, combined with 3D fluorescence spectroscopy and multivariate analysis, demonstrates clear utility as a diagnostic tool for sludge characterisation. Applied consistently across a diverse set of sludge-derived typologies, it represents a transferable and scalable characterisation framework applicable to the broadening range of sludge-derived products entering the organic fertiliser market under evolving European regulatory frameworks.

Some limitations of the present work should be acknowledged. Chemical sequential extraction provides a proxy for bioaccessibility under defined chemical conditions and does not directly measure biological availability. This would require complementary bioassay data, such as biochemical methane potential (BMP). The hydrochar samples originate from different processing facilities, introducing feedstock and process variability that limits direct comparison with typologies originating from a single WWTP, but demonstrate its reduced variability as a sludge product.

Future work should prioritise the integration of phosphorus speciation analysis, biological availability assays and a broader contaminant screening to complement the organic matter characterisation presented here. A further priority for future work is the validation of the ISBAMO-derived complexity and accessibility indicators against measured carbon mineralisation rates. Establishing these correlations would enable the use of fractionation and fluorescence-derived indicators as input variables for dynamic process models predicting organic matter fate in soil following land application, such as the PLS model for carbon biodegradability in soil proposed by Jimenez et al., 2017. This would advance the framework from a descriptive characterisation tool toward a predictive model for carbon turnover in agroecosystems. For the agronomic valorisation of sludge-derived products, accurate prediction of organic carbon mineralisation in soil is particularly meaningful, as it directly informs estimates of carbon sequestration potential, greenhouse gas emissions associated with land application, and the contribution of sludge-derived

organic matter to long-term soil carbon stocks (Fernández-Domínguez et al., 2021; Jimenez et al., 2017). These aspects are critical considerations for evaluating the environmental sustainability of sludge recycling in agriculture.

Beyond characterisation, these findings support evidence-based selection of valorisation pathways and can inform regulatory decision-making on the agronomic use of the growing suite of sludge-derived fertiliser products. Altogether, the characterisation database established in this study offers a reference to improve the efficiency and safety of sludge-derived product recycling and provides a foundation for designing future strategies that align nutrient circularity with soil health and environmental safety goals.

Contribution Statement

Unless otherwise stated, all work presented in this thesis, including laboratory analyses, data processing, statistical analysis, and interpretation of results was carried out by the author. Other contributions are outlined below:

The sample collection was completed by different treatment plant operators. Sample pretreatment (centrifugation, filtration, freeze-drying and grinding) and several physicochemical measurements (TS, VS, pH, EC and CHNS) were completed by Erika Sinisgalli, prior to the author's work.

Declaration of generative AI and AI-assisted technologies in the manuscript preparation process

During the preparation of this work, the author used Claude AI for language editing and rephrasing, and for troubleshooting support related to data analysis (R, Excel). After using this tool, the author reviewed, verified, and edited all content as needed, and takes full responsibility for the final text and its scientific content.

7 Bibliography

Abou Jaoude, L., H. Mohtar, R., Kamaleddine, F., Dbaibo, R., Bou Said, R., Keniar, I., & F. Yanni, S. (2025). Impact of treated wastewater sludge on soil and wheat growth characteristics in a semi-arid climate. *Science of The Total Environment*, *974*, 179166. https://doi.org/10.1016/j.scitotenv.2025.179166

Aboulfoth, A. M., Gohary, E. H. E., & Monayeri, O. D. E. (2015). EFFECT OF THERMAL PRETREATMENT ON THE SOLUBILIZATION OF ORGANIC MATTERS IN A MIXTURE OF PRIMARY AND WASTE ACTIVATED SLUDGE. *Journal of Urban and Environmental Engineering*.

Adhikari, K., Pearce, C. I., Sanguinet, K. A., Bary, A. I., Chowdhury, I., Eggleston, I., Xing, B., & Flury, M. (2024). Accumulation of microplastics in soil after long-term application of biosolids and atmospheric deposition. *Science of The Total Environment*, *912*, 168883. https://doi.org/10.1016/j.scitotenv.2023.168883

Aemig, Q., Doussiet, N., Danel, A., Delgenès, N., Jimenez, J., Houot, S., & Patureau, D. (2019). Organic micropollutants' distribution within sludge organic matter fractions explains their dynamic during sewage sludge anaerobic digestion followed by composting. *Environmental Science and Pollution Research*, *26*(6), 5820–5830. https://doi.org/10.1007/s11356-018-4014-7

Ahmad, M., Rajapaksha, A. U., Lim, J. E., Zhang, M., Bolan, N., Mohan, D., Vithanage, M., Lee, S. S., & Ok, Y. S. (2014). Biochar as a sorbent for contaminant management in soil and water: A review. *Chemosphere*, *99*, 19–33. https://doi.org/10.1016/j.chemosphere.2013.10.071

Alipour, M., Asadi, H., Chen, C., & Besalatpour, A. A. (2022). Fate of organic pollutants in sewage sludge during thermal treatments: Elimination of PCBs, PAHs, and PPCPs. *Fuel*, *319*, 123864. https://doi.org/10.1016/j.fuel.2022.123864

Álvarez, M. L., Gascó, G., Plaza, C., Paz-Ferreiro, J., & Méndez, A. (2017). Hydrochars from Biosolids and Urban Wastes as Substitute Materials for Peat. *Land Degradation & Development*, *28*(7), 2268–2276. https://doi.org/10.1002/ldr.2756

Amir, S., Hafidi, M., Merlina, G., Hamdi, H., & Revel, J.-C. (2004). Elemental analysis, FTIR and 13C-NMR of humic acids from sewage sludge composting. *Agronomie*, *24*(1), 13–18. https://doi.org/10.1051/agro:2003054

An-nori, A., Ezzariai, A., El Mejahed, K., El Fels, L., El Gharous, M., & Hafidi, M. (2022). Solar Drying as an Eco-Friendly Technology for Sewage Sludge Stabilization: Assessment of Micropollutant Behavior, Pathogen

Removal, and Agronomic Value. *Frontiers in Environmental Science*, *10*, 814590. https://doi.org/10.3389/fenvs.2022.814590

Arvaniti, O. S., Fountoulakis, M. S., Gatidou, G., Kalantzi, O.-I., Vakalis, S., & Stasinakis, A. S. (2024). Perfluoroalkyl and polyfluoroalkyl substances in sewage sludge: Challenges of biological and thermal treatment processes and potential threats to the environment from land disposal. *Environmental Sciences Europe*, *36*(1), 207. https://doi.org/10.1186/s12302-024-01031-3

Babić, S., & Mutavdžić Pavlović, D. (2013). Analysis of PhACs in Solid Environmental Samples (Soil, Sediment, and Sludge). In *Comprehensive Analytical Chemistry* (Vol. 62, pp. 129–167). Elsevier. https://doi.org/10.1016/B978-0-444-62657-8.00005-7

Balkrishna, A., Kaushik, P., Singh, S., Agrahari, P., Kumar, B., Kumar, P., & Arya, V. P. (2025). Potential use of sewage sludge as fertilizer in organic farming. *Cleaner Waste Systems*, *10*, 100245. https://doi.org/10.1016/j.clwas.2025.100245

Bolan, N., Sarkar, B., Vithanage, M., Singh, G., Tsang, D. C. W., Mukhopadhyay, R., Ramadass, K., Vinu, A., Sun, Y., Ramanayaka, S., Hoang, S. A., Yan, Y., Li, Y., Rinklebe, J., Li, H., & Kirkham, M. B. (2021). Distribution, behaviour, bioavailability and remediation of poly- and per-fluoroalkyl substances (PFAS) in solid biowastes and biowaste-treated soil. *Environment International*, *155*, 106600. https://doi.org/10.1016/j.envint.2021.106600

Bona, D., Bertoldi, D., Borgonovo, G., Mazzini, S., Ravasi, S., Silvestri, S., Zaccone, C., Giannetta, B., & Tambone, F. (2023). Evaluating the potential of hydrochar as a soil amendment. *Waste Management*, *159*, 75–83. https://doi.org/10.1016/j.wasman.2023.01.024

Bourdat-Deschamps, M., Ferhi, S., Bernet, N., Feder, F., Crouzet, O., Patureau, D., Montenach, D., Moussard, G. D., Mercier, V., Benoit, P., & Houot, S. (2017). Fate and impacts of pharmaceuticals and personal care products after repeated applications of organic waste products in long-term field experiments. *Science of The Total Environment*, *607–608*, 271–280. https://doi.org/10.1016/j.scitotenv.2017.06.240

Chen, H. (2023). *Effets à long terme d'apports répétés de produits résiduaires organiques en agriculture sur la production agricole et la fertilité des sols: Apports des résultats de deux essais au champ de longue durée*

en France [Doctorat ès Sciences de l'environnement, PhD, université Paris-Saclay]. https://doi.org/10.70675/1179d467z56daz40cdz87bazd45dde8f0215

Chen, H., Levavasseur, F., Montenach, D., Lollier, M., Morel, C., & Houot, S. (2022). An 18-year field experiment to assess how various types of organic waste used at European regulatory rates sustain crop yields and C, N, P, and K dynamics in a French calcareous soil. *Soil and Tillage Research*, *221*, 105415. https://doi.org/10.1016/j.still.2022.105415

Chiaramonti, D., Lotti, G., Vaccari, F. P., & Sanei, H. (2024). Assessment of long-lived Carbon permanence in agricultural soil: Unearthing 15 years-old biochar from long-term field experiment in vineyard. *Biomass and Bioenergy*, *191*, 107484. https://doi.org/10.1016/j.biombioe.2024.107484

Ciaciuch, A., Gaca, J., & Lelewer, K. (2017). Effect of the two-stage thermal disintegration and anaerobic digestion of sewage sludge on the COD fractions. *Polish Journal of Chemical Technology*, *19*(3), 130–135. https://doi.org/10.1515/pjct-2017-0059

Collard, M., Teychené, B., & Lemée, L. (2017). Comparison of three different wastewater sludge and their respective drying processes: Solar, thermal and reed beds – Impact on organic matter characteristics. *Journal of Environmental Management*, *203*, 760–767. https://doi.org/10.1016/j.jenvman.2016.05.070

Colombini, G., Rumpel, C., Houot, S., Biron, P., & Dignac, M.-F. (2022). A long-term field experiment confirms the necessity of improving biowaste sorting to decrease coarse microplastic inputs in compost amended soils. *Environmental Pollution*, *315*, 120369. https://doi.org/10.1016/j.envpol.2022.120369

Dominguez, D. F. (2023). *Characterize and control the organic matter fate during anaerobic digestion to optimize the agronomic value of digestates*.

Durak, H. (2023). Comprehensive Assessment of Thermochemical Processes for Sustainable Waste Management and Resource Recovery. *Processes*, *11*(7), 2092. https://doi.org/10.3390/pr11072092

Eid, E. M., Ahmed, M. T., Alrumman, S. A., Salama, S. G., Khattab, K. A., Kumar, P., Širić, I., & Sewelam, N. (2026). Application of sewage sludge as a soil biofertilizer enhances crop productivity of alfalfa plants (Medicago sativa L.) and improves soil quality without heavy metal toxicity. *Scientific Reports*, *16*(1), 8524. https://doi.org/10.1038/s41598-026-39561-w

EU Commission. (2019). EU, 2019. EU Law and Publications. Regulation (EU) 2019/1009 of the European Parliament and of the Council of 5 June 2019 Laying Down Rules on the Making Available on the Market of EU Fertilising Products and Amending Regulations (EC) No 1069/2009 and (EC) No 1107/2009 and Repealing Regulation (EC) No 2003/2003; UE 2019/1009; EU Law and Publications: Luxembourg, 2019, http://data.europa.eu/eli/reg/2019/1009/oj. *EU 2019/1009*, *1009*(1009).

EurEau. (2021). *Note on sludge management*.

European Comission. (1986). *"Council Directive 86/278/EEC of 12 June 1986 on the protection of the environment, and in particular of the soil, when sewage sludge is used in agriculture."*

Eurostat. (2022). *Sewage sludge production and disposal* [Dataset]. Eurostat. https://doi.org/10.2908/ENV_WW_SPD

Fan, Y., Hornung, U., & Dahmen, N. (2022). Hydrothermal liquefaction of sewage sludge for biofuel application: A review on fundamentals, current challenges and strategies. *Biomass and Bioenergy*, *165*, 106570. https://doi.org/10.1016/j.biombioe.2022.106570

Feng, J., Burke, I. T., Chen, X., & Stewart, D. I. (2023). Assessing metal contamination and speciation in sewage sludge: Implications for soil application and environmental risk. *Reviews in Environmental Science and Bio/Technology*, *22*(4), 1037–1058. https://doi.org/10.1007/s11157-023-09675-y

Fernández-Domínguez, D., Guilayn, F., Patureau, D., & Jimenez, J. (2022). Characterising the stability of the organic matter during anaerobic digestion: A selective review on the major spectroscopic techniques. *Reviews in Environmental Science and Bio/Technology*, *21*(3), 691–726. https://doi.org/10.1007/s11157-022-09623-2

Fernández-Domínguez, D., Patureau, D., Houot, S., Sertillanges, N., Zennaro, B., & Jimenez, J. (2021). Prediction of organic matter accessibility and complexity in anaerobic digestates. *Waste Management*, *136*, 132–142. https://doi.org/10.1016/j.wasman.2021.10.004

Gebretsadkan, A. A., Belete, Y. Z., Krounbi, L., Gelfand, I., Bernstein, R., & Gross, A. (2024). Soil application of activated hydrochar derived from sewage sludge enhances plant growth and reduces nitrogen loss. *Science of The Total Environment*, *949*, 174965. https://doi.org/10.1016/j.scitotenv.2024.174965

Gizaw, D. G., Periyasamy, S., Redda, Z. T., John, B. I., Baylie Mengstie, H., & Asaithambi, P. (2024). A comprehensive review on sewage sludge as sustainable feedstock for bioenergy production. *Environmental Quality Management*, *33*(3), 223–238. https://doi.org/10.1002/tqem.22116

Green Horizon Farmers Network. (2019). *Note on Fertilising Products Regulation (EU) 2019/1009)*.

Guilayn, F., Rouez, M., Crest, M., Patureau, D., & Jimenez, J. (2020). Valorization of digestates from urban or centralized biogas plants: A critical review. *Reviews in Environmental Science and Bio/Technology*, *19*(2), 419–462. https://doi.org/10.1007/s11157-020-09531-3

Guo, L., Zhang, B., Xiao, K., Zhang, Q., & Zheng, M. (2009). Levels and distributions of polychlorinated biphenyls in sewage sludge of urban wastewater treatment plants. *Journal of Environmental Sciences*, *21*(4), 468–473. https://doi.org/10.1016/S1001-0742(08)62293-7

Horttanainen, M., Deviatkin, I., & Havukainen, J. (2017). Nitrogen release from mechanically dewatered sewage sludge during thermal drying and potential for recovery. *Journal of Cleaner Production*, *142*, 1819–1826. https://doi.org/10.1016/j.jclepro.2016.11.102

Hudcová, H., Vymazal, J., & Rozkošný, M. (2019a). Present restrictions of sewage sludge application in agriculture within the European Union. *Soil and Water Research*, *14*(2), 104–120. https://doi.org/10.17221/36/2018-SWR

Hudcová, H., Vymazal, J., & Rozkošný, M. (2019b). Present restrictions of sewage sludge application in agriculture within the European Union. *Soil and Water Research*, *14*(2), 104–120. https://doi.org/10.17221/36/2018-SWR

IEA. (2021). *Bioenergy HTC-Valorisation-of-organic-wastes-and-sludges-for-hydrochar-production-and-biofertilizers-Full-Report*.

Ippolito, J. A., Ducey, T. F., Diaz, K., & Barbarick, K. A. (2021). Long-term biosolids land application influences soil health. *Science of The Total Environment*, *791*, 148344. https://doi.org/10.1016/j.scitotenv.2021.148344

Jimenez, J., Aemig, Q., Doussiet, N., Steyer, J.-P., Houot, S., & Patureau, D. (2015). A new organic matter fractionation methodology for organic wastes: Bioaccessibility and complexity characterization for treatment optimization. *Bioresource Technology*, *194*, 344–353. https://doi.org/10.1016/j.biortech.2015.07.037

Jimenez, J., Gonidec, E., Cacho Rivero, J. A., Latrille, E., Vedrenne, F., & Steyer, J.-P. (2014). Prediction of anaerobic biodegradability and bioaccessibility of municipal sludge by coupling sequential extractions with fluorescence spectroscopy: Towards ADM1 variables characterization. *Water Research*, *50*, 359–372. https://doi.org/10.1016/j.watres.2013.10.048

Jimenez, J., Grigatti, M., Boanini, E., Patureau, D., & Bernet, N. (2020). The impact of biogas digestate typology on nutrient recovery for plant growth: Accessibility indicators for first fertilization prediction. *Waste Management*, *117*, 18–31. https://doi.org/10.1016/j.wasman.2020.07.052

Jimenez, J., Lei, H., Steyer, J.-P., Houot, S., & Patureau, D. (2017). Methane production and fertilizing value of organic waste: Organic matter characterization for a better prediction of valorization pathways. *Bioresource Technology*, *241*, 1012–1021. https://doi.org/10.1016/j.biortech.2017.05.176

Kominko, H., Gorazda, K., & Wzorek, Z. (2024). Sewage sludge: A review of its risks and circular raw material potential. *Journal of Water Process Engineering*, *63*, 105522. https://doi.org/10.1016/j.jwpe.2024.105522

Laera, A., Shakeri Yekta, S., Hedenström, M., Buzier, R., Guibaud, G., Dario, M., Esposito, G., & Van Hullebusch, E. D. (2019). A simultaneous assessment of organic matter and trace elements bio-accessibility in substrate and digestate from an anaerobic digestion plant. *Bioresource Technology*, *288*, 121587. https://doi.org/10.1016/j.biortech.2019.121587

Lamastra, L., Suciu, N. A., & Trevisan, M. (2018). Sewage sludge for sustainable agriculture: Contaminants' contents and potential use as fertilizer. *Chemical and Biological Technologies in Agriculture*, *5*(1), 10. https://doi.org/10.1186/s40538-018-0122-3

Landeros Gonzalez, G. V., Dominguez Cortinas, G., Hudson, M., Shaw, P., & Williams, I. D. (2022). A Review of the Origins of Microplastics arriving at Wastewater Treatment Plants. *Detritus*, (20), 41–55. https://doi.org/10.31025/2611-4135/2022.15224

Lashermes, G., Nicolardot, B., Parnaudeau, V., Thuriès, L., Chaussod, R., Guillotin, M. L., Linères, M., Mary, B., Metzger, L., & Morvan, T. (2009). Typology of exogenous organic matters based on chemical and biochemical composition to predict potential nitrogen mineralization. *Bioresource Technology*, S0960852409010529. https://doi.org/10.1016/j.biortech.2009.08.025

Li, Y., Zhang, Q., Xiao, S., Yang, Q., Wang, L., & Hao, J. (2024). Review of Melanoidins as By-Product from Thermal Hydrolysis of Sludge: Properties, Hazards, and Removal. *Processes*, *12*(1), 135. https://doi.org/10.3390/pr12010135

Liu, L., Wang, Y., Wang, J., He, C., & Zhang, J. (2026). Recovery of nitrogen and phosphorus in sewage sludge treatment technologies. *Chinese Chemical Letters*, *37*(3), 111431. https://doi.org/10.1016/j.cclet.2025.111431

Lucia, C., Badalucco, L., Corsino, S. F., Galati, A., Iovino, M., Muscarella, S. M., Paliaga, S., Torregrossa, M., & Laudicina, V. A. (2025a). Management and valorisation of sewage sludge to foster the circular economy in the agricultural sector. *Discover Soil*, *2*(1), 80. https://doi.org/10.1007/s44378-025-00105-9

Lucia, C., Badalucco, L., Corsino, S. F., Galati, A., Iovino, M., Muscarella, S. M., Paliaga, S., Torregrossa, M., & Laudicina, V. A. (2025b). Management and valorisation of sewage sludge to foster the circular economy in the agricultural sector. *Discover Soil*, *2*(1), 80. https://doi.org/10.1007/s44378-025-00105-9

Mailler, R., Gasperi, J., Patureau, D., Vulliet, E., Delgenes, N., Danel, A., Deshayes, S., Eudes, V., Guerin, S., Moilleron, R., Chebbo, G., & Rocher, V. (2017). Fate of emerging and priority micropollutants during the sewage sludge treatment: Case study of Paris conurbation. Part 1: Contamination of the different types of sewage sludge. *Waste Management*, *59*, 379–393. https://doi.org/10.1016/j.wasman.2016.11.010

McGrath, S. P., Chaudri, A. M., & Giller, K. E. (1995). Long-term effects of metals in sewage sludge on soils, microorganisms and plants. *Journal of Industrial Microbiology*, *14*(2), 94–104. https://doi.org/10.1007/BF01569890

Melo, T. M., Bottlinger, M., Schulz, E., Leandro, W. M., Botelho De Oliveira, S., Menezes De Aguiar Filho, A., El-Naggar, A., Bolan, N., Wang, H., Ok, Y. S., & Rinklebe, J. (2019). Management of biosolids-derived hydrochar (Sewchar): Effect on plant germination, and farmers' acceptance. *Journal of Environmental Management*, *237*, 200–214. https://doi.org/10.1016/j.jenvman.2019.02.042

Melo, T. M., Bottlinger, M., Schulz, E., Leandro, W. M., Menezes De Aguiar Filho, A., Wang, H., Ok, Y. S., & Rinklebe, J. (2018). Plant and soil responses to hydrothermally converted sewage sludge (sewchar). *Chemosphere*, *206*, 338–348. https://doi.org/10.1016/j.chemosphere.2018.04.178

Meng, X., Huang, Q., Xu, J., Gao, H., & Yan, J. (2019). A review of phosphorus recovery from different thermal treatment products of sewage sludge. *Waste Disposal & Sustainable Energy*, *1*(2), 99–115. https://doi.org/10.1007/s42768-019-00007-x

Michaud, A. M., Caradec, L., Tampio, E., Laakso, J., Jimenez, J., & Houot, S. (2026). Clustering of Exogenous Organic Material Properties to Improve Their Efficient Recycling in European Agriculture. *European Journal of Soil Science*, *77*(1), e70261. https://doi.org/10.1111/ejss.70261

Michaud, A. M., Dunsin Saliu, T., Munoz, G., Feder, F., Sappin-Didier, V., Watteau, F., Houot, S., & Sauvé, S. (2025). In situ occurrence and mobility of per and polyfluoroalkyl substances in soils amended with organic waste products. *Science of The Total Environment*, *984*, 179708. https://doi.org/10.1016/j.scitotenv.2025.179708

Mohammed, R., Zhang, Z.-F., Kan, Z., Jiang, C., Liu, L.-Y., Ma, W.-L., Song, W.-W., Nikolaev, A., & Li, Y.-F. (2021). Determination of Polycyclic Aromatic Hydrocarbons and Their Methylated Derivatives in Sewage Sludge from Northeastern China: Occurrence, Profiles and Toxicity Evaluation. *Molecules*, *26*(9), 2739. https://doi.org/10.3390/molecules26092739

Muller, M., Jimenez, J., Antonini, M., Dudal, Y., Latrille, E., Vedrenne, F., Steyer, J.-P., & Patureau, D. (2014). Combining chemical sequential extractions with 3D fluorescence spectroscopy to characterize sludge organic matter. *Waste Management*, *34*(12), 2572–2580. https://doi.org/10.1016/j.wasman.2014.07.028

Munoz, G., Michaud, A. M., Liu, M., Vo Duy, S., Montenach, D., Resseguier, C., Watteau, F., Sappin-Didier, V., Feder, F., Morvan, T., Houot, S., Desrosiers, M., Liu, J., & Sauvé, S. (2022). Target and Nontarget Screening of PFAS in Biosolids, Composts, and Other Organic Waste Products for Land Application in France. *Environmental Science & Technology*, *56*(10), 6056–6068. https://doi.org/10.1021/acs.est.1c03697

Mustonen, K., Deviatkin, I., Havukainen, J., & Horttanainen, M. (2018). Nitrogen behaviour during thermal drying of mechanically dewatered biosludge from pulp and paper industry. *Environmental Technology*, *39*(8), 1052–1060. https://doi.org/10.1080/09593330.2017.1319879

Nahar, K., Thulasiraman, A. V., Vuppaladadiyam, A. K., Hakeem, I. G., & Shah, K. (2024). Current understanding on the fate of contaminants during hydrothermal treatment of sewage sludge. *Current Opinion in Green and Sustainable Chemistry*, *49*, 100960. https://doi.org/10.1016/j.cogsc.2024.100960

Park, J., Park, S., & Kim, M. (2014). Anaerobic degradation of amino acids generated from the hydrolysis of sewage sludge. *Environmental Technology*, *35*(9), 1133–1139. https://doi.org/10.1080/09593330.2013.863951

Parnaudeau, V., Nicolardot, B., & Pagès, J. (2004). Relevance of Organic Matter Fractions as Predictors of Wastewater Sludge Mineralization in Soil. *Journal of Environmental Quality*, *33*(5), 1885–1894. https://doi.org/10.2134/jeq2004.1885

Peng, N., Li, Y., Liu, T., Lang, Q., Gai, C., & Liu, Z. (2017). Polycyclic Aromatic Hydrocarbons and Toxic Heavy Metals in Municipal Solid Waste and Corresponding Hydrochars. *Energy & Fuels*, *31*(2), 1665–1671. https://doi.org/10.1021/acs.energyfuels.6b02964

Pokharel, U., Neelgund, G., Ray, R. L., Balan, V., & Kumar, S. (2025). Biochar for Soil Amendment: Applications, Benefits, and Environmental Impacts. *Bioengineering*, *12*(11), 1137. https://doi.org/10.3390/bioengineering12111137

Qin, Y., & Hu, S. (2018). Study on Release Characteristics and Recovery of Nitrogen and Phosphorus during the Anaerobic Fermentation of Excess Sludge. *IOP Conference Series: Earth and Environmental Science*, *108*, 042018. https://doi.org/10.1088/1755-1315/108/4/042018

Racek, J., Sevcik, J., Chorazy, T., Kucerik, J., & Hlavinek, P. (2020). Biochar – Recovery Material from Pyrolysis of Sewage Sludge: A Review. *Waste and Biomass Valorization*, *11*(7), 3677–3709. https://doi.org/10.1007/s12649-019-00679-w

Rombolà, A. G., Meredith, W., Snape, C. E., Baronti, S., Genesio, L., Vaccari, F. P., Miglietta, F., & Fabbri, D. (2015). Fate of Soil Organic Carbon and Polycyclic Aromatic Hydrocarbons in a Vineyard Soil Treated with Biochar. *Environmental Science & Technology*, *49*(18), 11037–11044. https://doi.org/10.1021/acs.est.5b02562

Romero-Güiza, M. S., Flotats, X., Asiain-Mira, R., & Palatsi, J. (2022). Enhancement of sewage sludge thickening and energy self-sufficiency with advanced process control tools in a full-scale wastewater treatment plant. *Water Research*, *222*, 118924. https://doi.org/10.1016/j.watres.2022.118924

Saliu, T. D., Michaud, A. M., Munoz, G., Dinh, Q. T., Feder, F., Arrouy, L., Sappin-Didier, V., Watteau, F., Houot, S., Liu, J., & Sauvé, S. (2025). Influence of organic waste amendments on uptake of per and polyfluoroalkyl substances from soil to crops: Insights from long-term field experiments. *Science of The Total Environment*, *996*, 180156. https://doi.org/10.1016/j.scitotenv.2025.180156

Salva, J., Sečkár, M., Schwarz, M., Samešová, D., Mordáčová, M., Poništ, J., & Veverková, D. (2025). Analysis of the current state of sewage sludge treatment from the perspective of current European directives. *Environmental Sciences Europe*, *37*(1), 59. https://doi.org/10.1186/s12302-025-01097-7

Schnell, M., Horst, T., & Quicker, P. (2020). Thermal treatment of sewage sludge in Germany: A review. *Journal of Environmental Management*, *263*, 110367. https://doi.org/10.1016/j.jenvman.2020.110367

Sutton, P. M. A., Thornton, C., & Montanarella, D. L. (2016). *Nutrient Recovery and Reuse (NRR) in European agriculture. A review of the issues, opportunities, and actions. RISE Foundation, Brussels*.

Tarpagkou, R., & Pantokratoras, A. (2014). The influence of lamellar settler in sedimentation tanks for potable water treatment—A computational fluid dynamic study. *Powder Technology*, *268*, 139–149. https://doi.org/10.1016/j.powtec.2014.08.030

Tasca, A. L., Puccini, M., Gori, R., Corsi, I., Galletti, A. M. R., & Vitolo, S. (2019). Hydrothermal carbonization of sewage sludge: A critical analysis of process severity, hydrochar properties and environmental implications. *Waste Management*, *93*, 1–13. https://doi.org/10.1016/j.wasman.2019.05.027

Tekin, K., Karagöz, S., & Bektaş, S. (2014). A review of hydrothermal biomass processing. *Renewable and Sustainable Energy Reviews*, *40*, 673–687. https://doi.org/10.1016/j.rser.2014.07.216

Ternes, T. A., Herrmann, N., Bonerz, M., Knacker, T., Siegrist, H., & Joss, A. (2004). A rapid method to measure the solid–water distribution coefficient (Kd) for pharmaceuticals and musk fragrances in sewage sludge. *Water Research*, *38*(19), 4075–4084. https://doi.org/10.1016/j.watres.2004.07.015

Vaissie, P., Monge, A., & Husson, F. (2025). *Factoshiny: Perform Factorial Analysis from "FactoMineR" with a Shiny Application* (Version 2.7) [Computer software]. https://cran.r-project.org/web/packages/Factoshiny/index.html

Voulvoulis, N., & Lester, J. N. (2006). Fate of organotins in sewage sludge during anaerobic digestion. *Science of The Total Environment*, *371*(1–3), 373–382. https://doi.org/10.1016/j.scitotenv.2006.08.024

Wang, T., Zhai, Y., Zhu, Y., Li, C., & Zeng, G. (2018). A review of the hydrothermal carbonization of biomass waste for hydrochar formation: Process conditions, fundamentals, and physicochemical properties. *Renewable and Sustainable Energy Reviews*, *90*, 223–247. https://doi.org/10.1016/j.rser.2018.03.071

Yang, N., Zhang, Y., Hua, Y., Yang, S., & Dai, X. (2026). Why does organics dissolution reach “equilibrium-limited dissolution” during sludge thermal hydrolysis: The competitive effects between hydrolysis, repolymerization, and solid phase adsorption. *Water Research*, *298*, 125845. https://doi.org/10.1016/j.watres.2026.125845

Yin, S., Gao, L., Fan, X., Gao, S., Zhou, X., Jin, W., He, Z., & Wang, Q. (2024). Performance of sewage sludge treatment for the removal of antibiotic resistance genes: Status and prospects. *Science of The Total Environment*, *907*, 167862. https://doi.org/10.1016/j.scitotenv.2023.167862

Yu, Z., & Schanbacher, F. L. (2010). Production of Methane Biogas as Fuel Through Anaerobic Digestion. In O. V. Singh & S. P. Harvey (Eds.), *Sustainable Biotechnology* (pp. 105–127). Springer Netherlands. https://doi.org/10.1007/978-90-481-3295-9_6

Zhang, C., Yan, H., Li, F., Hu, X., & Zhou, Q. (2013). Sorption of short- and long-chain perfluoroalkyl surfactants on sewage sludges. *Journal of Hazardous Materials*, *260*, 689–699. https://doi.org/10.1016/j.jhazmat.2013.06.022

Zhang, J., Lin, Q., & Zhao, X. (2014a). The Hydrochar Characters of Municipal Sewage Sludge Under Different Hydrothermal Temperatures and Durations. *Journal of Integrative Agriculture*, *13*(3), 471–482. https://doi.org/10.1016/S2095-3119(13)60702-9

Zhang, J., Lin, Q., & Zhao, X. (2014b). The Hydrochar Characters of Municipal Sewage Sludge Under Different Hydrothermal Temperatures and Durations. *Journal of Integrative Agriculture*, *13*(3), 471–482. https://doi.org/10.1016/S2095-3119(13)60702-9

Zhang, X., Ye, P., & Wu, Y. (2022). Enhanced technology for sewage sludge advanced dewatering from an engineering practice perspective: A review. *Journal of Environmental Management*, *321*, 115938. https://doi.org/10.1016/j.jenvman.2022.115938

Zhao, X., Li, B., Ni, J., & Xie, D. (2016). Effect of four crop straws on transformation of organic matter during sewage sludge composting. *Journal of Integrative Agriculture*, *15*(1), 232–240. https://doi.org/10.1016/S2095-3119(14)60954-0

Zielińska, A., & Oleszczuk, P. (2015). Evaluation of sewage sludge and slow pyrolyzed sewage sludge-derived biochar for adsorption of phenanthrene and pyrene. *Bioresource Technology*, *192*, 618–626. https://doi.org/10.1016/j.biortech.2015.06.032

8 Annex

8.1 Annex A: Supplementary Figures and Tables

8.1.1 Complexity Index of ISBAMO Fractions

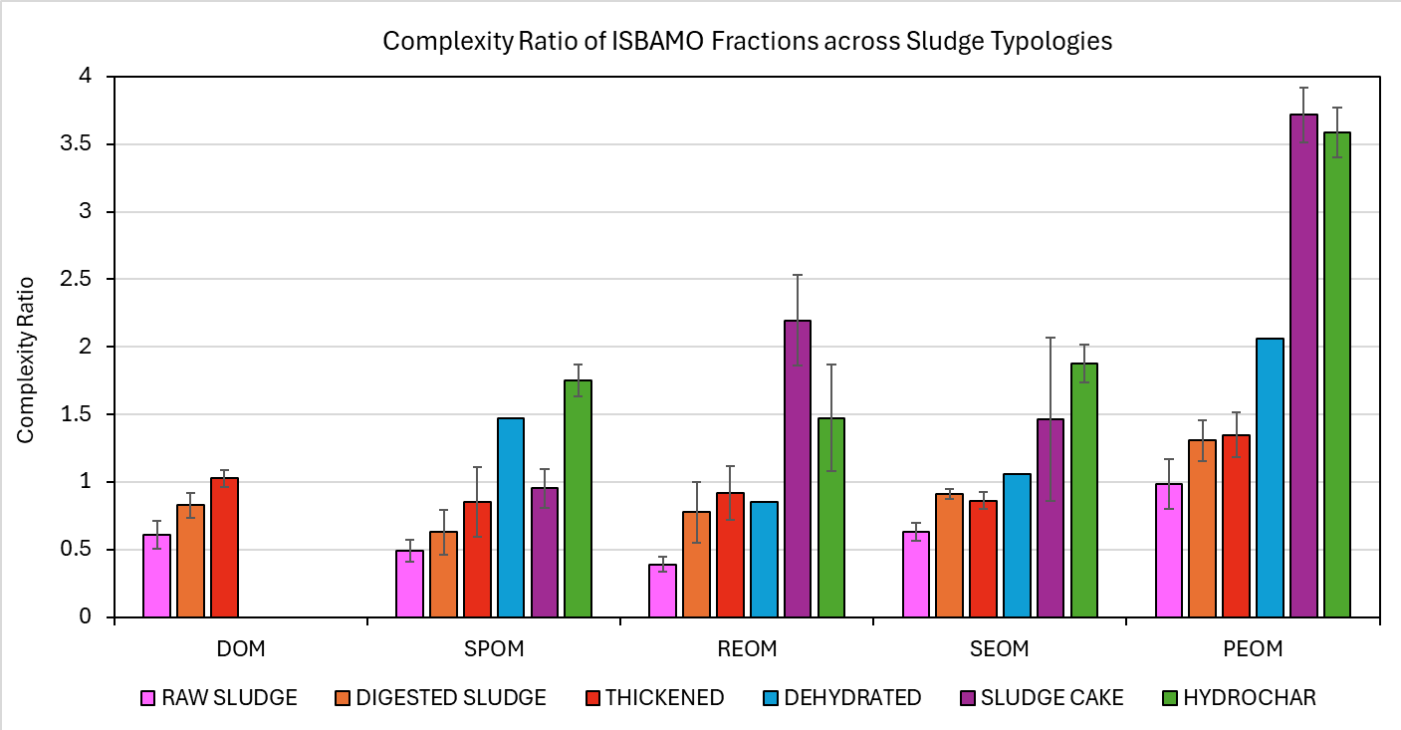

Figure A 1: The complexity ratio (CR) of each typology (raw sludge, digested sludge, thickened sludge, sludge cake and hydrochar), across fractions (DOM, SPOM, REOM, SEOM, PEOM). n=4 for each typology. Black error bars show standard deviation.

8.1.2 PCA and HCA of Physicochemical Properties, with Biochar Included

Scores and loadings from the PCA of the physicochemical properties, including biochar (29 samples in total) are presented in Figure A 2. The first two components accounted for 62.67% of the total variance (Dim 1: 39.43%; Dim 2: 23.24). The distribution of variables is consistent with the analysis excluding biochar and correlation values for the variables on dimensions 1 and 2 are shown in Table A 1. Biochar (sample 29) is positioned at the extreme negative end of dimension 1 and elevated dimension 2, clearly isolated from all other sludge-derived typologies.

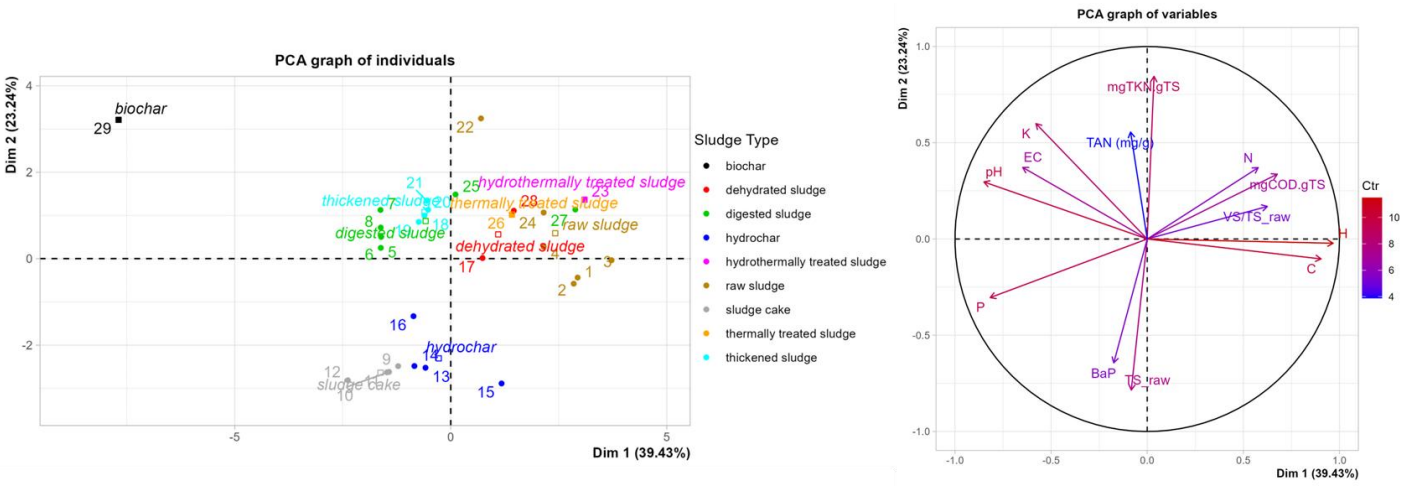

Figure A 2: Scores plot (a) and loadings (b) obtained from the PCA analysis of the database including biochar with the considered set of physicochemical characteristics (pH, EC, TS, VS/TS, COD, TKN, N, C, H, P, K, BaP, TAN) as active variables; left is the graph of individuals (sludge types) and right is the PCA graph of variables (physicochemical properties).

Table A 1: Correlation data of the variables for dimension 1 and dimension 2 of PCA graph of physicochemical characteristics using data including biochar.

Correlation of quantitative variables on **Dimension1**		**Correlation** of quantitative variables on **Dimension2**	
H	0.9672	mgTKN.gTS	0.845
C	0.9045	K	0.5995
mgCOD.gTS	0.6768	TAN (mg/g)	0.5559
VS/TS_raw	0.6251	EC	0.3719
N	0.5773	N	0.3707
K	-0.5789	BaP	-0.6435
EC	-0.6479	TS_raw	-0.7845
P	-0.817		
pH	-0.8496		

8.2 Annex B: Raw Data

Table A 2: Raw data for the mean COD distribution (% of extracted COD) across ISBAMO fractions and total organic carbon content (tCOD, mg/g TS) for each sludge typology (n = 4 replicates). Values in parentheses indicate mean % COD extracted relative to tCOD of the raw solid. Standard deviations are reported for tCOD values. DOM_COD data were unavailable for sludge cake and hydrochar. Data underlying Figure 8.

Sample	RAW (55%)	DIGESTED (48%)	THICKENED (51%)	SLUDGE CAKE (32%)	HYDROCHAR (55%)
DOM_COD	9%	1%	1%		
SPOM_COD	4%	2%	2%	3%	2%
REOM_COD	7%	3%	4%	2%	3%
SEOM_COD	12%	10%	12%	4%	6%
PEOM_COD	23%	32%	32%	23%	43%
NEOM_COD	45%	52%	49%	68%	45%
% COD extracted	55%	48%	51%	32%	55%
mean tCOD mg/g TS	1485.2975	1044.035	1044.0775	875.0275	1170.4125
st dev	206.279724	45.49015754	32.38556301	51.11117123	106.4787567

Table A 3: Raw data for the mean nitrogen distribution (% of extracted TN) across ISBAMO fractions and total nitrogen content (TKN, mg/g TS) for each sludge typology (n = 4 replicates). Values in parentheses indicate mean % TN extracted relative to TKN. Standard deviations are reported for TKN values. DOM_TN data are unavailable for sludge cake and hydrochar. Data underlying Figure 9.

Sample (extracted TN)	RAW (68%)	DIGESTED (75%)	THICKENED (69%)	SLUDGE CAKE (23%)	HYDROCHAR (36%)
DOM_TN	11%	57%	47%		
SPOM_TN	12%	4%	4%	7%	18%
REOM_TN	14%	4%	5%	6%	7%
SEOM_TN	32%	10%	12%	10%	12%
PEOM + NEOM	32%	25%	32%	77%	64%
% TN extracted	68%	75%	68%	23%	36%
TKN mg/g TS	41.357	74.5435	80.21775	21.76225	26.01575
st dev	15.677801	8.360602231	11.53481716	0.558152533	6.799173203

Table A 4: Raw data for the mean percentage fluorescence intensity distribution across zones I–VII and split line values for each ISBAMO fraction and sludge typology. Relevant typology is indicated in each table. Values represent the proportion (%) of total fluorescence intensity attributed to each zone within a given fraction. DOM fraction data are unavailable for sludge cake and hydrochar. This table underlies Figure 12.

RAW					
Zone	DOM	SPOM	REOM	SEOM	PEOM
I	13.60161	6.107009	18.26478	8.015924	10.32305
II	32.51117	40.55509	37.85348	36.95267	30.25746
III	17.79702	20.86018	16.59752	16.60354	10.66228
IV	20.44969	18.44927	15.42078	21.52567	22.91918
V	9.887049	8.312534	6.492849	9.13572	12.26636
VI	4.718493	4.592597	4.388115	6.361118	9.768549
VII	1.034967	1.123315	0.98247	1.405365	3.803116
Split line	63.9098	67.52228	72.71579	61.57213	51.24279

DIGESTED					
Zone	DOM	SPOM	REOM	SEOM	PEOM
I	9.592267	5.855976	10.6782	4.681442	5.006241
II	41.92042	36.58646	30.95218	31.19997	29.65227
III	3.380058	19.11205	14.31608	16.19653	8.692396
IV	23.88263	22.59814	22.54257	24.82673	23.06612
V	10.1676	8.721374	10.89296	11.59553	13.96608
VI	8.098442	5.794044	8.718475	9.731081	12.93679
VII	2.958588	1.331955	1.899551	1.768715	6.6801
split line	54.89274	61.55448	55.94645	52.07795	43.35091

THICKENED					
Zone	DOM	SPOM	REOM	SEOM	PEOM
I	7.235516	2.90439	8.172882	5.14272	7.171092
II	30.65378	34.30151	31.14488	33.68495	26.62229
III	11.33165	14.84295	12.78986	14.95613	9.202191
IV	29.3983	26.80691	23.49438	24.66271	24.13328
V	11.45757	11.7874	11.29739	10.77671	15.03176
VI	8.058328	7.715557	10.86663	9.030763	12.30135
VII	1.864849	1.641272	2.233978	1.746005	5.538045
split line	49.22095	52.04886	52.10763	53.7838	42.99557

SLUDGE CAKE				
Zone	SPOM	REOM	SEOM	PEOM
I	1.190124	5.162882	3.659402	2.223291
II	39.53842	18.07636	26.7912	14.19534
III	12.46657	8.754425	11.13296	5.160862
IV	30.43005	30.80156	29.93091	33.92189
V	9.020596	14.50637	13.99476	25.03277
VI	6.232007	20.23084	12.01237	14.2141
VII	1.122223	2.467558	2.478394	5.251754
split line	53.19512	31.99366	41.58357	21.57949

HYDROCHAR				
Zone	SPOM	REOM	SEOM	PEOM
I	1.626236	3.193279	1.928121	2.271566
II	24.35454	25.04929	22.77594	13.20305
III	10.22303	11.14996	10.56237	6.191462
IV	36.7954	34.19853	35.66275	41.74933
V	14.69556	14.89911	16.50728	24.40411
VI	10.41771	9.546921	10.26612	9.743626
VII	1.88752	1.962912	2.297414	2.43687
split line	36.2038	39.39253	35.26643	21.66607

Table A 5: Raw data for the mean complexity ratio (CR) and standard deviation across ISBAMO fractions for each sludge typology (n=4 per typology), underlying Figure 13.

TYPOLOGY	VALUE	DOM	SPOM	REOM	SEOM	PEOM
RAW SLUDGE	mean	0.608782	0.49325	0.392376	0.630568	0.985431
	st dev	0.104527	0.07916	0.058421	0.06549	0.181652
DIGESTED SLUDGE	mean	0.827826	0.628662	0.777804	0.914392	1.306537
	st dev	0.092237	0.168187	0.225143	0.036677	0.149075
THICKENED	mean	1.026722	0.851852	0.922899	0.863753	1.346982
	st dev	0.059905	0.257017	0.199072	0.063659	0.165752
SLUDGE CAKE	mean		0.95329	2.197509	1.464876	3.71809
	st dev		0.142008	0.334105	0.607238	0.203129
HYDROCHAR	mean		1.752623	1.473256	1.876367	3.583015
	st dev		0.117891	0.394431	0.141053	0.184418